# Subpart RR Monitoring, Reporting, and Verification (MRV) Plan
# Kinder Morgan Permian CCS LLC

Prepared for *Kinder Morgan Permian CCS LLC*
Houston, TX

By

*Lonquist Sequestration, LLC*
Austin, TX

Version 4.0
June 2023

# INTRODUCTION

Kinder Morgan Production Co. LLC (Kinder Morgan) currently has a Class II disposal permit issued by the Texas Railroad Commission (TRRC) for the Katz Strawn Unit 2361 well (KSU 2361), API# 42-433-33712. The permit was originally issued in November 2011 for saltwater disposal operations, and the well has actively injected saltwater since 2013. This permit currently authorizes Kinder Morgan to inject up to 30,000 barrels saltwater per day (bbls/d), equating to 65 million standard cubic feet per day (MMscf/day) of carbon dioxide, into the Ellenburger and Cambrian formations at a depth of 5,800' to 6,800' with a maximum allowable surface pressure of 2,900 psi. The KSU 2361 well is located in a rural, sparsely populated area of Stonewall County, Texas, approximately twelve miles west of the town of Knox City, as shown in Figure 1.

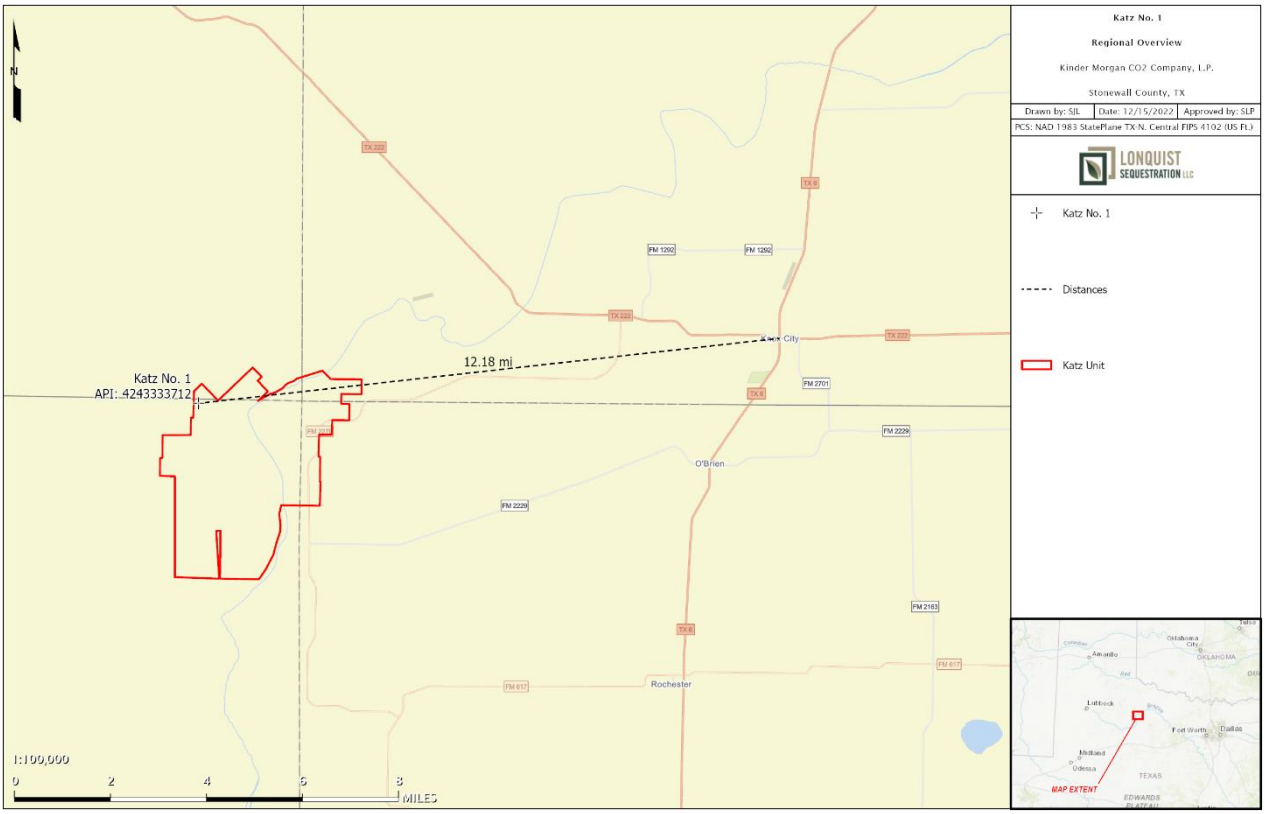


Figure 1 – Location of KSU 2361 Well

Kinder Morgan is seeking TRRC approval to amend the existing KSU 2361 Class II saltwater disposal permit to inject treated acid gas (TAG), including $CO_2$. In the future, Kinder Morgan may provide surplus injection capacity to dispose oil and gas waste derived TAG from similar third-party gas processing facilities. Kinder Morgan intends to inject into this well for 21 years at a capacity ranging up to 65 million standard cubic feet per day (MMSCF/d). The source of this injected $CO_2$ gas is from Red Cedar natural gas processing plants in southern Colorado. Table 1 below shows the expected composition of the gas stream to be injected. Table 2 shows the expected average volume of $CO_2$ gas commitments from similar type emission sources in the same area, along with the contract status as of March 2023.

Table 1 – Expected Gas Composition at KSU 2361

| Component | Mol Percent |
|---|---|
| Carbon Dioxide | 99.20% |
| Methane | 0.25% |
| Ethane | 0.03% |
| Propane | 0.04% |
| Nitrogen | 0.48% |
| Hydrogen Sulfide | 0.00% |

Table 2 – Expected Sequestered Gas Volumes for KSU 2361

| Contract Status | Avg. Rate (MMcfd) |
|---|---|
| Committed | 22 |
| Proposal | 8 |
| Proposal | 23 |
| Proposal | 9 |
| **Total** | 62 |

Kinder Morgan is submitting this Monitoring, Reporting, and Verification (MRV) plan to the EPA for approval under 40 CFR §98.440(a), Subpart RR, of the Greenhouse Gas Reporting Program (GHGRP).

# ACRONYMS AND ABBREVIATIONS

| | |
|---|---|
| ‘ | Feet |
| % | Percent (Percentage) |
| °C | Degrees Celsius |
| °F | Degrees Fahrenheit |
| AMA | Active Monitoring Area |
| BCF | Billion Cubic Feet |
| $CH_4$ | Methane |
| CMG | Computer Modelling Group |
| $CO_2$ | Carbon Dioxide (may also refer to other Carbon Oxides) |
| E | East |
| EOS | Equation of State |
| EPA | U.S. Environmental Protection Agency |
| ESD | Emergency Shutdown |
| FG | Fracture Gradient |
| ft | Foot (Feet) |
| GAPI | Gamma Units of the American Petroleum Institute |
| GAU | Groundwater Advisory Unit |
| GEM | Computer Modelling Group’s GEM 2020.11 |
| GHGs | Greenhouse Gases |
| GHGRP | Greenhouse Gas Reporting Program |
| GL | Ground Level Elevation |
| $H_2S$ | Hydrogen Sulfide |
| JPHIE | Effective Porosity (corrected for clay content) |
| mD | MilliDarcy(ies) |
| mi | Mile(s) |
| MIT | Mechanical Integrity Test |
| MM | Million |

| | |
|---|---|
| MMA | Maximum Monitoring Area |
| MCF | Thousand Cubic Feet |
| MMCF | Million Cubic Feet |
| MMSCF | Million Standard Cubic Feet |
| MSCF/D | Thousand Cubic Feet per Day |
| MMSCF/d | Million Standard Cubic Feet per Day |
| MRV | Monitoring, Reporting, and Verification |
| $\nu$ | Poisson's Ratio |
| N | North |
| NW | Northwest |
| OBG | Overburden Gradient |
| PG | Pore Gradient |
| pH | Scale of Acidity |
| ppm | Parts per Million |
| psi | Pounds per Square Inch |
| psig | Pounds per Square Inch Gauge |
| S | South |
| SE | Southeast |
| SF | Safety Factor |
| SWD | Saltwater Disposal |
| TAC | Texas Administrative Code |
| TAG | Treated Acid Gas |
| TOC | Total Organic Carbon |
| TRRC | Texas Railroad Commission |
| UIC | Underground Injection Control |
| USDW | Underground Source of Drinking Water |
| W | West |

# TABLE OF CONTENTS

LIST OF FIGURES

LIST OF TABLES

# SECTION 1 – UIC INFORMATION

This section contains key information regarding the UIC Permit.

## 1.1 Underground Injection Control (UIC) Permit Class: Class II

The TRRC regulates oil and gas activities in Texas and has primacy to implement the Underground Injection Control (UIC) Class II program. TRRC classifies the KSU 2361 well as UIC Class II. A Class II permit was issued to Kinder Morgan under TRRC Rule 9 (entitled "Disposal into Non-Productive Formations") and Rule 36 (entitled "Oil, Gas, or Geothermal Resource Operation in Hydrogen Sulfide Areas").

## 1.2 UIC Well Identification Number:

Katz Strawn Unit 2361, API No. 42-433-33712, UIC #000104281.

# SECTION 2 – PROJECT DESCRIPTION

This Project Description discusses the geologic setting, planned injection process and volumes, and the reservoir and plume modeling performed for the KSU 2361 well.

The injection interval for KSU 2361 is approximately 670’ below the base of the Strawn formation, the primary producing formation in the area, and approximately 5,900’ below the base of the lowest useable-quality aquifer. Therefore, the location, facility, and the well design of the KSU 2361 well are planned to protect against the migration of $CO_2$ out of the injection interval, protect against contamination of subsurface resources and, most critical, to prevent surface releases.

## 2.1 Regional Geology

The KSU 2361 well is located on the Eastern Shelf, a broad marine shelf located in the eastern portion of the Permian Basin, shown in Figure 2. Figure 3 depicts an Eastern Shelf stratigraphic column representative of the strata found at the KSU 2361 well location. The red stars reference the injection formations, and a green star indicates the historically productive interval in the area.

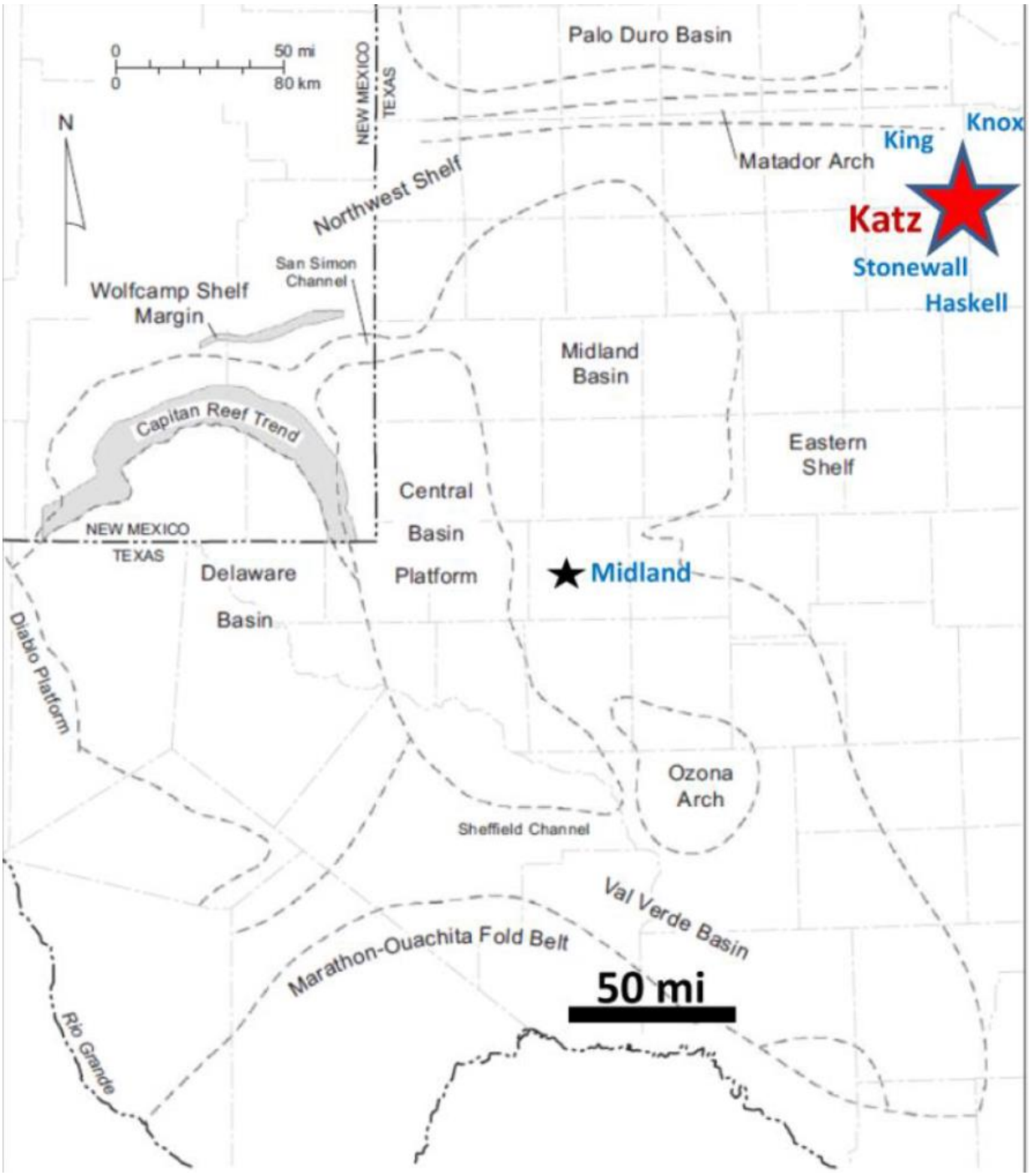


Figure 2 – Regional Map of the Permian Basin. The red star is the approximate location of KSU 2361 well.

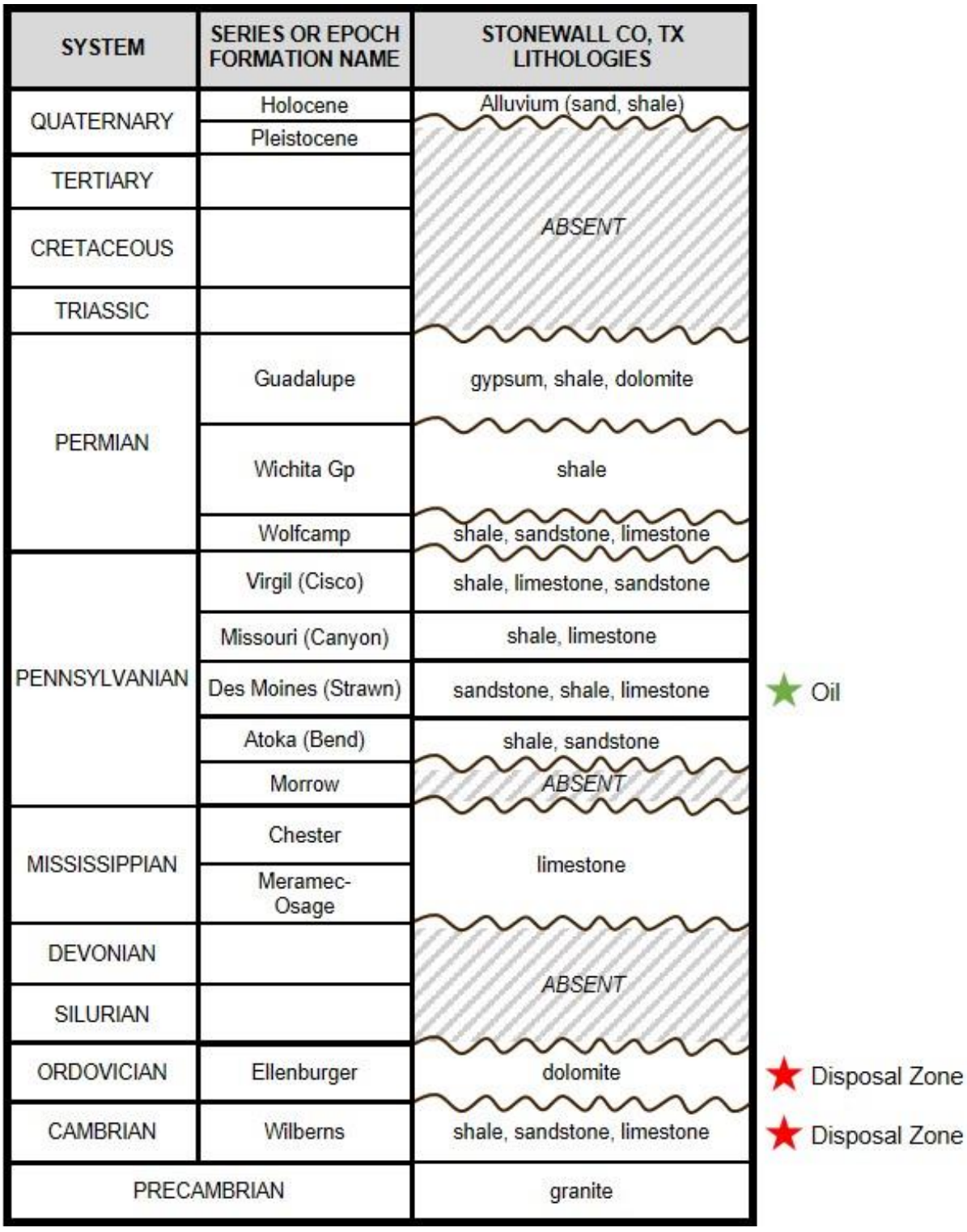


Figure 3 – Stratigraphic Column of the Eastern Shelf.

The upper target injection interval is the lower Ordovician-age Ellenburger Group, which is subdivided into the Honeycut, Gorman, and Tanyard Formations, as seen in Figure 4. Upper Cambrian-age sandstone units of the Wilberns Formation, comprise the lower target injection interval.

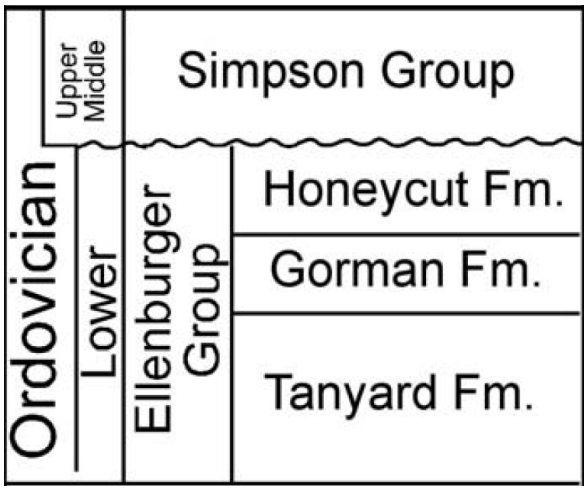


Figure 4 – Stratigraphic Column Depicting the Composition of the Ordovician-age Formations (Kupecz, 1992).

The Ellenburger Group is present at varying depths in each of the provinces of the Permian Basin. In the Midland Basin area, the top of Ellenburger carbonate is as deep as 11,000' (GL) (Loucks, 2003). Due to regional structural dip of the Eastern Shelf, in northeast Stonewall County, the top of Ellenburger is found at only approximately 6,000' deep (GL). The depositional environment over the Stonewall, King, Knox, and Haskell County intersection during the Ordovician Period was a broad, shallow water carbonate platform with an interior of dolomite and an outer area of limestone. This was interpreted by Kerans (1990) as the dolomite being a restricted shelf interior and the limestone being an outer rim of more open-shelf deposits (Loucks, 2003).

Kerans (1990) performed the most complete regional analysis on Ellenburger depositional systems and facies. He recognized six general lithofacies as follows: litharenite: fan delta – marginal marine depositional system; mixed siliciclastic-carbonate packstone/grainstone: lower tidal-flat depositional system; ooid and peloid grainstone: high-energy restricted-shelf depositional system; mottled mudstone: low-energy restricted-shelf depositional system; laminated mudstone: upper tidal-flat depositional system; and gastropod-intraclast-peloid packstone/grainstone: open shallow-water-shelf depositional system.

According to Loucks, the diagenesis of the Ellenburger Group is complex, and the processes that produced the diagenesis spanned millions of years. The three major diagenetic processes of note are dolomitization, karsting, and tectonic fracturing. Dolomitization favors the preservation of fractures and pores due to its greater chemical and mechanical stability relative to limestone. Kupecz and Land (1991) delineated generations of dolomite into early-stage and late-stage. They attributed 90% of the dolomite as early-stage, wherein the source of magnesium was probably seawater. The other 10% of dolomite was attributed as late-stage, in which warm, reactive fluids were expelled from basinal shales during the Ouachita Orogeny. Karsting can affect only the surface of a carbonate terrain, forming terra rosa, or it can extensively dissolve the carbonate surface,

forming karst towers (Loucks, 2003). It can also produce extensive subsurface dissolution in the form of caves and other structures, which increases porosity and permeability. Fracturing can be tectonic or karst-related. Tectonic fractures are commonly the youngest fractures in the rock and generally crosscut karst-related fractures (Kerans, 1989). Holtz and Kerans (1992) divided Ellenburger reservoirs into three groups based on these fracture types. The Eastern Shelf of the Permian Basin falls within the ramp carbonates group, in which predominant pore types are intercrystalline and interparticle. These reservoirs are characterized by the thinnest net pay, highest porosity, moderate permeability, highest initial water saturation, and highest residual oil saturation.

Figures 5 and 6 show the regional structure contours and isopachs of the Ellenburger Group, respectively. Figure 7 shows isopachs of Cambrian and lower Ordovician strata. Stars depict the KSU 2361 well location in each of these figures. In Figure 8, formation tops from gamma-ray data indicate the net pay thickness of the Ellenburger and Cambrian is approximately 223' within this interval in the KSU 2361 well location.

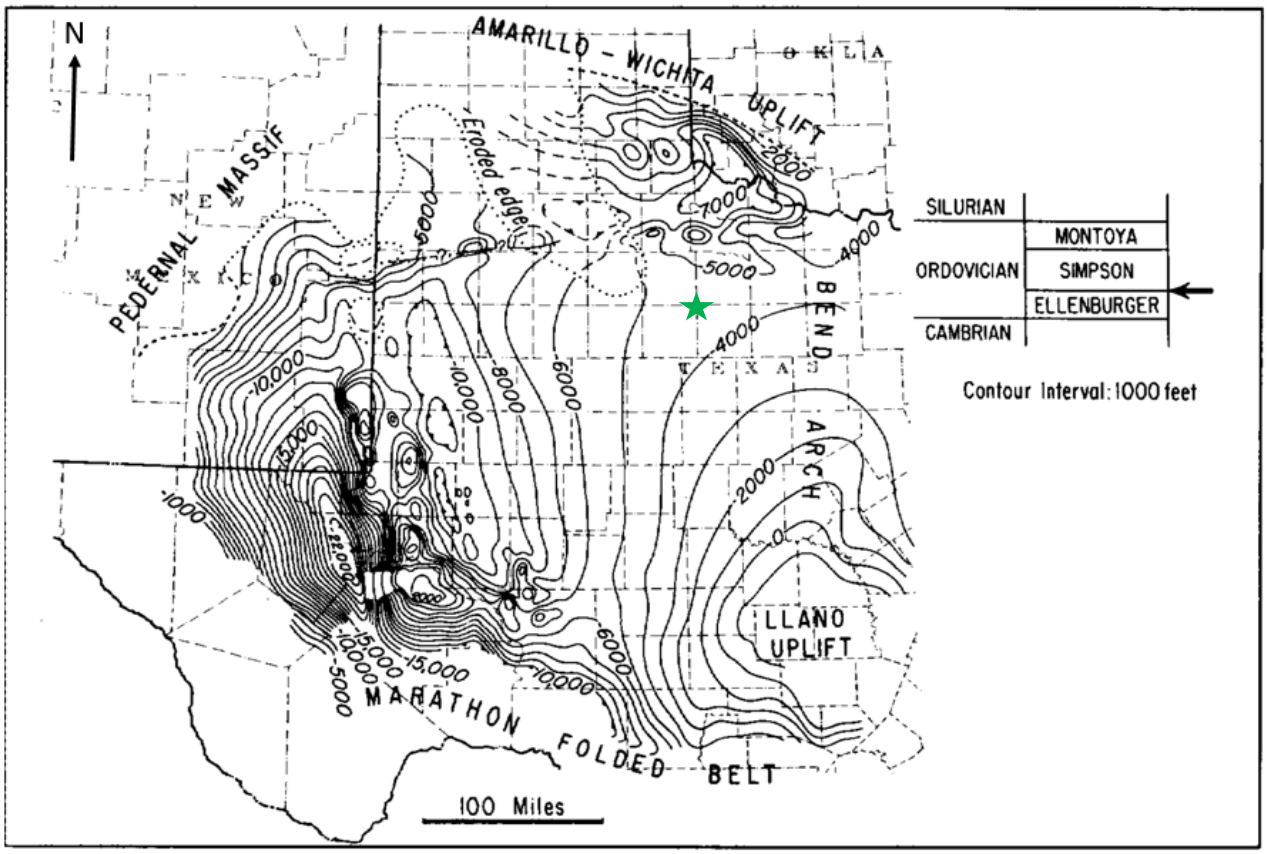


Figure 5 – Top of Structure Map of the Ellenburger Group in West Texas (Subsea Values) (Galley, 1955).

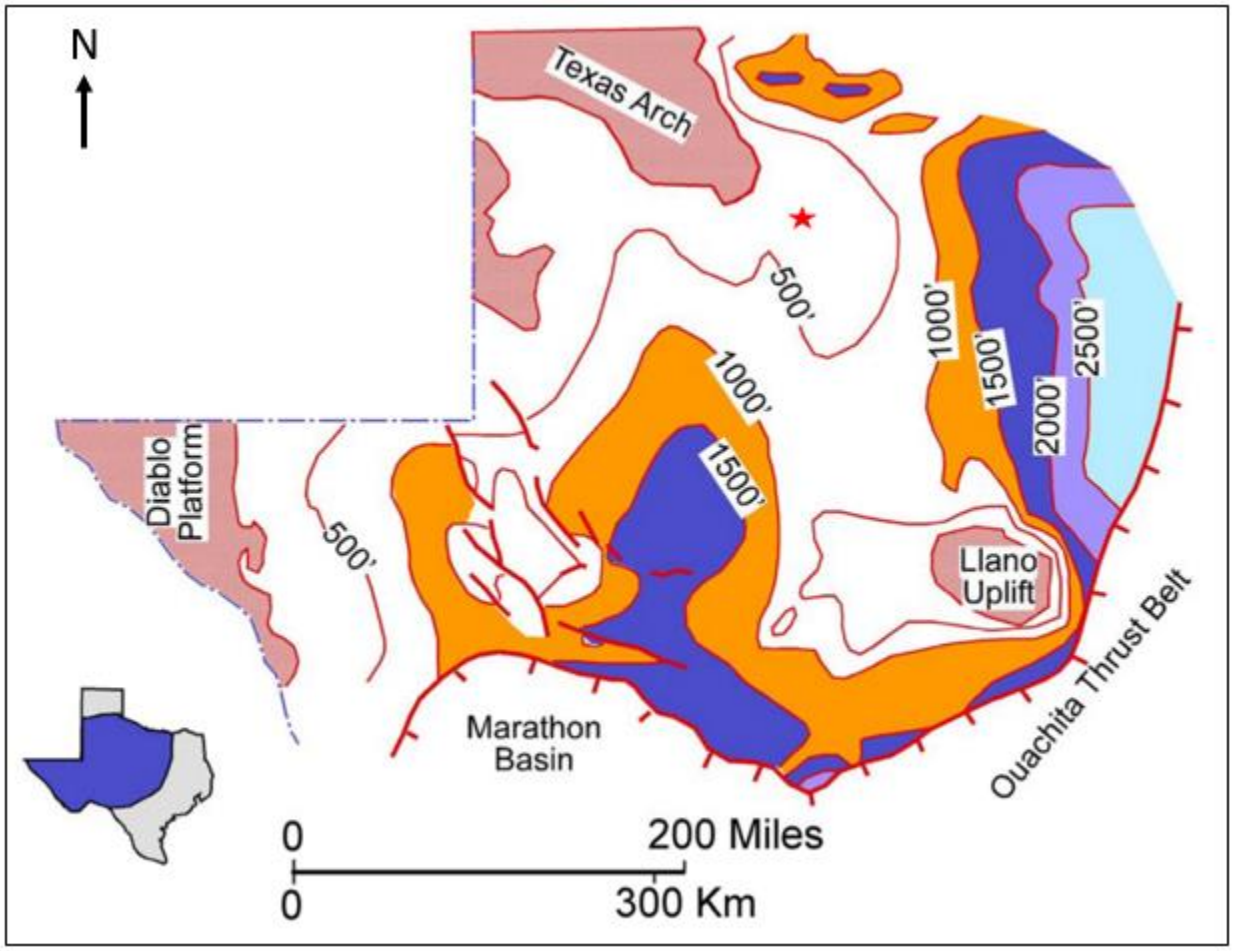


Figure 6 – Generalized Isopach Map of the Ellenburger Group in West Texas (Kerans, 1989).

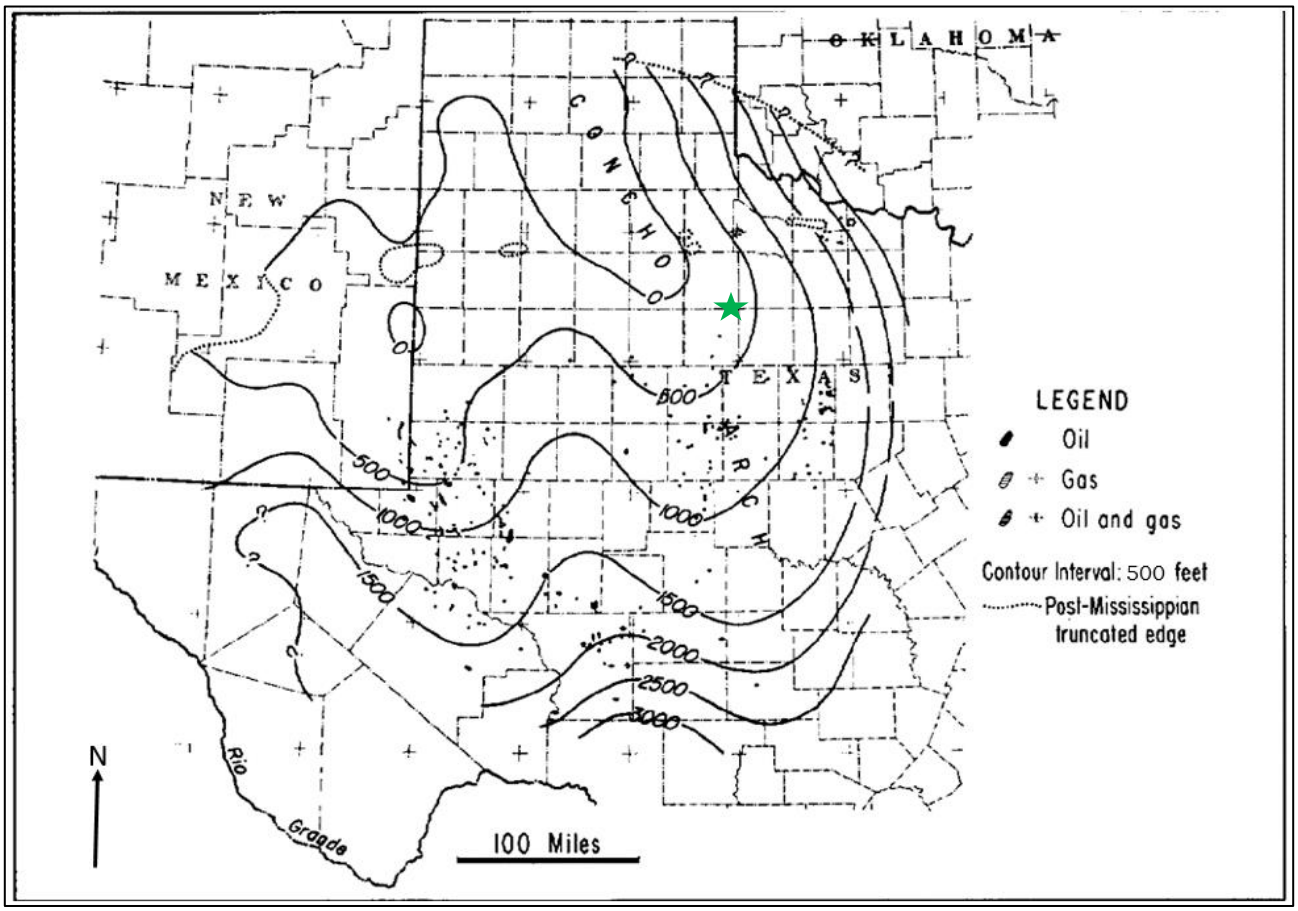


Figure 7 – Thickness of Cambrian and Lower Ordovician Strata (Galley, 1955).

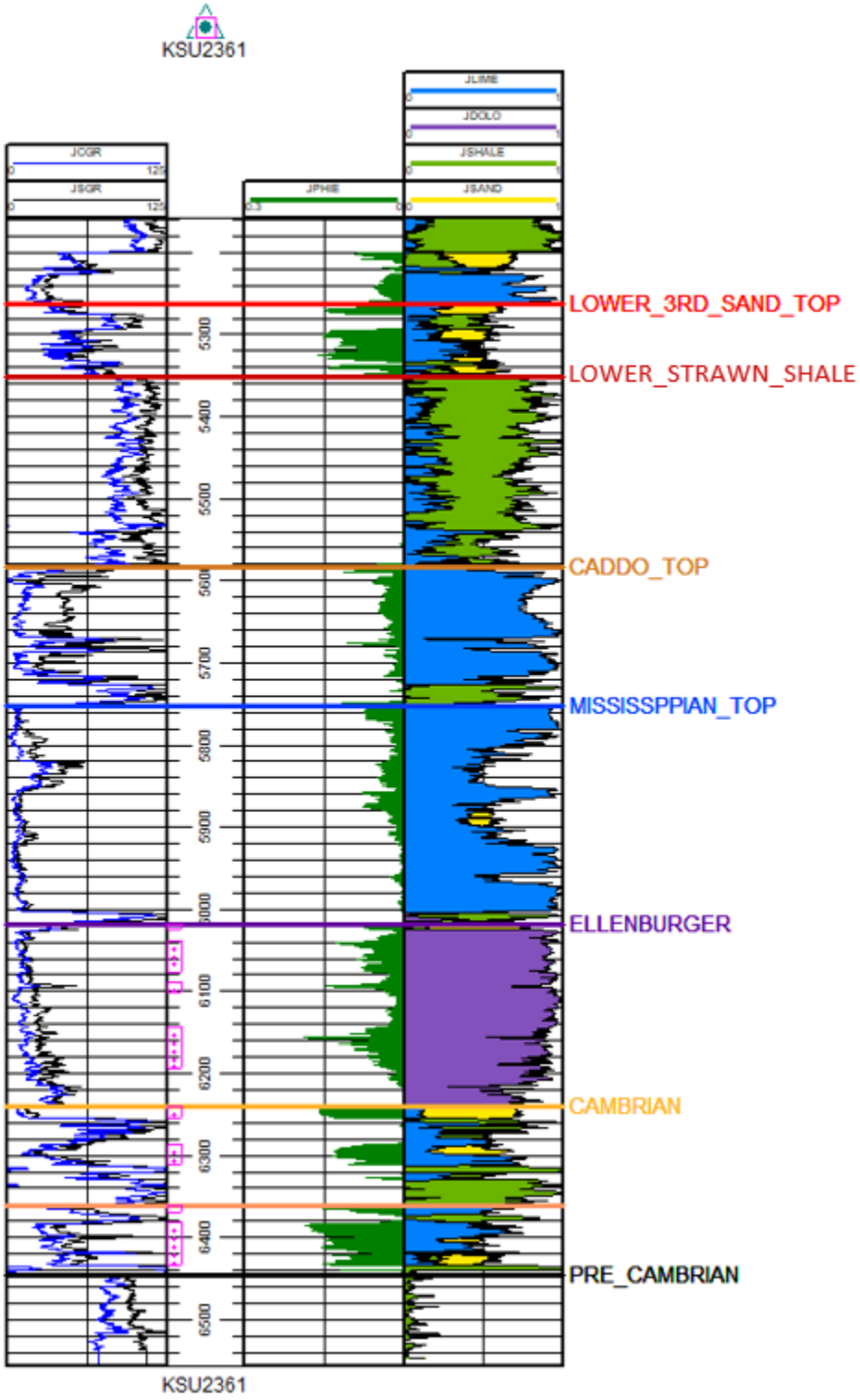


Figure 8 – Formation Tops at KSU 2361. Purple represents dolomite and the upper injection interval. Yellow represents sandstone, which is present in the pay interval. Pink boxes within depth column indicate active perforated intervals.

Cambrian-age strata consist of interbedded sandstone, limestone, and shale members. The initial deposits laid down on the eroded surface of Precambrian rocks were sandstone and arenaceous carbonates. Shale members are thickest in the southeast and nonexistent on the west side of the Permian Basin (Galley, 1955).

Overlying the Precambrian basement rock is the Riley Formation. This, in turn, is overlain by transgressive and progradational shallow-water marine sandstone, siltstone, limestone, and dolomite of the Wilberns Formation. The Riley Formation consists of sandstone packages whose thicknesses vary from place to place in response to the paleotopography of the underlying Precambrian surface (Kyle and McBride, 2014). The depositional environment in this area during the Cambrian was influenced by the sea, which advanced from the southeast (Galley, 1955). This led to the formation of a complex succession of transgressive and regressive sandstone units, both glauconitic and non-glauconitic (Kyle and McBride, 2014).

The Riley Formation is probably thickest south of the Llano region and laps out about 100 miles west and a slightly greater distance northwestward from the Llano region. It has accumulated in a northwestward-extending arm of the sea and likely extended beyond its present limits since there is a disconformity at its top. The Wilberns Formation thins appreciably northwestward from the Llano region to about 230’ in Nolan County and to 70’ in Lubbock County. West and north of the Llano region, usage suggested by Cloud and Barnes and adopted by petroleum geologists places the Tanyard-Wilberns boundary in the vicinity of the first appearance downward of glauconite (Barnes et al., 1959).

Figure 9 indicates that the Riley Formation’s northwestern extent ends in Jones and Fisher counties, which implies that Cambrian strata at KSU 2361 may be limited to the Wilberns Formation only.

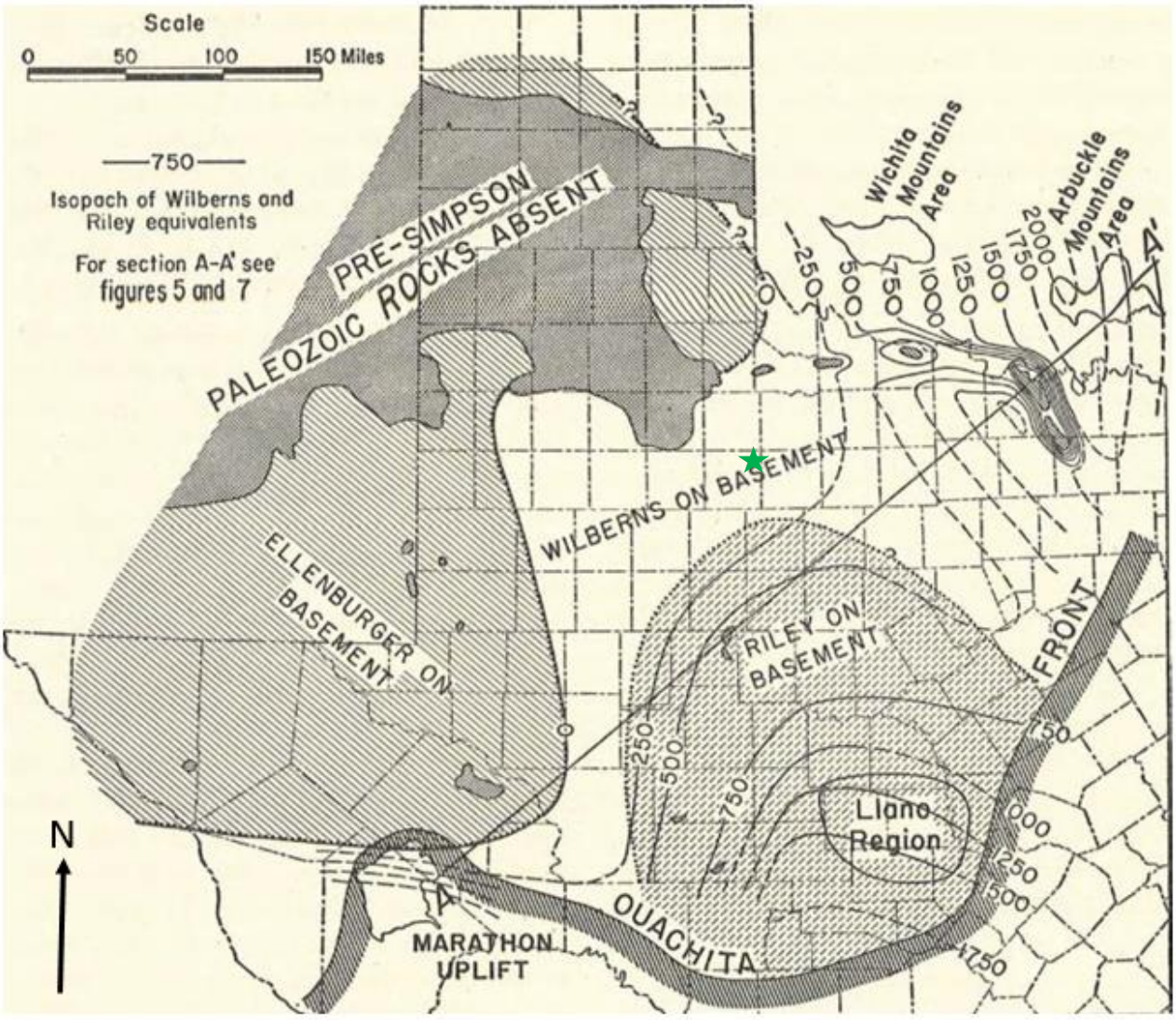


Figure 9 – Isopach Map of Riley and Wilberns equivalents in Texas and Southern Oklahoma. The green star approximates the location of KSU 2361 (Barnes et al., 1959).

### 2.1.1 Regional Faulting

Regional faulting in the KSU 2361 area trends primarily N-S in direction. This is the result of the dip rotation from a SW-NE trend seen in the Fort Worth basin to the east that rotates N-S as you move west towards the Bend-Arch and the edge of the basin (Hornhach, 2016). This trend then carries towards the Eastern Shelf closer to the KSU 2361 location. The most common faults are high-angle basement faults that primarily die within the Pennsylvanian in the KSU 2361 well area. Faulting is discussed in more detail in the Site characterization.

## 2.2 Site Characterization

The following section discusses site-specific geological characteristics of the KSU 2361 well.

### 2.2.1 Stratigraphy and Lithologic Characteristics

Figure 10 depicts an annotated open hole log from the surface to the total depth of the KSU 2361 well, with regional formation tops indicating the injection and primary upper confining units. Figure 11 provides a magnified view of the zones of interest, from above the Lower Strawn to the Precambrian, with general lithologic descriptions along the right edge of the figure.

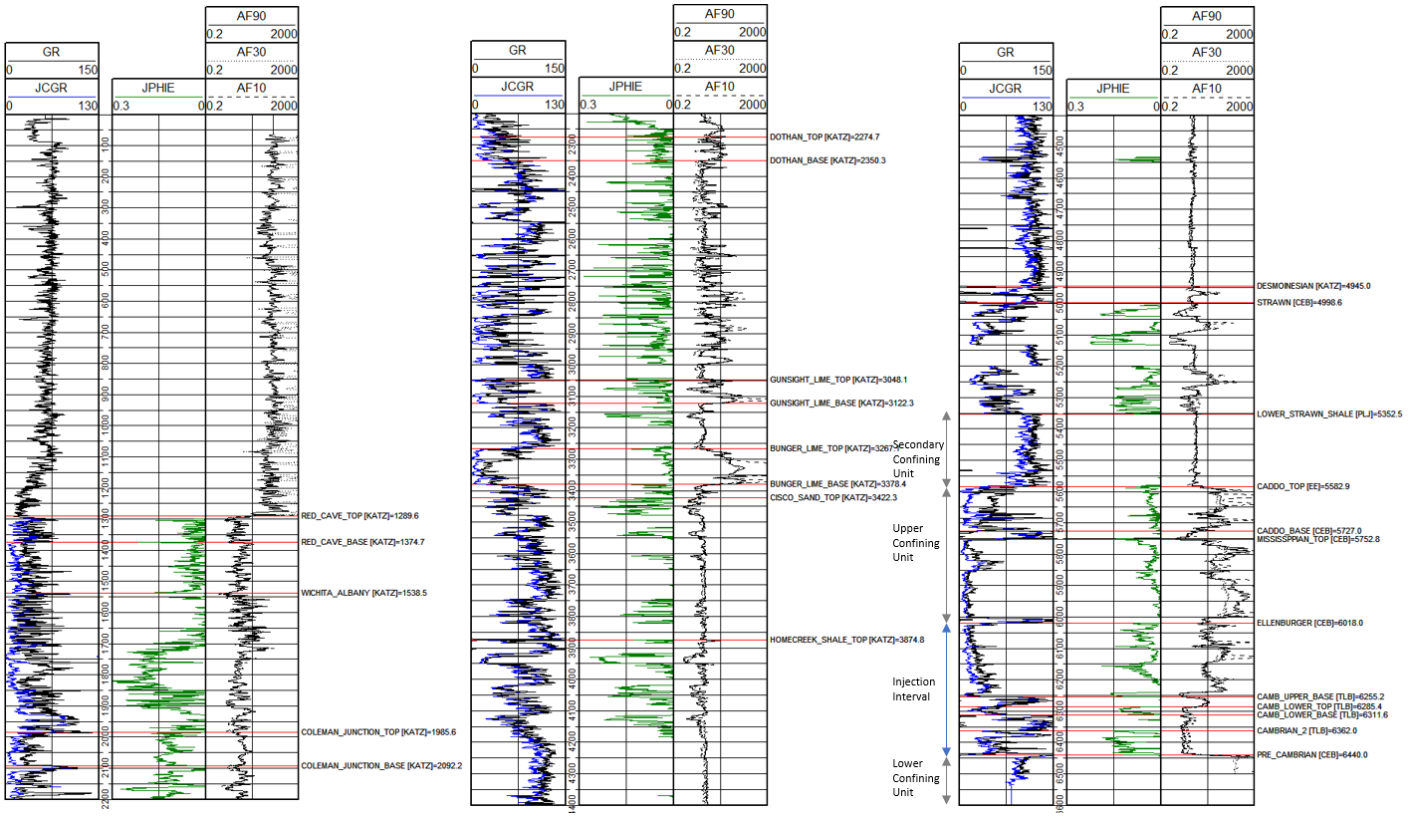


Figure 10 – KSU 2361 Type Log

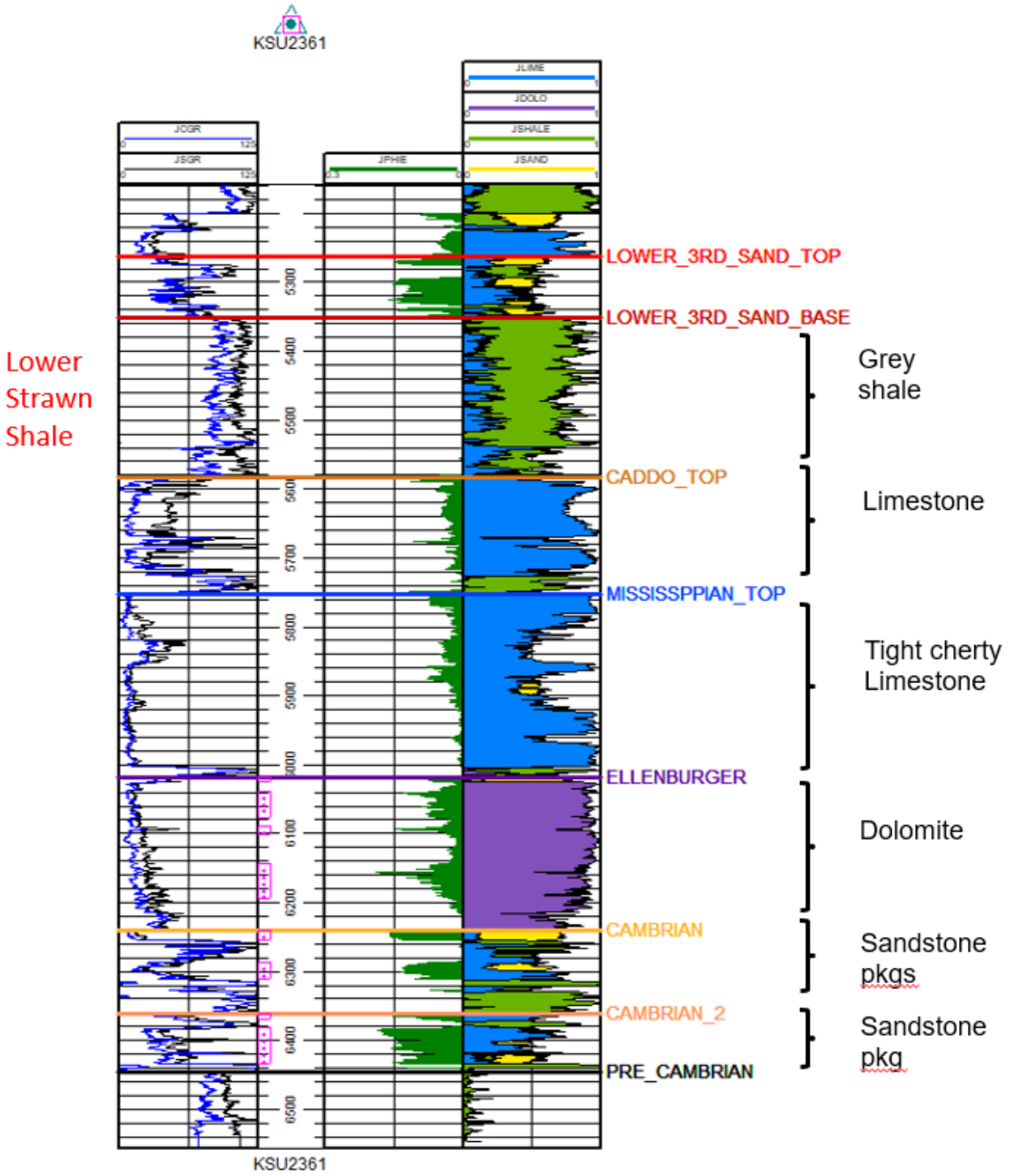


Figure 11 – Type Log of Zones of Interest

### 2.2.2 Upper Confining Zone – Mississippian Lime

The Mississippian Lime is the primary confining unit for the KSU 2361. This formation is the product of a large extensive shallow water carbonate platform that covered much of the southern and western Laurussia (Kane). Figure 12 shows the location of the KSU 2361 well to be found within the Chappel Shelf of the Mississippian Age. Representative cores of the Mississippian Lime formation found on the Chappel Shelf in the Llano uplift area consist of light-colored, fine- to coarse-grained, skeletal packstone (Kane). The open hole log seen in Figure 11 depicts the Mississippian Lime as predominantly cherty limestone. The basal carbonate section has little to no effective porosity development, which should translate to no permeability development. The Mississippian Platform Carbonate play is the smallest oil-producing play in the Permian Basin, which is tied to the abundance of crinoidal, grain-rich facies in platform successions. Most production from Mississippian reservoirs comes from more porous upper Mississippian ooid grainstones (Kane). This indicates that little to no reservoir characteristics are developed within the lower Mississippian Lime, creating an optimal seal.

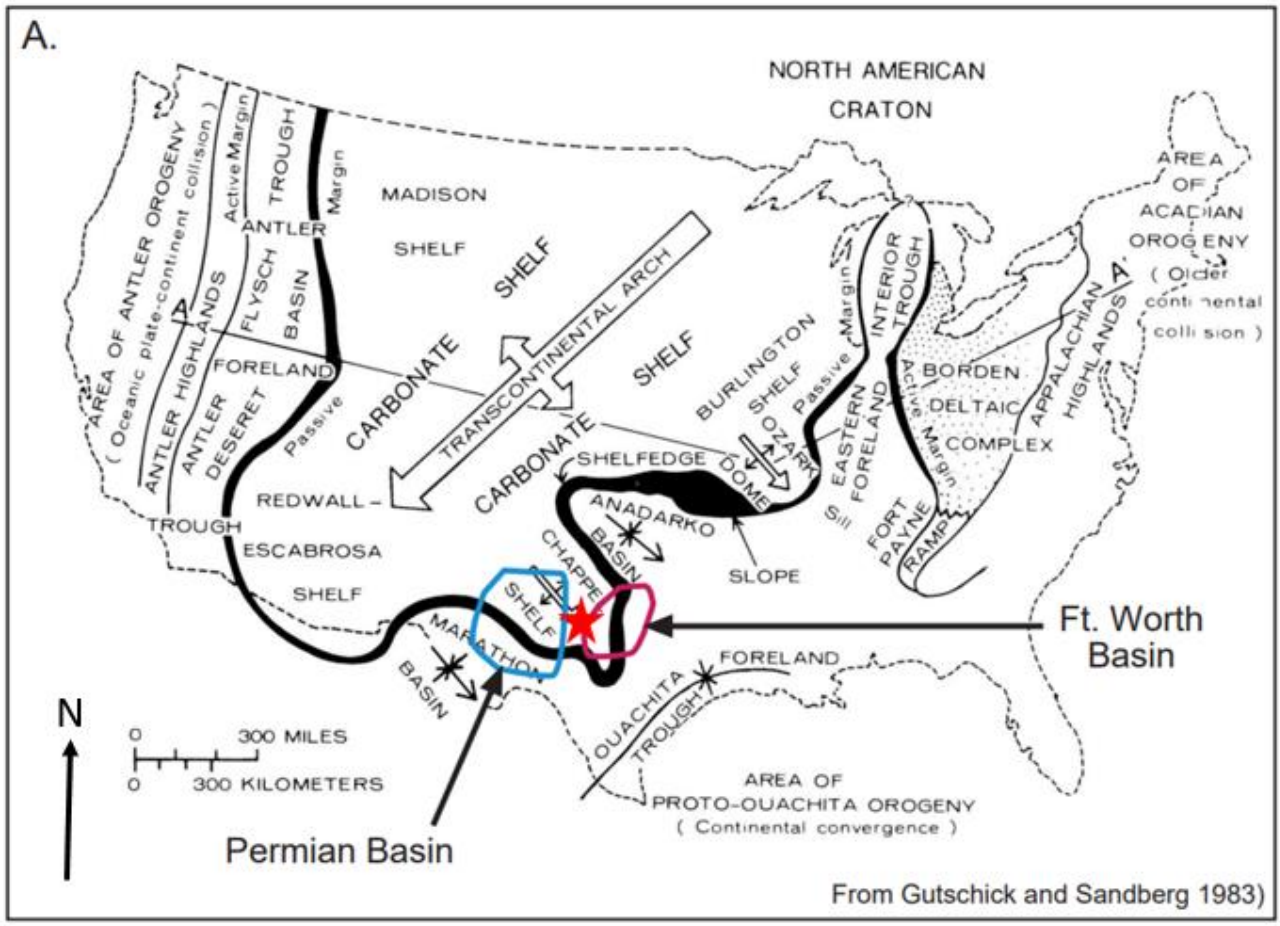


Figure 12 – Depositional Map of the Mississippian (Kane)

### 2.2.3 Secondary Confining Interval – Lower Strawn Shale

The Lower Strawn Shale (LSS) is Desmoinesian in age and was heavily influenced by the Knox Baylor Trough, which is near the KSU 2361 location and is late-Desmoinesian in age. The trough resulted from the Ouachita-Marathon overthrust movement that disrupted the Fort Worth basin depositional center, moving the Desmoinesian depocenter further to the west to form the Knox Baylor Trough. This trough allowed sediments to be transported west to the Midland Basin. These sediments were derived from the destruction of the elongated Bowie Delta System, which derived its sediments from the Muenster-Wichita Mountain system (Gunn, 1982).

Depositional facies within the Strawn unit resemble assemblages typical of a mixed siliciclastic-carbonate continental-to-shelf transitional succession found along a complex embayed coastline. Six petrophysically distinct lithofacies were identified: (1) lenticular to wavy-bedded mudstone, (2) flaser to wavy-bedded sandstone, (3) carbonate-rich sandstone, (4) ripple-to-trough cross-laminated sandstone with common convolute bedding, (5) trough cross-laminated sandstone with abundant mud rip ups and mud balls, and (6) heavily bioturbated sandstone. Combined lithofacies and ichnofacies observations suggest that paleoenvironments of the Katz Field included a bayhead delta, back-barrier estuary embayment, tidal flood delta, tidal flat, and upper to middle shoreface (Jesse G. White, 2014). The LSS is associated with the back-barrier estuary embayment depositional environment, evidenced by the abundance of mudstone.

Figure 13 provides core photos and associated descriptions of a core sample taken in the Katz field within an embayment environment. Core descriptions of this core sample observed characteristics that serve as excellent sealant properties to prohibit the migration of injection fluids above the injection zone. Conventional core data was collected in an offset well near the LSS depths in the API #42-433-33534 well, 5,089’ away from the KSU 2361 well. Figure 14 is a cross-section relating the KSU 2361 well and the API #42-433-33534 well, indicating the cored interval alongside pictures of the lower portion of the core that most closely resembles the LSS. Horizontal permeabilities within the pictured core data range from 0.05 to 0.3 mD, with a vertical permeability value of less than 0.01 mD.

Along with the core reports and descriptions, Figure 14 plots calculated log curves from petrophysical analyses run on open-hole log data from the KSU 2361 well. Figure 14 indicates no effective porosity within the LSS (JPHIE green curve, 2$^{nd}$ track from the left) with a shale lithology reading (JHSHALE, green shading, 3$^{rd}$ track from the left). The petrophysical properties and lithology indicated by core and log data demonstrate that the LSS possesses characteristics of an excellent sealing formation.

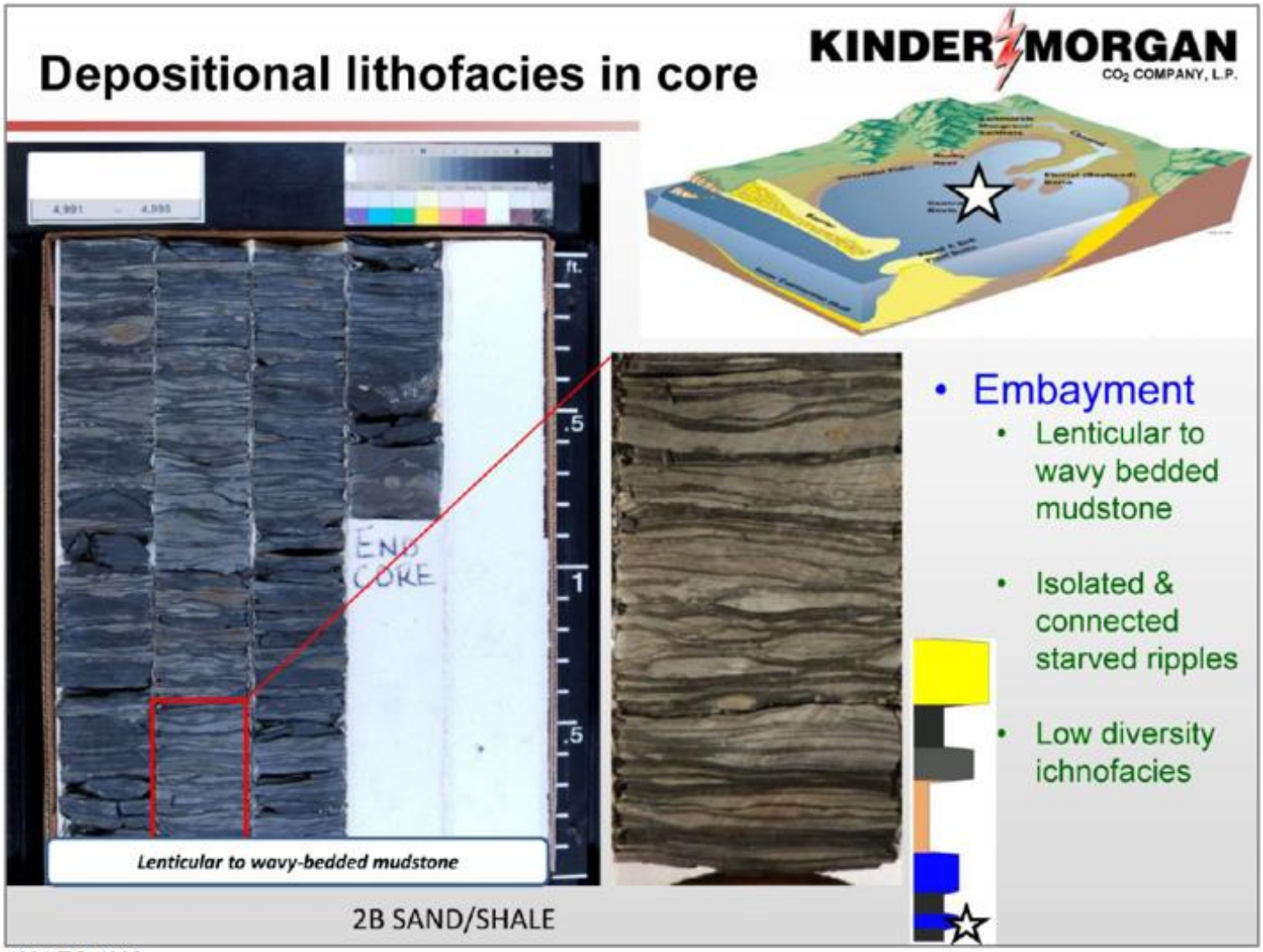


**4991 TO 4998:**

4991.00 – 4997.4: Black to dark gray lenticular to wavy bedded mudstone encasing light gray lenticular siltstone to muddy very-fine sandstone. Abundant light gray calcareous horizons. Note zones of reddish color.

4997.4 – 4997.5: Burrowed transgressive bioclastic lag deposit? Abundant crinoid and bioclastic debris over burrowed laminated to contorted black shale.

4997.5 - 4997.7: Black laminated shale

4997.7 - 4998.0: Dark gray to gray black crinoid mudstone interbedded with a single tan algal mudstone-wackestone hardground exhibiting mudcracks.

Trace fossils shown in blow-ups include *Paleophycus, Planolites, Thalassinoides* and *Teichichnus*.

Sedimentology infers **brackish water deposits** (Brackish water is water that has more salinity than fresh water, but not as much as seawater. It may result from mixing of seawater with fresh water, as in estuaries.

4991 - 4998: Estuary – embayment. Brackish water deposit. Muddy.

Figure 13 – Core Description

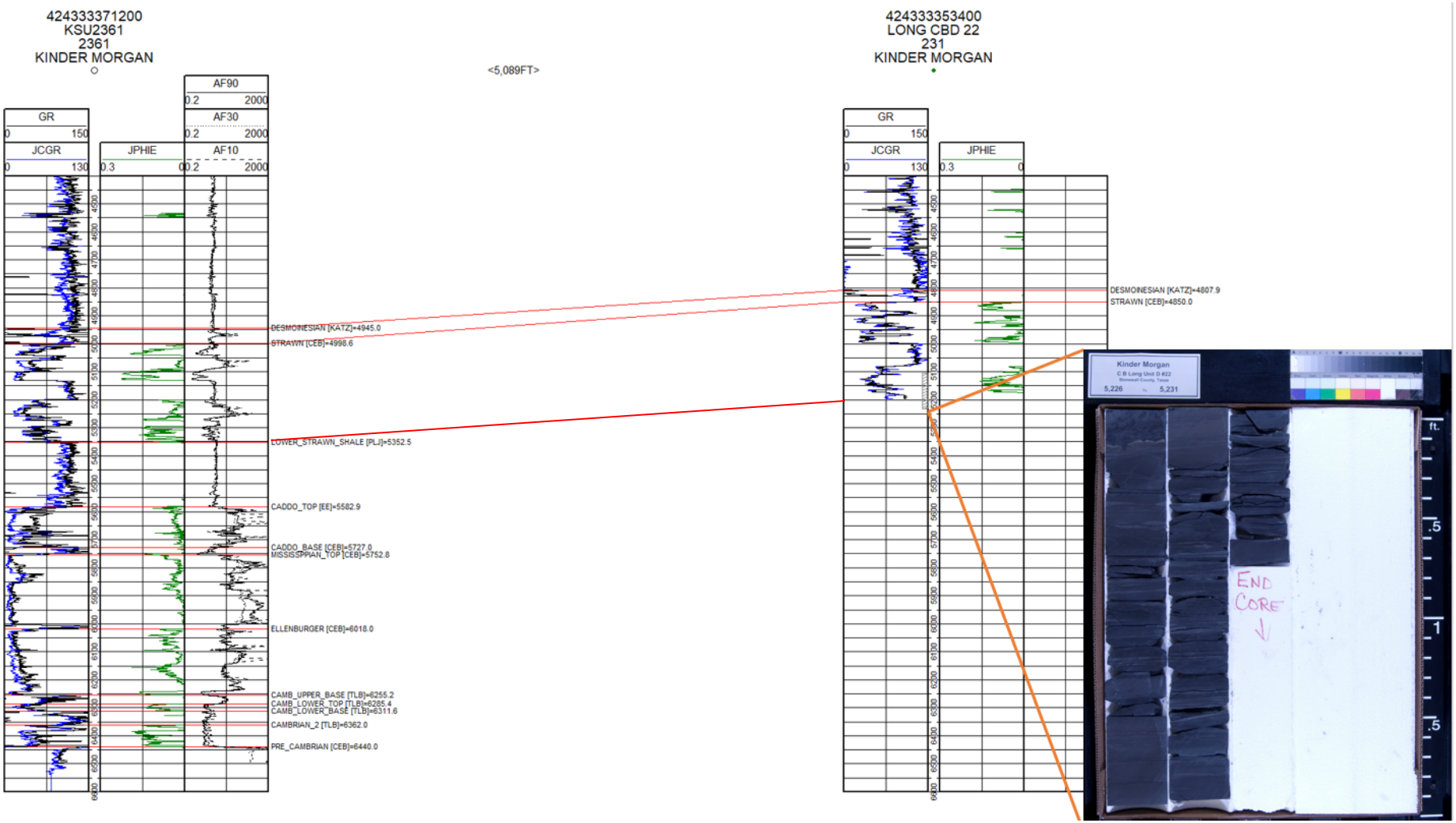


Figure 14 – Cross Section Depicting Correlative Offset Core with Lower Strawn Shale

## 2.2.4 Injection Interval – Ellenburger/Cambrian Sands

### Ellenburger

The Ellenburger is a widespread lower Ordovician carbonate deposited over the entire north Texas area, indicating a relatively uniform depositional condition (Hendricks, 1964). North Central Texas experienced a low-energy, restricted shelf environment comprised of a homogeneous sequence of gray to dark-gray, fine to medium crystalline dolomite containing irregular mottling (probable bioturbation structures) and lesser parallel-laminated mudstone and peloid-wackestone (Kerans, 1990). Figure 15 is a map depicting the different depositional environments of the lower Ordovician, with associated lithologies. This map confirms the inferred dolomite lithology of the open hole log analysis in Figure 11 of the KSU 2361 well.

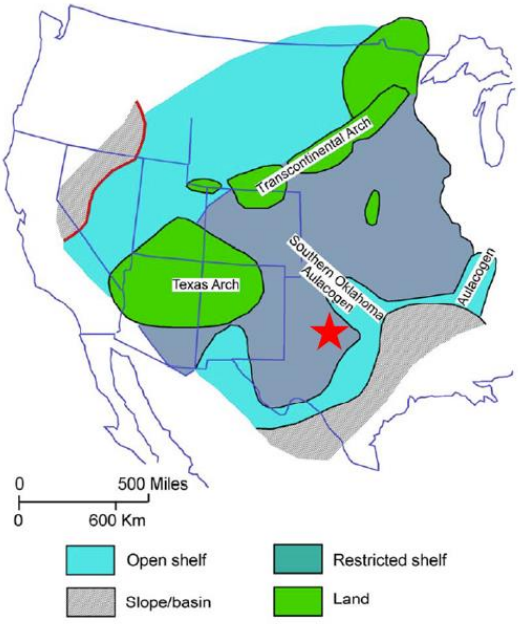


Figure 3. Interpreted regional depositional setting during Early Ordovician time. After Ross (1976) and Kerans (1990).

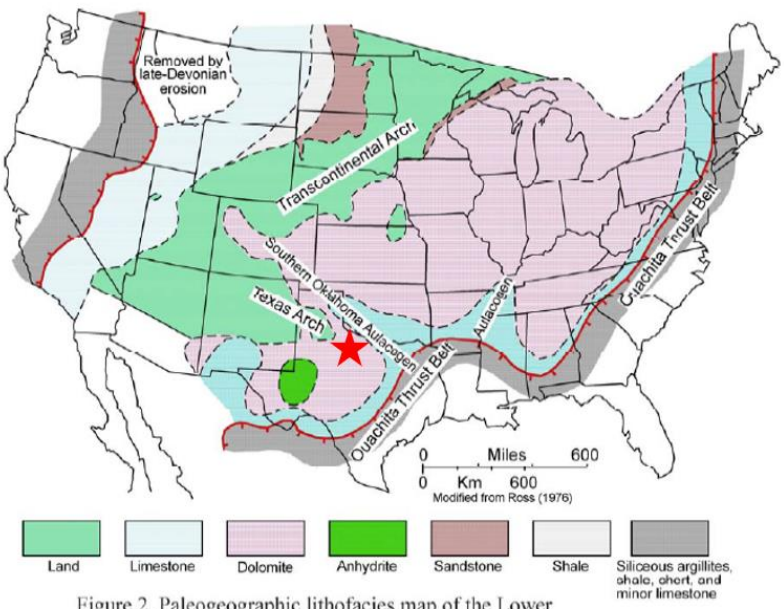


Figure 2. Paleogeographic lithofacies map of the Lower Ordovician section in the United States. From Ross (1976).

Figure 15 – Depositional Environments of the Lower Ordovician and Associated Lithofacies (Loucks, 2003)

### Ellenburger Porosity/Permeability Development

Within the low-energy, restricted shelf environment, facies are highly dolomitized and have a heavy presence of bioturbation resulting in mottling (Loucks, 2003). The dolomitization led to porosity development within the Ellenburger, along with diagenetic leaching processes and other secondary porosity features such as karsts and vugs. The tables in Figure 16 show permeability and porosity values tabulated from Ellenburger reservoirs within Texas, categorized by their diagenetic facies into three groups: Karst Modified, Ramp Carbonates, and Tectonically Fractured Dolostones. Based on the descriptions in Figure 16, the Ellenburger of the KSU 2361 would fall within the Karst Modified Reservoirs category outlined in red with average porosity and permeability values of 3% and 32 mD, respectively. This corresponds with the data collected from the KSU 2361 well. As shown in Figure

11 above, the calculated effective porosity curve in green (JPHIE) is an average of roughly 3% over the Ellenburger formation. Permeability was estimated from volumes injected plotted against pressure responses within the KSU 2361 well; these permeabilities ranged from 12-20 mD. Similarities between these two datasets validate reservoir characteristics used for model inputs.

**Cambrian**

The deposition of Cambrian and lower Ordovician strata on the early Paleozoic shelf was initiated by a transgressing sea which, entering the area from the south, first laid down a clastic sequence. Initial deposits were sandstone and arenaceous carbonates that grade upward into the slightly cherty carbonates of the Ellenburger group (Galley, 1958). Lithologies include glauconitic and phosphatic to clean sandstones of various textures, intergrading and alternating with chemical, clastic, and even local limestones and dolomites, together with intercalated thin shales (Conselman, 1954).

**Cambrian Porosity/Permeability Development**

Few reservoir characteristics have been published on the Cambrian sands. Porosity and permeability were estimated based on the KSU 2361 wells open hole log and injection data. There are three discreet sandstone intervals within the Cambrian at this location. The upper two sands identified in the CAMBRIAN package have an average effective porosity of 12.9% and 8.8%. The average effective porosity of the third sand is 8.4%. These effective porosity values are plotted as the JPHIE (effective porosity) curve in Figure 11. Due to nature of the Ellenburger and Cambrian zones being commingled during injection tests, modeling makes the assumption of 12-20mD average permeability for the interval, for history matched injection volumes and pressures.

Table 2. Geologic characteristics of the three Ellenburger reservoir groups. From Holtz and Kerans (1992).

| | Karst Modified | Ramp Carbonate | Tectonically Fractured Dolostone |
|---|---|---|---|
| **Lithology** | Dolostone | Dolostone | Dolostone |
| **Depositional setting** | Inner ramp | Mid- to outer ramp | Inner ramp |
| **Karst facies** | Extensive sub-Middle Ordovician | Sub-Middle Ordovician, sub-Silurian/Devonian, sub-Mississippian, sub-Permian/ Pennsylvanian | Variable intra-Ellenburger, sub-Middle Ordovician |
| **Fault-related fracturing** | Subsidiary | Subsidiary | Locally extensive |
| **Dominant pore type** | Karst-related fractures and interbreccia | Intercrystalline in dolomite | Fault-related fractures |
| **Dolomitization** | Pervasive | Partial, stratigraphic and fracture-controlled | Pervasive |

| Parameter | Karst Modified | Ramp Carbonate | Tectonically Fractured Dolostone |
|---|---|---|---|
| **Net pay (ft)** | Avg. = 181, Range = 20 - 410 | Avg. = 43 Range = 4 - 223 | Avg. = 293, Range = 7 - 790 |
| **Porosity (%)** | Avg. = 3 Range = 1.6 - 7 | Avg. = 14 Range = 2 - 14 | Avg. = 4 Range = 1 - 8 |
| **Permeability (md)** | Avg. = 32 Range = 2 - 750 | Avg. = 12 Range = 0.8 - 44 | Avg. = 4 Range = 1 - 100 |
| **Initial water saturation (%)** | Avg. = 21 Range = 4 - 54 | Avg. = 32 Range = 20 - 60 | Avg. = 22, Range = 10 - 35 |
| **Residual oil saturation (%)** | Avg. = 31 Range = 20 - 44 | Avg. = 36 Range = 25 - 62 | NA |

Figure 16 – Geologic and Petrophysical Parameters of the Ellenburger (Loucks, 2003)

**Formation Fluid**

Four wells were identified within approximately 20 miles of the KSU 2361 well through a review of oil-field brine compositions of the Ellenburger formation from the U.S. Geological Survey National Produced Waters Geochemical Database v2.3. None of these four wells are salt water disposal wells. The location of these wells is shown in Figure 17. Results from the synthesis of this data are provided in Table 3. The fluids have higher than 20,000 parts per million (ppm) total dissolved solids. Therefore, these aquifers are considered saline. These analyses indicate that the in situ reservoir fluid of the Ellenburger Formation is compatible with the proposed injection fluids.

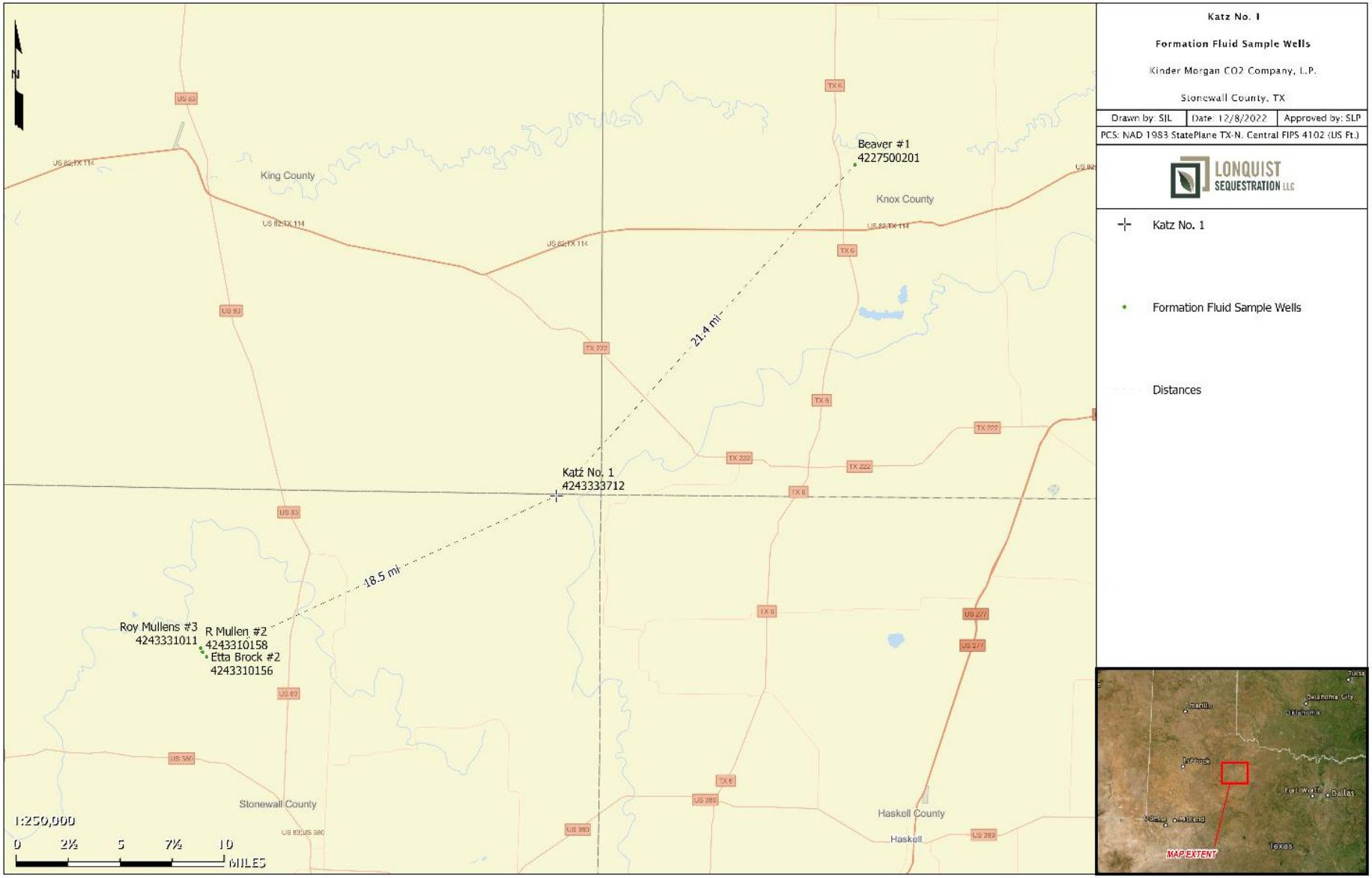


Figure 17 – Offset Wells used for Formation Fluid Characterization.

Table 3 – Analysis of Ordovician-age formation fluids from nearby oil-field brine samples

| | Average | Low | High |
|---|---|---|---|
| Total Dissolved Solids (ppm) | 144065 | 98802 | 210131 |
| pH | 6.15 | 5 | 7 |
| Sodium (ppm) | 43391 | 30833 | 64222 |
| Calcium (ppm) | 9275 | 5128 | 13200 |
| Chlorides (ppm) | 88355 | 60061 | 128685 |

### 2.2.5 Lower Confining Zone – Precambrian

The Precambrian outcrops to the south at the Llano uplift and the west in the Trans-Pecos regions of Texas and central New Mexico. Outcrops near the Llano Uplift in McCulloch County consist of highly weathered granite, schist, and gneiss. The granite is fine- to coarse-grained and contains numerous pegmatite veins. The schist has a high percentage of biotite, which gives it a dark-gray color, and it is often referred to as "gray shale" or "blue mud" by well drillers. The gneiss is pinkish and fine-grained (Mason, 1961). A study in 1996 was performed by Adams and Keller to better understand the Precambrian distribution in Texas indicates that Precambrian at the Katz 2361 location should contain an average metamorphic rock, as seen in Figure 18. This agrees with the open hole log response in the Precambrian formation in the open hole log section of Katz 2361. Gamma-ray log values of the Precambrian section are consistently above 90 GAPI (Gamma Units of the American Petroleum Institute), indicating a high radioactive response. A very high resistivity reading within this section indicates little to no porosity, as shown in the JPHIE, validating the characteristics described above. These traits are ideal attributes of a tight, lower confining basement.

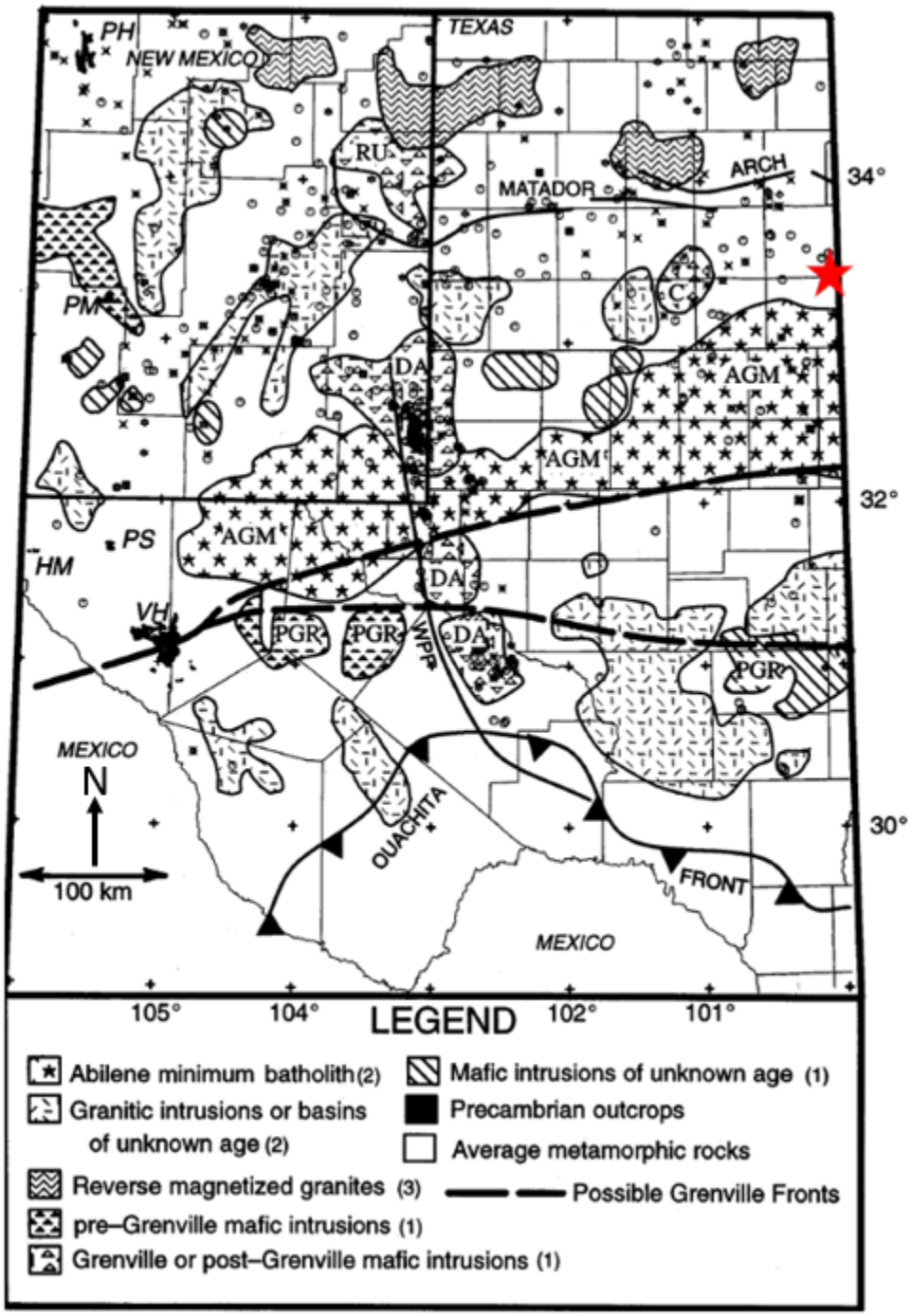


Figure 18 – Pre-Cambrian Distribution Map (Adams and Keller, 1996)

## 2.3 Fracture Pressure Gradient

Fracture pressure gradients were estimated using Eaton's equation. Eaton's equation is commonly accepted as the standard practice for determining fracture gradients. Poisson's ratio ($\nu$), overburden gradient (OBG), and pore gradient (PG) are all variables that can be changed to match the site-specific injection zone. The expected fracture gradient was determined using industry standards and a literature review. The overburden gradient was assumed to be 1.05 psi/ft. This value is considered best practice when there are no site-specific numbers available. The pore pressure gradient was calculated to be 0.43 psi/ft from the bottom hole pressure data. For limestone/dolomite rock in the injection zone, the Poisson's ratio was assumed to be 0.3 through literature review (Molina, Vilarras, Zeidouni 2016). Using these values in the equation below, a fracture gradient of 0.70 psi/ft was calculated for the injection zone.

For the upper confining interval, a similar fracture gradient was calculated. The upper confining shale has an increased chance to vertically fracture if the injection interval below is fractured (Molina, Vilarras, Zeidouni 2016). Therefore, a Poisson's ratio equal to that of the injection interval was used as a conservative estimate. The lower confining zone was assumed to be of a similar matrix to the injection interval, with the key difference being that the formation is much tighter (lower porosity/permeability). Therefore, the Poisson's ratio was assumed to be slightly higher in this rock. As seen in Table 4, the fracture gradient of .64 psi/ft is slightly higher in the lower confining zone.

Multiple approaches can be taken to manage reservoir pressure. Current engineering practices for acid gas $CO_2$ injection recommend applying a 10% safety factor to the fracture pressure of the geology being injected into, resulting a 0.63 psi/ft gradient. This new value represents the maximum allowable bottom-hole pressure during injection. Another approach is to maintain a maximum wellhead pressure (WHP). In the reservoir model, a WHP of 1,850 psi was used to constrain the simulated well. This translates to a value that is 84% of the frac gradient or a 16% safety factor. By using either approach, there is a reduced risk of fracture propagation in the injection zone.

A conservative maximum pressure constraint of 0.60 psi/ft was used for injection modeling, which is well below the calculated fracture gradient for each zone. This was done to ensure that the injection pressure would never exceed the fracture pressure of the injection zone.

Table 4 – Fracture Gradient Assumptions

| | Injection Interval | Upper Confining | Lower Confining |
|---|---|---|---|
| Overburden Gradient (psi/ft) | 1.05 | 1.05 | 1.05 |
| Pore Gradient (psi/ft) | 0.43 | 0.43 | 0.43 |
| Poisson's Ratio | 0.30 | 0.30 | 0.31 |
| Fracture Gradient (psi/ft) | 0.70 | 0.70 | 0.71 |
| **FG + 10% Safety Factor (psi/ft)** | **0.63** | **0.63** | **0.64** |

The following calculations were used to obtain fracture gradient estimates:

$$FG = \frac{\mathrm{n}}{1-\mathrm{n}}(OBG - PG) + PG$$

$$FG = \frac{0.3}{1-0.3}(1.05 - 0.43) + 0.43 = 0.70$$

$$FG\ with\ SF = 0.70 \times (1 - 0.1) = \mathbf{0.63}$$ **(Injection and Upper Confining intervals)**

$$FG\ with\ SF = 0.71 \times (1 - 0.1) = \mathbf{.64}$$ **(Lower Confining interval)**

## 2.4 Local Structure

Regional structure in the area of the KSU 2361 well is influenced by a shallow angle ramp down dip to the southwest towards the Midland Basin, which is set up by a north-south regional fault to the east. Specifically, the KSU 2361 well is located on the western portion of a shelf-like feature that dips slightly away from the fault to the east. Figure 19 is a structure map on the top of the Ellenburger with the KSU 2361 well indicated by the black star.

Subsurface interpretations of the Ellenburger formation heavily relied on 3D seismic coverage in the area. The seismic coverage outline is represented by the purple boundary seen in Figure 19. Only two wells penetrated the Ellenburger formation within the 3D seismic data volume and are shown in the northwest to southeast seismic profile along with the cross-section in Figure 22. These two wells are active injection wells within the proposed injection interval operated by Kinder Morgan, one being the Katz 2361 well while the other is the Katz #3741 well. Both wells were used to create time-to-depth conversions for the Ellenburger horizon. Shallower formations provide additional well control to assist in creating time-to-depth conversions displayed in the seismic profiles in Figures 21 and 22.

The KSU 2361 well is located roughly 12,000’ west of the mapped fault seen in Figure 19. This distance provides a buffer between the injection plume and the fault that alleviates concerns regarding the interaction between the injectate and the fault. As shown in the seismic profile, this fault does not project above the Caddo formation and is not present in the LSS. As this fault does not project into the upper confining shale layer, there is little risk of the fault acting as a conduit for the injectate to leak outside the proposed injection interval.

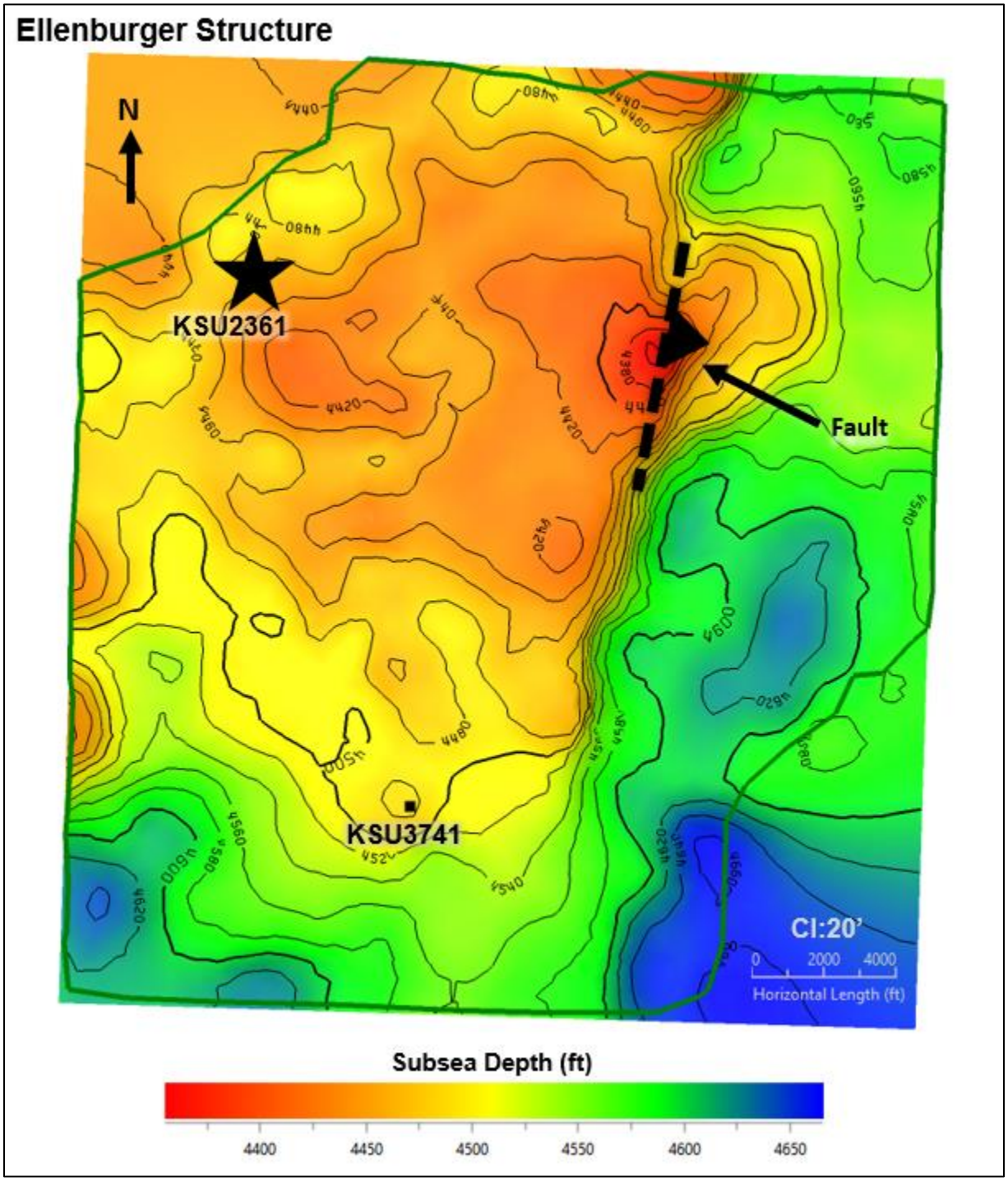


Figure 19 – Ellenburger Structure Map (Subsea Depths). Contour Interval (CI) on Ellenburger Structure map is 20'. The green outline is the boundary of the seismic data.

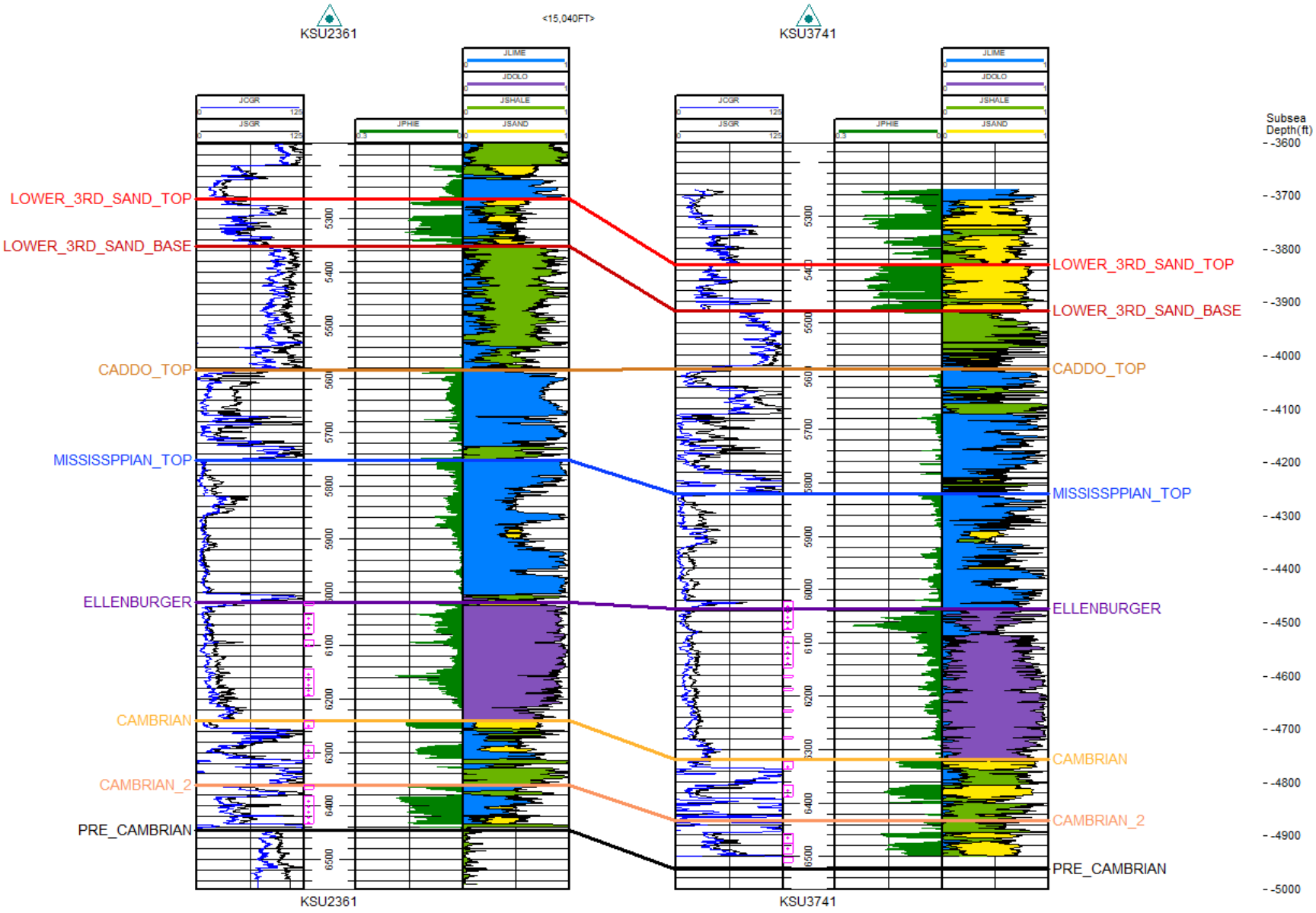


Figure 20 – Structural Northwest-Southeast Cross Section

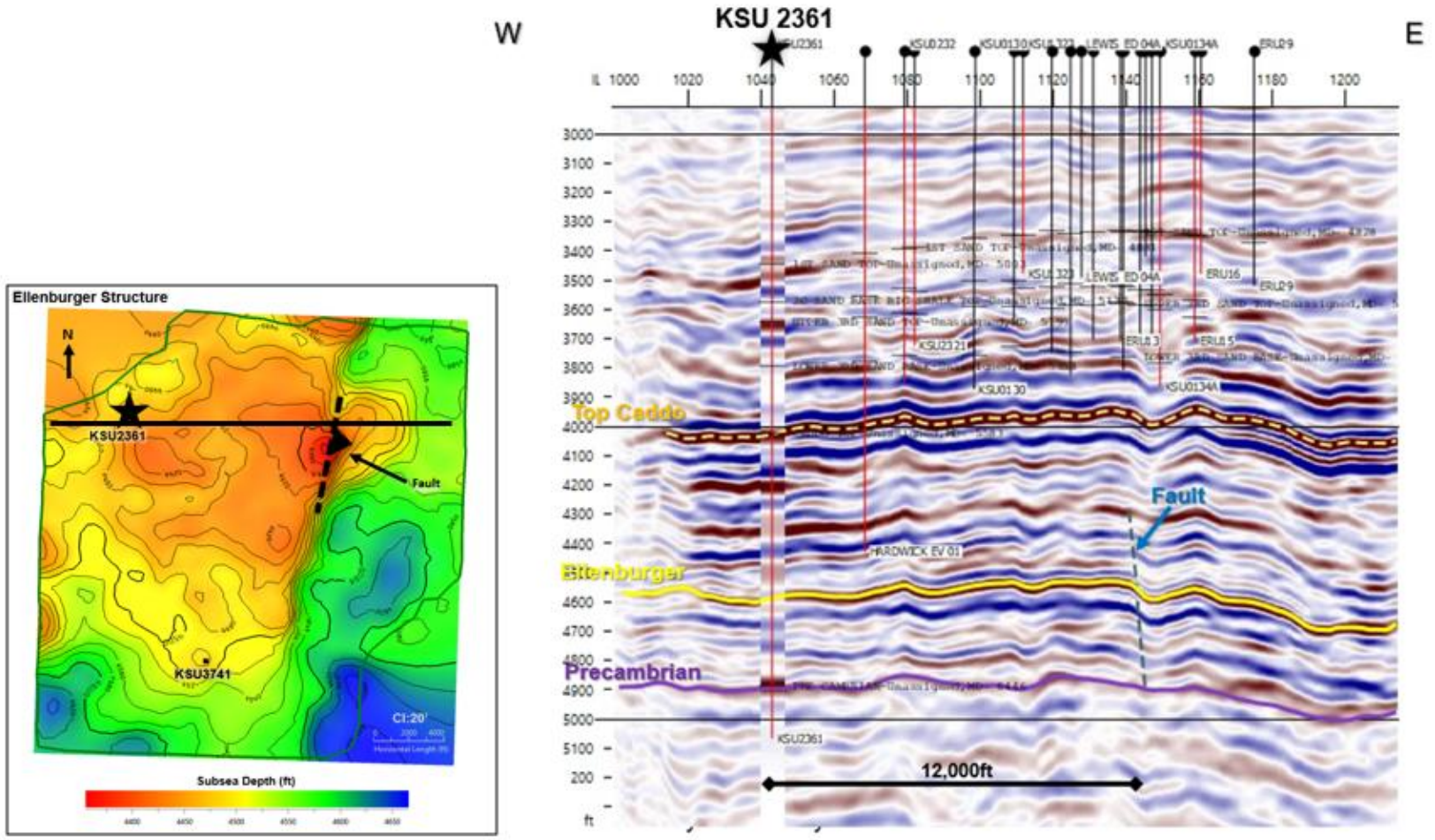


Figure 21 – Structural West to East Seismic Profile. Ellenburger structure map modified from Figure 19.

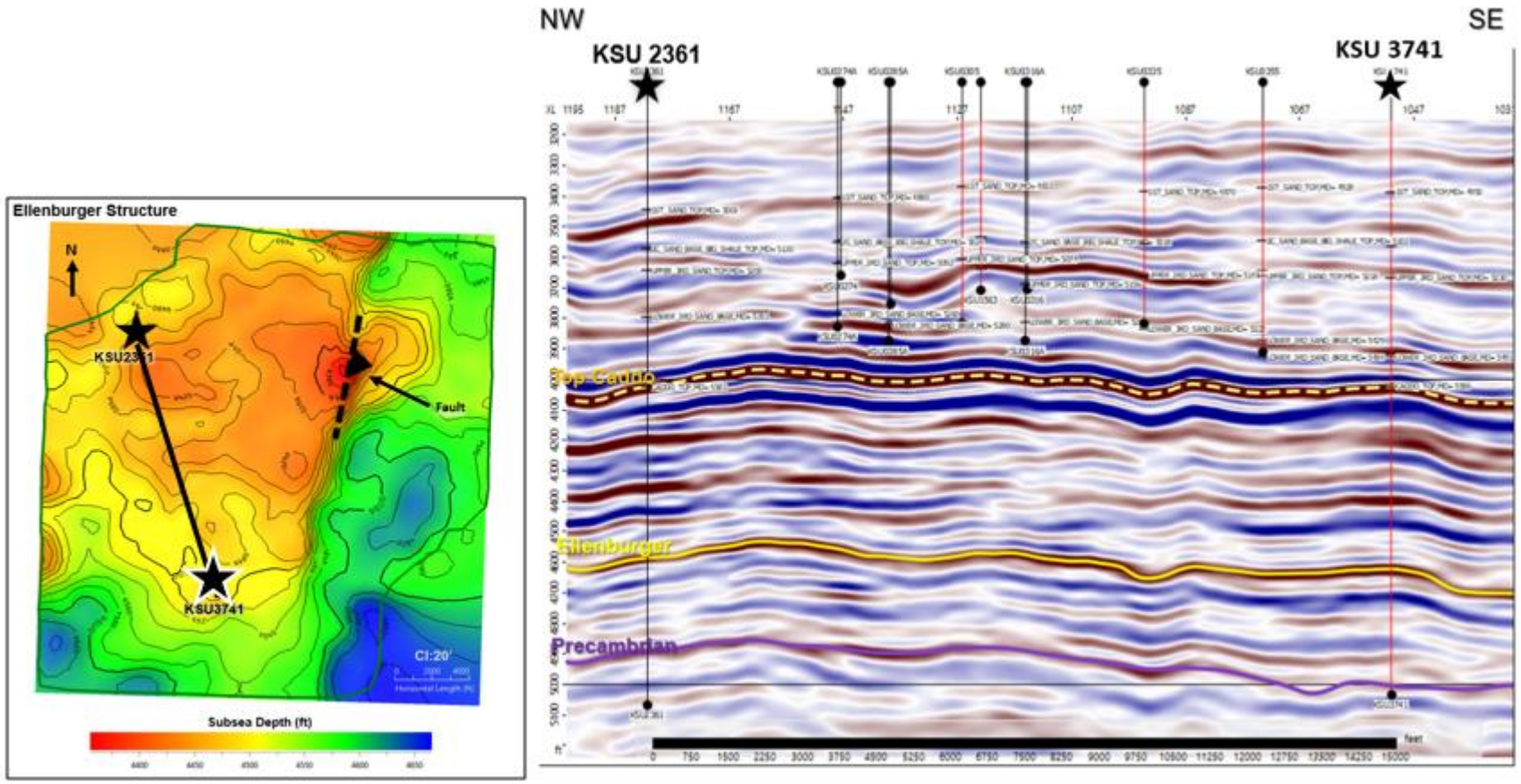


Figure 22 – Structural Northwest to Southeast Seismic Profile between the two wells that penetrate the Ellenburger within the seismic volume. Ellenburger structure map modified from Figure 19.

## 2.5 Injection and Confinement Summary

The lithologic and petrophysical characteristics of the Ellenburger and Cambrian sand formations at the KSU 2361 well location indicate that the formations have sufficient thickness, porosity, permeability, and lateral continuity to accept the proposed injection fluids. The Mississippian Lime formation at the KSU 2361 well has low permeability. It is of sufficient thickness and lateral continuity to serve as the upper confining zone, with the Lower Strawn Shale acting as a secondary confining unit. Beneath the injection interval, the low permeability, low porosity Precambrian formation is unsuitable for fluid migration and serves as the lower confining zone.

The area of review has been studied to identify potential subsurface features that may affect the ability of these injection and confinement units to retain the injectate within the requested injection interval. Faults have been identified, characterized, and determined to be low risk to the containment of injectate and do not increase the risk of migration of fluids above the injection interval.

## 2.6 Groundwater Hydrology

Stonewall, Haskell, Knox, and King Counties fall within the boundary of the Texas Water Development Board's (TWDB) Groundwater Management Area 6. The Seymour Aquifer is identified by the TWDB's *Aquifers of Texas* report in the vicinity of the KSU 2361 well (George et al., 2011). Table 5 references the Seymour Aquifer's position in geologic time and the associated geologic formations, which include the Seymour Formation, Lingos Formation, and Quaternary alluvium (Ewing et al., 2004). A depiction of the general stratigraphy of the Seymour Aquifer is shown in Figure 23.

Table 5 – Geologic and Hydrogeologic Units near Stonewall, Haskell, Knox, and King Counties, Texas (Ewing et al., 2004).

| System | Series | Group | Formation |
|---|---|---|---|
| Quaternary | Recent to Pleistocene | | Alluvium |
| | | | Seymour |
| Tertiary | missing | | |
| Cretaceous | | | |
| Jurassic | | | |
| Triassic | | | |
| Permian | Ochoa | | Quartermaster |
| | Guadalupe | Whitehorse | |
| | | Pease River | Dog Creek Shale |
| | | | Blaine Gypsum |
| | | | Flowerpot Shale |
| | | | San Angelo |
| | Leonard | Clear Fork | Choza |
| | | | Vale |
| | | | Arroyo |
| | | Wichita (upper portion only) | Lueders |
| | | | Clyde |

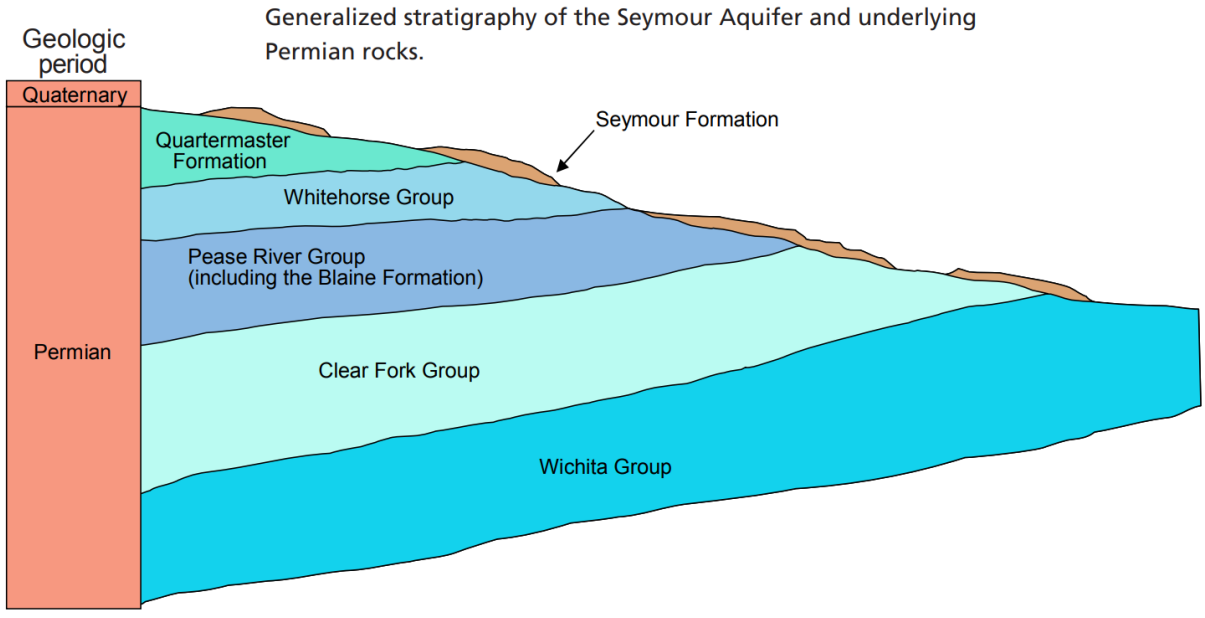


Figure 23 – Generalized Stratigraphy of the Seymour Aquifer (George et al., 2011)

The Seymour Aquifer, as defined by the TWDB, consists of isolated pods of alluvium deposits of Quaternary age, depicted in Figure 24. It extends from the southern Brazos River watershed northward to the border of Oklahoma. The Seymour Aquifer overlies Permian-age deposits that generally dip to the west. Topography, structure, and permeability variation control groundwater flow within the pods. The aquifer generally follows the topographical gradient along the major axis of the pod and discharges laterally to springs, seeps, and alluvium. Similar mechanisms can be expected within the majority of the other pods (Ewing et al., 2004).

A map showing the inferred groundwater flow pattern within a portion of one of the pods in Haskell and Knox counties is shown in Figure 25. The map approximates the natural direction of flow unaffected by pumping from wells. North of the Rule, TX, groundwater divide, the flow is toward the north, northwest, or northeast. Based on the contours of the water table and the permeabilities for the formation indicated by pumping tests, the estimated natural rate of water movement in the Seymour Aquifer, unaffected by pumping, ranges locally from approximately 200’ to 5,000’ per year. Over several miles, the estimated average rate of movement is typically between 800’ and 1,200’ per year (R.W. Harden and Associates, 1978).

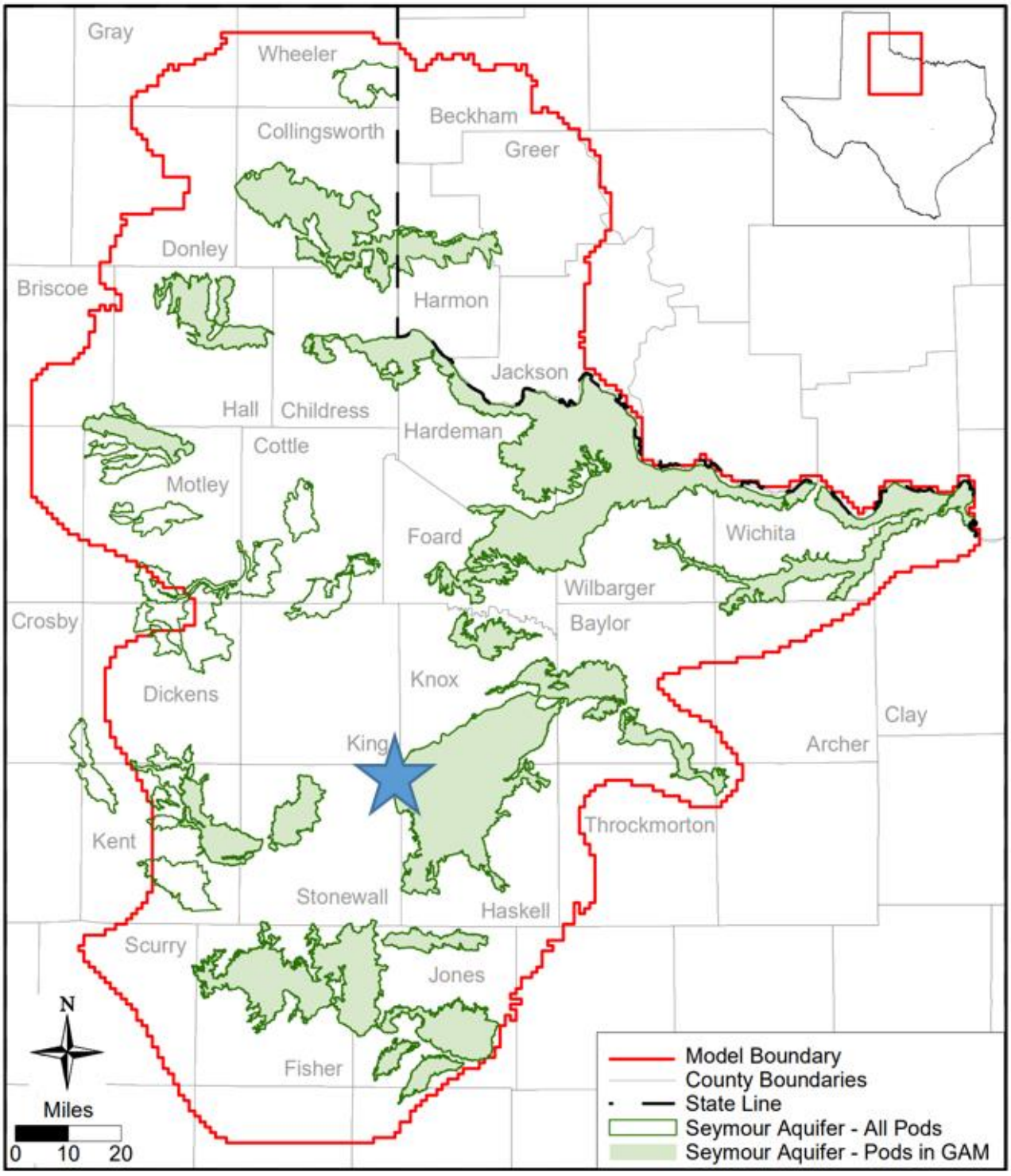


Figure 24 – Regional Extent of the Seymour Aquifer Pods (Ewing et al., 2004)


Figure 25 – Direction of Groundwater Flow in a Portion of one Pod of the Seymour Aquifer (R.W. Harden and Associates, 1978).

Total dissolved solids (TDS) are a measure of water saltiness, the sum of concentrations of all dissolved ions (such as sodium, calcium, magnesium, potassium, chloride, sulfate, and carbonates) plus silica. As shown in Figure 26, the total dissolved solids in 41% of the wells within the Seymour Aquifer exceed 1,000 milligrams per liter (mg/L), Texas' secondary maximum contaminant level (MCL). Therefore, the utility of water from the Seymour Aquifer as a drinking water supply is limited in many areas for health reasons, primarily due to elevated nitrate concentrations, and for taste reasons due to saltiness (Ewing et al., 2004).

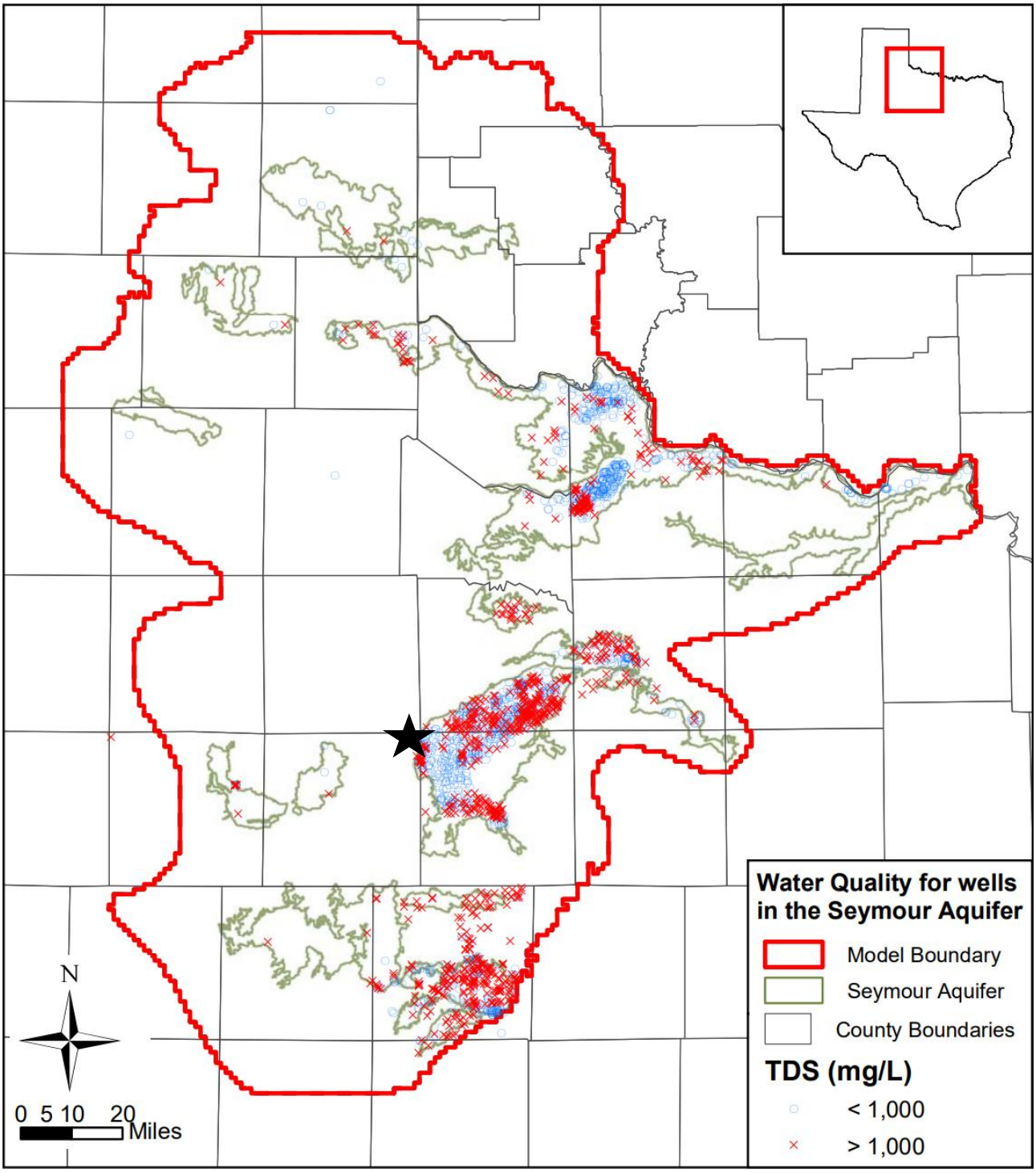


Figure 26 – Total Dissolved Solids (TDS) in Groundwater from the Seymour Aquifer (Ewing et al., 2004)

The TRRC's Groundwater Advisory Unit (GAU) specified for the KSU 2361 well that the interval from the land surface to a depth of 100' must specifically protect usable-quality groundwater. Therefore, the base of Underground Sources of Drinking Water (USDW) can be approximated at 100' at the location of the KSU 2361 well, and there is approximately 5,920' separating the base of the USDW and the injection interval. A copy of the GAU's Groundwater Protection Determination letter issued

by the TRRC as part of the Class II permitting process for the KSU 2361 well is provided in Appendix A. Though unlikely for reasons outlined in the confinement and potential leaks sections, if migration of injected fluid did occur above the Mississippian limestone, thousands of feet of tight limestone and shale beds occur between the injection interval and the lowest water-bearing aquifer.

## 2.6.1 Reservoir Characterization Modeling

### Introduction

KSU 2361 is located in Kinder Morgan's Katz Oil Field in northeast Stonewall County. A geologic model was constructed of this area to forecast the movement of $CO_2$ and any pressure increases. The model is comprised of the Ellenburger and Cambrian formations, which cover 13,774 acres (~22 square miles). A single $CO_2$ injector was simulated for 100 years, where approximately 25 million metric tons (MMT) of $CO_2$ was safely stored.

### Software

Paradigm's software suite was used to build the geologic and dynamic models. SKUA-GOCAD™ was utilized in building the geomodel, while Tempest™ designed the dynamic model. The EPA recognizes these software packages for an area of review delineation modeling as listed in the Class VI Well Area of Review Evaluation and Corrective Action Guidance document.

SKUA-GOCAD™ is a software tool for geology that offers a range of features for structure and stratigraphy, structural analysis, fault seal, well correlation, facies interpretation, 2D/3D restoration, and basin modeling. The structure and stratigraphy module allows users to construct fully sealed structural models, while the structural analysis module provides tools for analyzing fracture probability, stress, and strain. The fault seal module enables the computation of fault displacement maps and fault SGR properties, and the well correlation module allows users to create well sections and digitize markers. The facies interpretation module offers tools for paleo-facies interpretation, and the 2D/3D restoration module provides tools for restoring 3D basin and reservoir models. Finally, the basin modeling module enables users to construct 4D basin models for transfer to basin model simulation software.

Tempest™ is another of Paradigm's industry-leading software packages for reservoir engineering. Tempest™ has history-matching capabilities, allowing for more accurate reservoir characterization modeling. In addition, this software is used to build dynamic models for $CO_2$ injection. Tempest™ is comprised of three modules: Tempest™ VIEW, Tempest™ ENABLE and Tempest™ MORE. Tempest™ MORE is a black oil simulator with many features and applications to simulate $CO_2$ injection. The Tempest™ MORE module can accept data in standard GRDECL (RMS, Petrel) file formats. It can also produce output in the ECLIPSE, Nexus/VIP, Intersect, and IMEX/GEM/STARS formats. This allows users to easily import data into the software and export it in a format compatible with other tools and systems. The standard file formats improve the interoperability and compatibility of the MORE software with other systems and tools used in the oil and gas industry

**Trapping Mechanisms**

To accurately simulate the $CO_2$ injection and predict the subsequent plume migration, Tempest™ models $CO_2$ trapping mechanisms in the injection zone. There are five primary trapping mechanisms: structural, hydrodynamic, residual gas (hysteresis), solubility, and geochemical. For this simulation, geochemical reactions were not considered. Each of the five mechanisms is described in further detail below.

*Structural Trapping*

Structural traps, a physical trapping mechanism, are underground rock formations that trap and store the injected supercritical $CO_2$. These traps are created by the physical properties of the cap rock, such as its porosity and permeability. For example, a structural trap may be formed by a layer of porous rock above a layer of non-porous rock, with the $CO_2$ being trapped in the porous rock. Some other examples of structural traps are faults or pinch-outs. Faults can limit the horizontal migration of the plume in the injected formation. The injected $CO_2$ is lighter than the connate brine found already in the formation. Because of this, the $CO_2$ floats to the top of the formation and is stored underneath the impermeable cap rock. In this model, $CO_2$ mass density ranges between 34.9 to 38.5 $lb/ft^3$ from the shallow to deep injection intervals, whereas the formation brine density is approximately 63.3 $lb/ft^3$.

*Hydrodynamic Trapping*

Hydrodynamic traps are another form of physical trapping caused by the interaction between $CO_2$ and the formation brine. Hydrodynamic trapping is caused by supercritical $CO_2$ traveling vertically upwards until it reaches the impermeable cap rock and spreads laterally through the unconfined sand layers, driven by the buoyancy and higher density of the brine in the reservoir. Once the $CO_2$ reaches a caprock with a capillary entry pressure greater than the buoyancy, it is effectively trapped. This type of trapping works best in laterally unconfined sedimentary basins with little to no structural traps.

Equation-of-state (EOS) calculations are performed to determine the phase of $CO_2$ at any given location based on pressure and temperature for structural and hydrodynamic trapping mechanisms. Several well-known EOS formulae are used within the oil and gas industry for reservoir modeling. These formulae include the Van der Waals equation, the Peng-Robinson method, and the Soave-Redlich-Kwong (SRK) method. The Peng-Robinson is better suited for gas systems than the SRK method. The EOS implemented within the KSU 2361 well model was the Peng-Robinson method.

*Residual Gas Trapping*

Residual gas traps are also a physical form of trapping $CO_2$ within pore space by surface tension. This occurs when the porous rock acts as a sponge and traps the $CO_2$ as the displaced fluid is forced out of the pore space by the injected $CO_2$. As the displaced brine reenters the pore space once injection stops, small droplets of $CO_2$ remain in the pore space as residuals and become immobile.

*Solubility Trapping*

Solubility traps are a form of chemical trapping between the injected $CO_2$ and connate formation brine. Solubility trapping occurs when the $CO_2$ is dissolved in a liquid, such as the formation brine.

$CO_2$ is highly soluble in brine, with the resulting solution having a higher density than the connate brine. This feature affects the reservoir by causing the higher-density brine to sink within the formation, trapping the $CO_2$-entrained brine. This dissolution allows for an increased storage capacity and decreased fluid migration. Table 6 was designed to guide the model to determine the solubility of $CO_2$ at various pressures and a specified salinity.

Table 6 – $CO_2$ Solubility Table

| Pressure (psi) | CO2 Solubility (Mscf/Stb) | Salinity (ppm) |
|---|---|---|
| 14 | 0.00 | 66,000 |
| 50 | 0.00 | 66,000 |
| 150 | 0.01 | 66,000 |
| 500 | 0.0198 | 66,000 |
| 1000 | 0.0297 | 66,000 |
| 1500 | 0.0388 | 66,000 |
| 3000 | 0.0660 | 66,000 |

*Geochemical Trapping*

Geochemical trapping is another form of chemical trapping which refers to storing $CO_2$ in underground rock formations by using chemical reactions to transform the $CO_2$ into stable, solid minerals. This process is known as mineral carbonation, and it involves the reaction of $CO_2$ with the minerals and rocks in underground formations to form stable carbonates. During the process of injecting $CO_2$ into a disposal reservoir, four (4) primary chemical compounds may be present: $CO_2$ in the supercritical phase, the hydrochemistry of the naturally occurring brine in the reservoir, aqueous $CO_2$ (an ionic bond between $CO_2$ gas and the brine), and the geochemistry of the formation rock. These compounds can interact, leading to the precipitation of $CO_2$ as a new mineral, often calcium carbonate (limestone). This process is known as mineral carbonation, a key mechanism for the long-term storage of $CO_2$ in underground rock formations.

Mineral trapping can also occur through the adsorption of $CO_2$ onto clay minerals. When modeling this process, it is important to consider both hysteresis and solubility trapping. Geochemical formulae can be included in the model using an internal geochemistry database to describe the mineral trapping reactions. These formulae can describe aqueous reactions, such as those involving $CO_2$ and clay minerals. For aqueous reactions, the following chemical reactions are standard formulae used in $CO_2$ simulation:

$$CO_2(aq) + H_2O = H^+ + HCO_3^-$$
$$CO_3^{-2} + H^+ = HCO_3^-$$
$$OH^- + H^+ = H_2O$$

The following three formulae represent three common ionic reactions that can occur between water and $CO_2$ within a reservoir. These reactions involve the formation of solid minerals that can be found in sandstone aquifers, and they result in the precipitation of carbon oxides. These reactions are commonly included in modeling efforts to understand and predict the behavior of $CO_2$ in underground storage reservoirs:

$$Anorthite\ (CaAl_2Si_2O_8) + 8H^+ = 4\,H_2O + Ca^{2+} + 2Al^{4+}$$
$$Calcite\ (CaCO_3) + H^+ = Ca^{2+} + HCO3^-$$
$$Kaolinite\ \left(Al_2Si_2O_5(OH_4)\right) + 6H^+ = 5H_2O + 2Al^{3+} + 2SiO$$

Geochemical trapping has the potential to store $CO_2$ for hundreds or thousands of years, but the short-term effects of this method are relatively limited. Instead, the short-term movement and storage of $CO_2$ are more strongly influenced by hydrodynamic and solubility trapping mechanisms. These mechanisms involve the movement of fluids, such as water or oil, through porous rock formations and the solubilization of $CO_2$ in liquids, such as water or oil. As a result, these processes can be more effective in the short term at storing $CO_2$, although they may not have the same long-term stability as geochemical trapping.

**Static Model**

The geomodel was constructed to simulate the geologic structure of the Ellenburger and Cambrian formations. The grid contains 600 cells in the X-direction (East-West) and 400 cells in the Y-direction (North-South), totaling 240,000 cells per layer. Therefore, 55 layers were utilized in the model representing the gross thickness of the injection interval, totaling 13,200,000 grid blocks. The Ellenburger is comprised of 25 layers and the Cambrian is comprised of 30 layers. Each grid block is 50’ by 50’ by 10’, resulting in a model size of 5.7 miles by 3.8 miles by 550,’ as shown in Figure 27. This covers approximately 22 square miles (13,774 acres).

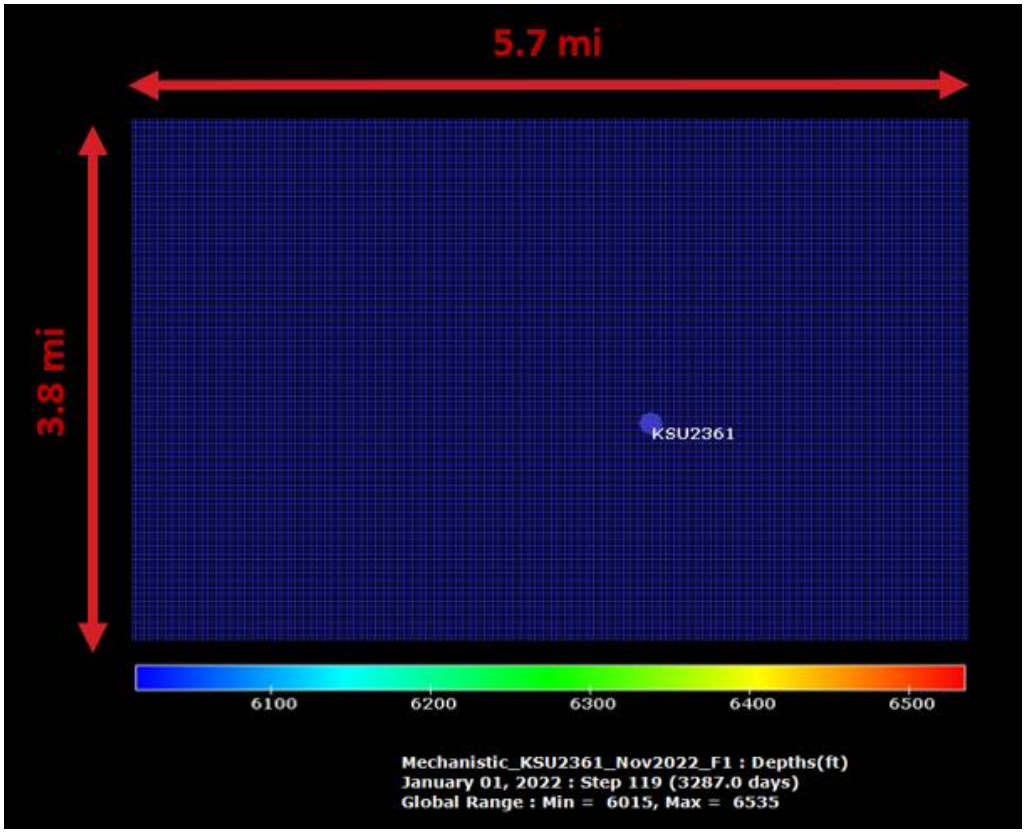


Figure 27 – Geomodel Dimensions

Well log analysis tied into seismic interpretation was used to identify any major formations tops. Four geologic units were identified and incorporated into the geomodel. Each geologic unit was used to determine the geologic structure of the injection zone. First, the Ellenburger is a carbonate formation comprised of dolomite/limestone matrix. Underlying the Ellenburger formation is the Cambrian sandstone. This sandstone was split into two geologic units, the Cambrian 1 and Cambrian 2. The Precambrian formation is at the bottom of the model. The Precambrian, comprised of granite, is the lower confining zone. Figure 28 highlights the overall structure of the target zone.

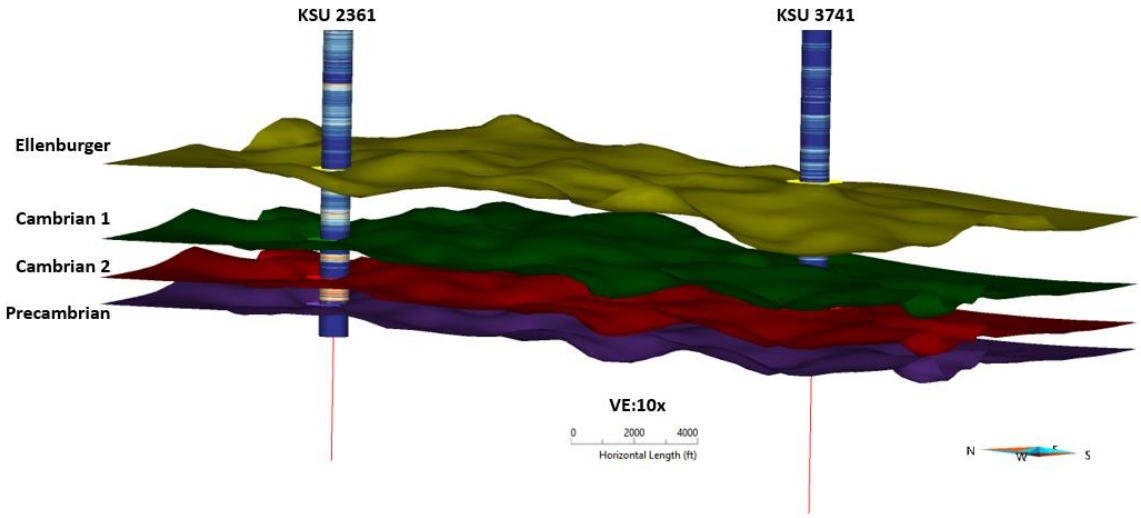


Figure 28 – Structural Horizons of the Geomodel

Permeability and porosity were distributed through the geomodel based on the formation. These rock properties were considered to be laterally homogenous in the simulation. However, vertical heterogeneity was incorporated into the model. Based on well log analysis, porosity was determined to be 10% in the Ellenburger carbonate and 12% in the Cambrian sandstone, as shown in Figure 29. Permeability was determined from history matching two wells. From this exercise, it was determined that the horizontal permeability ($K_H$) is 20 milliDarcy (mD) and vertical permeability ($K_V$) was assumed to be 10% of $K_H$ or 2 mD. Table 7 summarizes the rock properties in the model.

Table 7 – Rock Properties

| Assumptions | Values |
|---|---|
| Ellenburger Porosity (%) | 10 |
| Cambrian Porosity (%) | 12 |
| $K_H$ (mD) | 20 |
| $K_V/K_H$ Ratio | 0.1 |

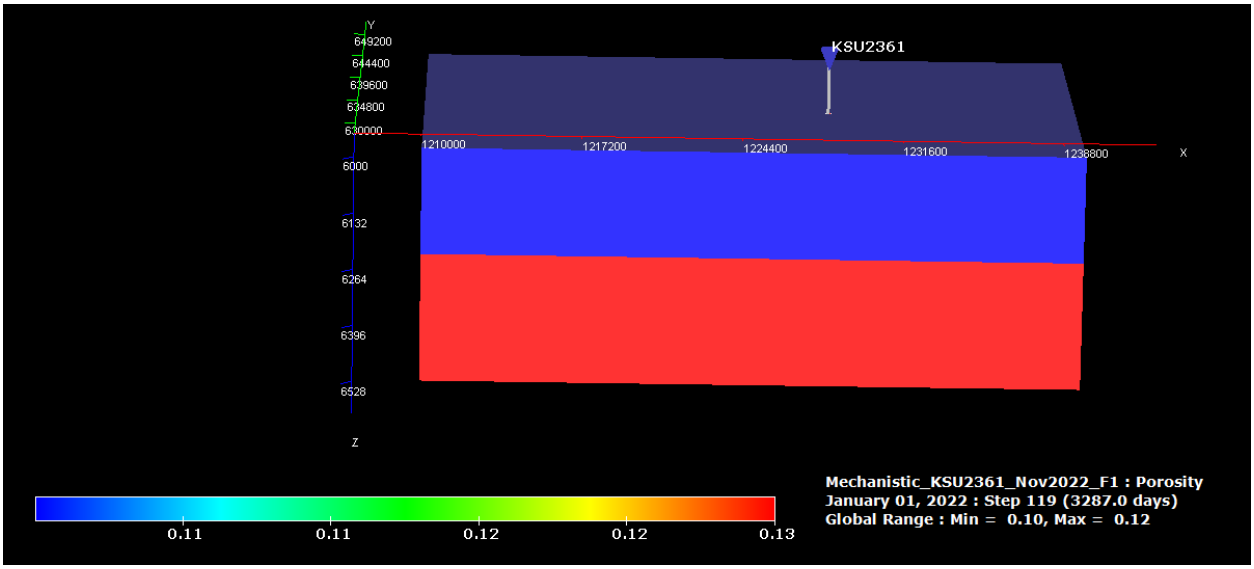


Figure 29 – Porosity Distribution in Plume Model

**Dynamic Model**

The primary objectives of the $CO_2$ plume model are as follows:

1. Determine the maximum possible injection rate without fracturing the target zone
2. Determine land acquisition strategy (i.e., maximum plume size)
3. Assess the likelihood of $CO_2$ leakage through potential conduits that may contaminate the Underground Source of Drinking Water (USDW)

Using the geomodel as an input, an infinite-acting model was built to simulate boundary conditions. The model assumes that the reservoir is 100% filled with brine. The formation fluid was estimated to have a salinity of 66,000 ppm. An offset step-rate test was utilized to estimate initial reservoir pressure and fracture pressure. Reservoir pressure was determined to be 2,600 psi which translates to a 0.435 psi/ft gradient. While pressure never reached high enough to propagate any fractures during the step-rate test, the fracture pressure was estimated to be approximately 4,390 psi. This translates to a fracture gradient of 0.683 psi/ft. Based off this data, a wellhead pressure of 1,850 psi was used to constrain the modelled well. An average temperature of 260 °F was also applied to the reservoir. Table 8 provides a summary of the initial conditions included in the simulation.

Table 8 – Initial Conditions Summary

| Assumptions | Values |
|---|---|
| Permeability (mD) | 20 |
| Porosity (%) | 10-12 |
| Pore Gradient (psi/ft) | 0.435 |
| Frac Gradient (psi/ft) | 0.683 |
| Reservoir Temperature (°F) | 260 |

To accurately and conservatively model the effective pore space of the rock, a net-to-gross (NTG) ratio was applied to the Ellenburger and Cambrian formations. The lateral plume extent is increased by reducing the total pore space $CO_2$ can flow through. Reducing the available pore space also limits

the $CO_2$ injection rate of the well due to higher increases in pressure. The Ellenburger had an NTG ratio of 0.5 applied, while the Cambrian formation had a 0.6 NTG ratio. This is further highlighted in Figure 30.

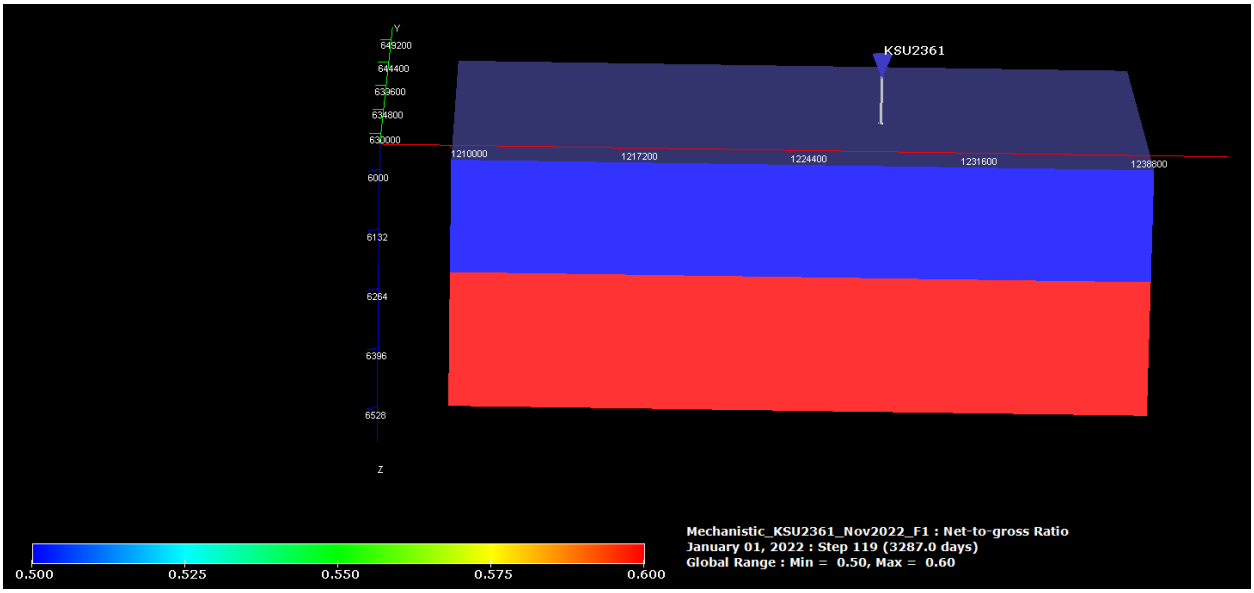


Figure 30 – NTG Ratio Applied to the Plume Model

**Relative Permeability**

Relative permeability curves were generated to represent a $CO_2$-brine system and how supercritical $CO_2$ will flow through a 100% brine-filled rock. Data from Kinder Morgan's McElmo Dome source models were utilized to create the relative permeability curves. The key inputs include a 9% irreducible water saturation and a 9% maximum residual gas saturation. Figure 31 shows the curves included in the simulation model.

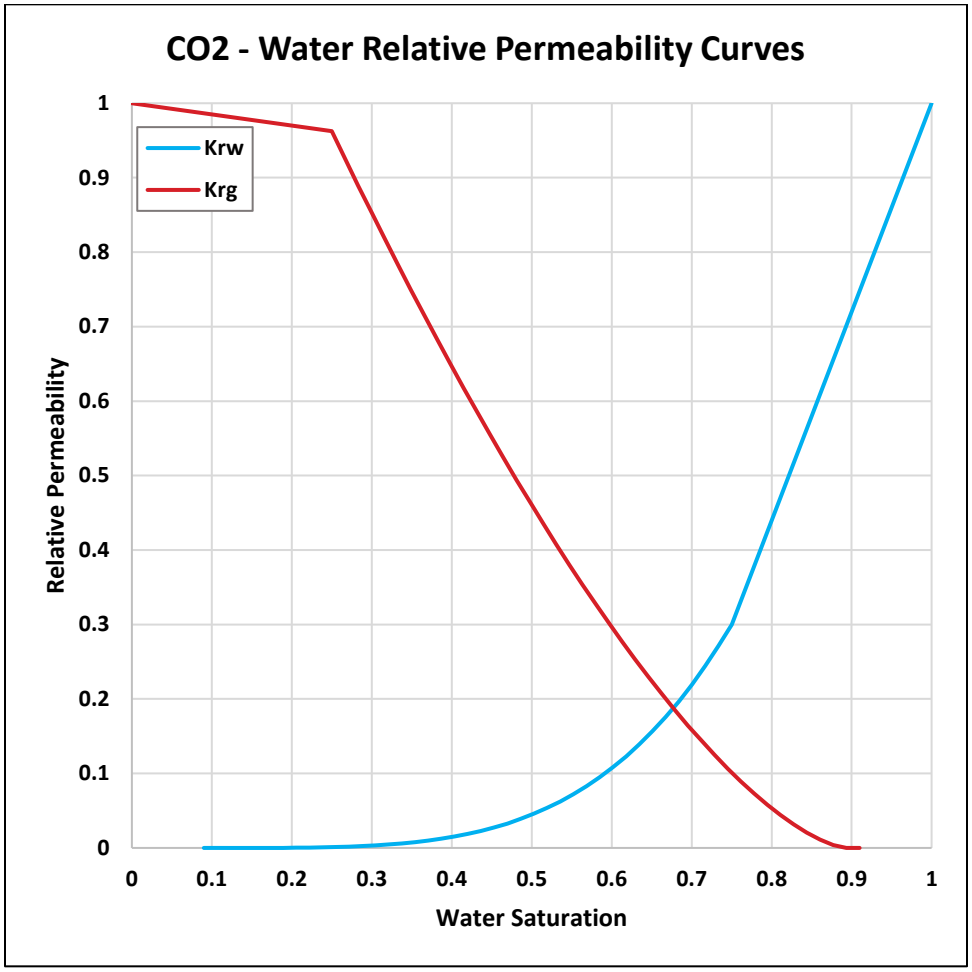


Figure 31 – $CO_2$-Water Relative Permeability Curves

**History Matching**

Two SWD wells were history-matched to determine permeability estimates. Historical injection rates were set in the model, and the simulated pressure response was compared to the recorded pressure data. This process was iterated multiple times until the simulated and real-life data matched. Monthly data points KSU 2361 (Figure 32) and KSU #3471 (Figure 33) were used to vary the injection rate in the model. These same intervals were used to compare the simulated results.

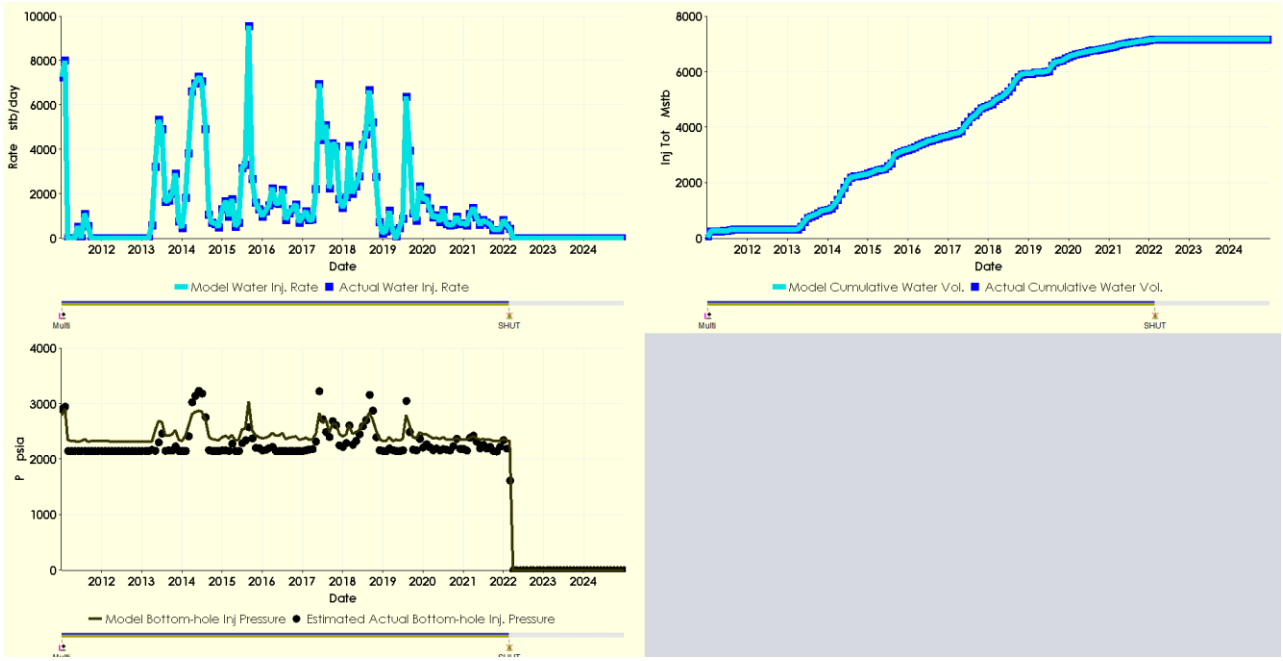


Figure 32 – History Match for KSU 2361

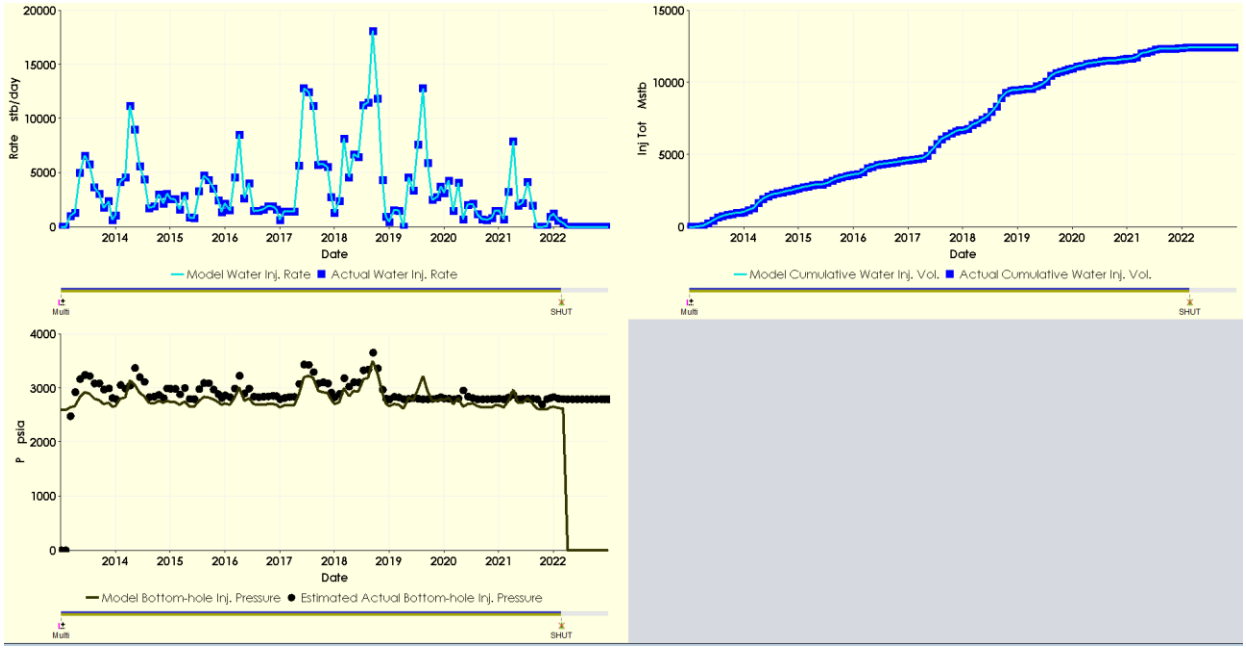


Figure 33 – History Match for KSU #3471

## $CO_2$ Injection Operations

KSU 2361 was simulated to inject supercritical $CO_2$ for 21 years. A maximum wellhead pressure (WHP) was used to limit the injection rate. This value was determined from the fracture gradient estimation, and an equivalent wellhead pressure was calculated. The WHP constraint was set to 1,850 psi, equal to 84% of the fracture pressure. The injection rate was then maximized to stay

below the expected frac gradient. Figure 34 shows the simulated WHP during active injection operations.

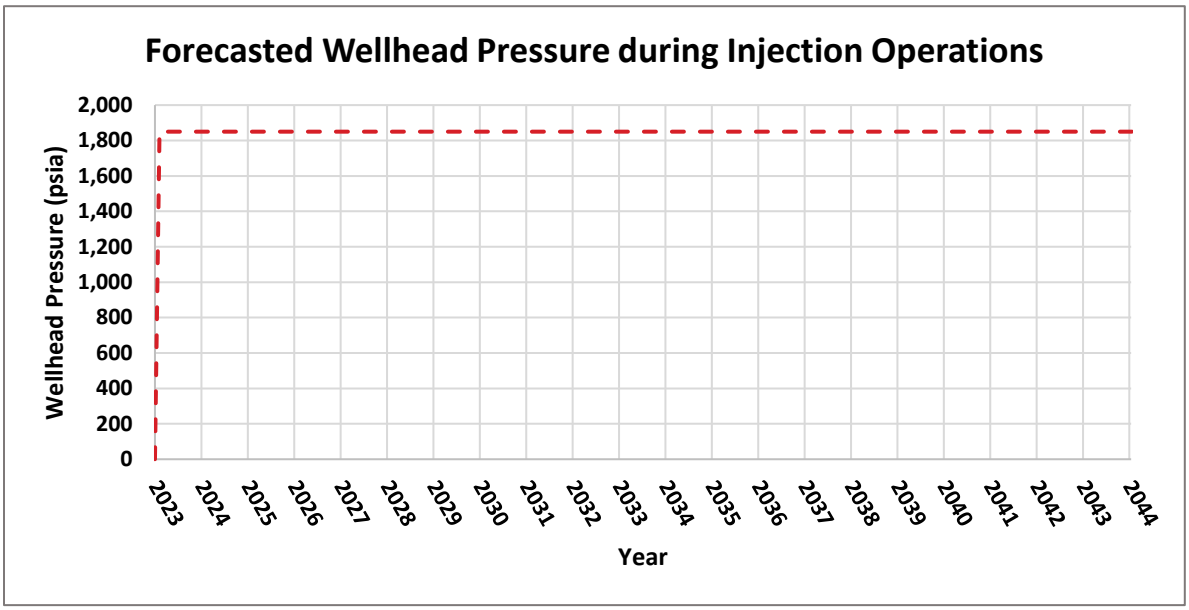


Figure 34 – Simulated Wellhead Pressure During Active Injection

During active injection, KSU 2361 achieved a maximum rate of approximately 1.22 MMT/yr. (~65 million cubic feet (MMscf)/day). During injection, the bottom hole pressure (BHP) reaches a maximum of 3,493 psi, which is safely below the fracture pressure. This is an 893-psi increase from the initial reservoir pressure. After injection ceases, the reservoir pressure decreases, reaching 65 psi buildup from the initial reservoir pressure. Figure 35 summarizes these results. The decreasing bottom-hole pressure from 2023 to 2044 is due to the relative permeability increasing over time.

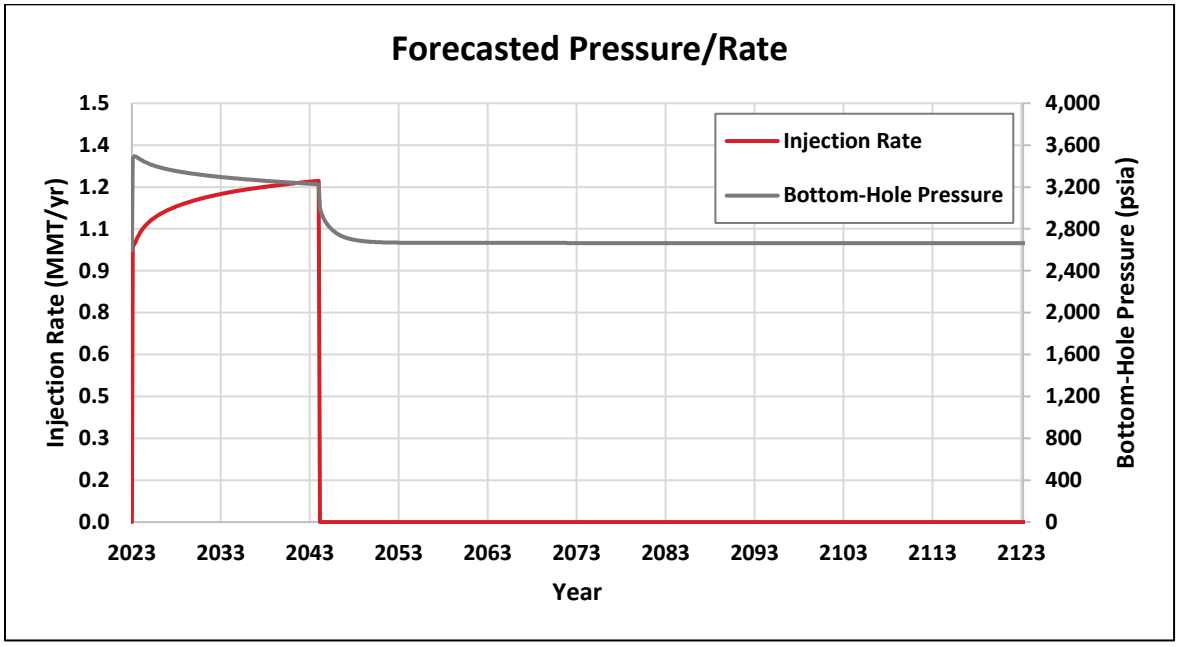


Figure 35 – Forecasted Injection Rate and BHP

## Model Results

The maximum plume was determined once the plume was considered stabilized and by using a gas saturation cutoff of 3%. The plume is considered stabilized once all lateral and vertical movement of $CO_2$ has stopped, which also marks the end of the initial monitoring period. Aerial plume sizes were taken at 10-year intervals to determine a growth rate. As seen in Figure 36, an annualized growth rate is determined at each interval. The plume is delineated based on the maximum extent of the plume when the growth rate reaches 0%. In this model, the plume stabilizes in 2074, 30 years after the end of the injection period.

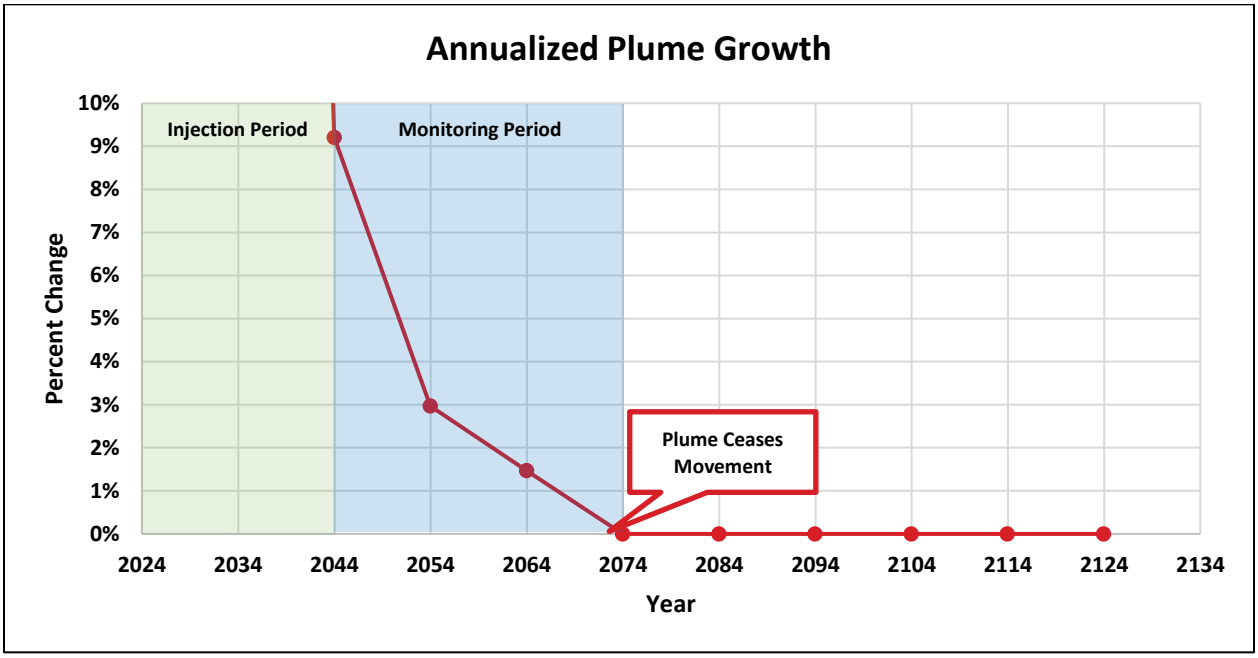


Figure 36 – Annualized Growth Rate of $CO_2$ Plume

The stabilized plume reaches a maximum of 3,384 ac (~5.3 sq mi). The furthest extent of this plume is to the South, as seen in Figure 37. The largest radius of the plume is 6,850' (~1.2 mi) from the wellbore. Due to the heterogeneity included in the model, the plume is not uniform from layer to layer, as seen in Figure 48. The maximum plume was chosen from the layer with the largest lateral extent of $CO_2$. Table 9 shows the plume radius and plume compared to time since injection starting in year zero. The results in Table 9 show that the modeled plume boundary is expected to stabilize 30 years after injection has ended. Additionally, the model was run a further 50 years to ensure the final plume boundary was stabilized, as shown in the table below.

Table 9 – Plume Model Radius and Area

| Date | Year | Plume Radius (ft.) | Plume Area (Acres) |
|---|---|---|---|
| Jan-23 | 0 | 0 | 0 |
| Jan-34 | 10 | 4650 | 1559 |
| Jan-44 | 20 | 6400 | 2954 |
| Jan-54 | 30 | 6700 | 3238 |
| Jan-64 | 40 | 6800 | 3335 |
| Jan-74 | 50 | 6850 | 3384 |
| Jan-84 | 60 | 6850 | 3384 |
| Jan-94 | 70 | 6850 | 3384 |
| Jan-04 | 80 | 6850 | 3384 |
| Jan-14 | 90 | 6850 | 3384 |
| Jan-24 | 100 | 6850 | 3384 |

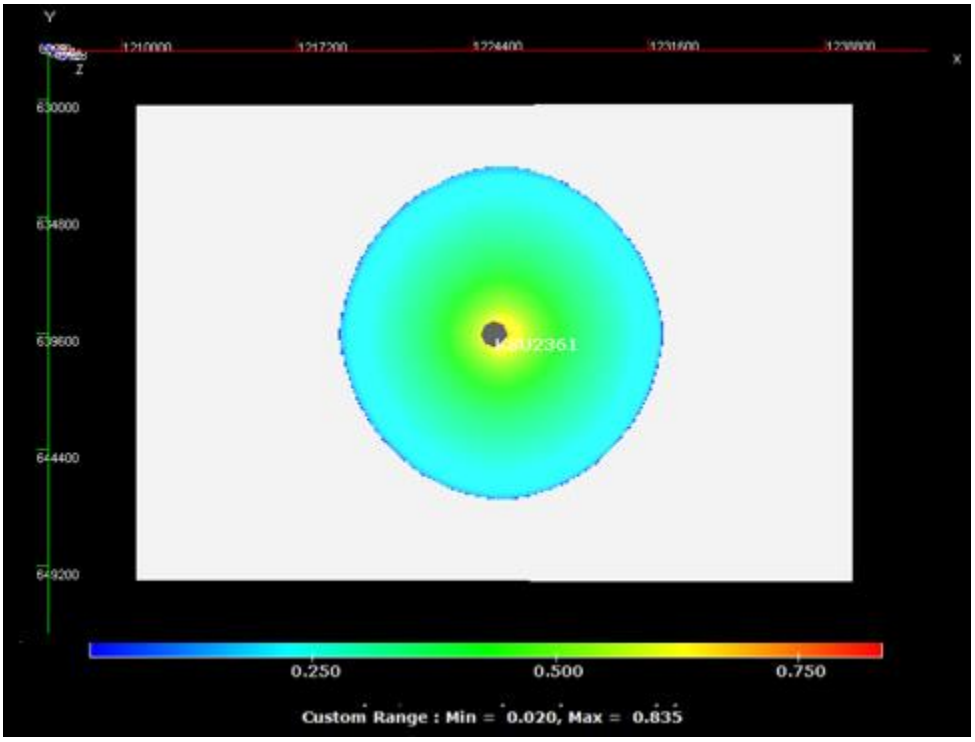


Figure 37 – Aerial View of $CO_2$ Plume

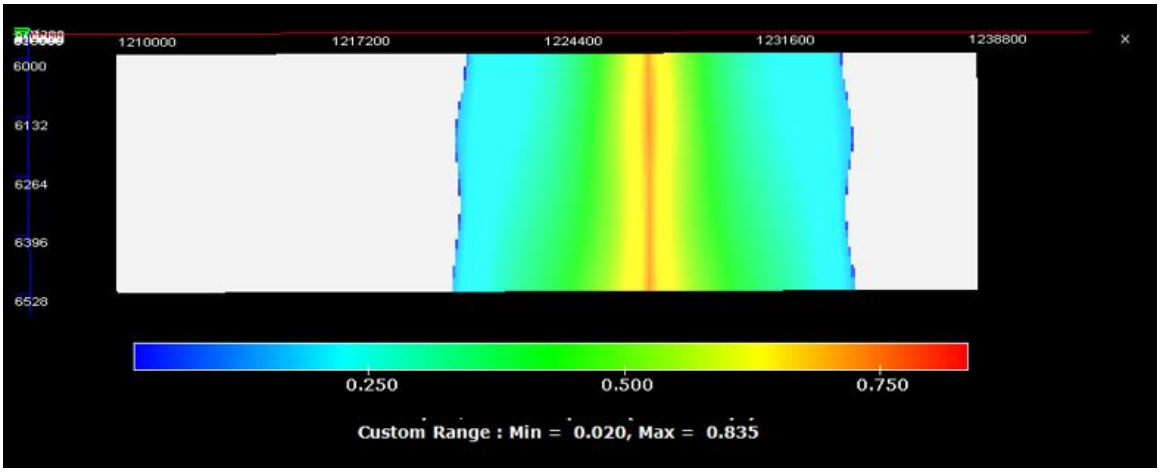


Figure 38 – Cross-Sectional View of $CO_2$ Plume

# SECTION 3 – DELINEATION OF MONITORING AREA

This section discusses the delineation of the Maximum Monitoring Area (MMA) and Active Monitoring Area (AMA) as described in EPA 40 CFR §**98.448(a)(1**).

## 3.1 Maximum Monitoring Area

The EPA defines the MMA as equal to, or greater than, the area expected to contain the free-phase $CO_2$-occupied plume until the $CO_2$ plume has stabilized, plus an all-around buffer zone of at least one-half mile. A numerical computer simulation was used to determine an estimate for the size and drift of the plume. Using a combination of Paradigm's SKUA-GOCAD and Aspen Technology's Tempest software packages, a geomodel, and reservoir model were used to determine the areal extent and density drift of the plume. The model accounts for the following considerations:

- Offset well logs to estimate geologic properties
- Petrophysical analysis to calculate the heterogeneity of the rock
- Geological interpretations to determine faulting and geologic structure
- Offset injection history to predict the density drift of the plume adequately

Kinder Morgan's pipeline gas specifications were used for the initial composition of the injectate in the model, as provided in Appendix B. The molar composition of the gas is mostly carbon dioxide, with some small amounts of nitrogen and hydrocarbons, and contained no $H_2S$. The molar composition was incorporated into the model as future $CO_2$ streams could be added for injection. As discussed in Section 2, the gas was modeled to be injected primarily into the Ellenburger and both Cambrian formations. The geomodel was created based on the rock properties seen in the Ellenburger and Cambrian rocks.

The weighted average gas saturation defined the plume boundary in the aquifer. A value of 3% gas saturation was used to determine the boundary of the plume. When injection ceases in 2044, the areal expanse of the plume will be 2,954 acres. After 30 additional years of density drift, the areal extent of the plume is 3,384 acres, with a maximum distance to the edge of the plume of approximately 6,850'. Since the stabilized plume shape is relatively circular, the maximum distance plus a one-half mile buffer from the injection well, was used to define the circular boundary of the MMA equal to 9500'.

The plume is expected to stabilize 30 years after injection ceases and does not migrate after 2050, the monitoring program of the MMA will remain active for the required amount of time.

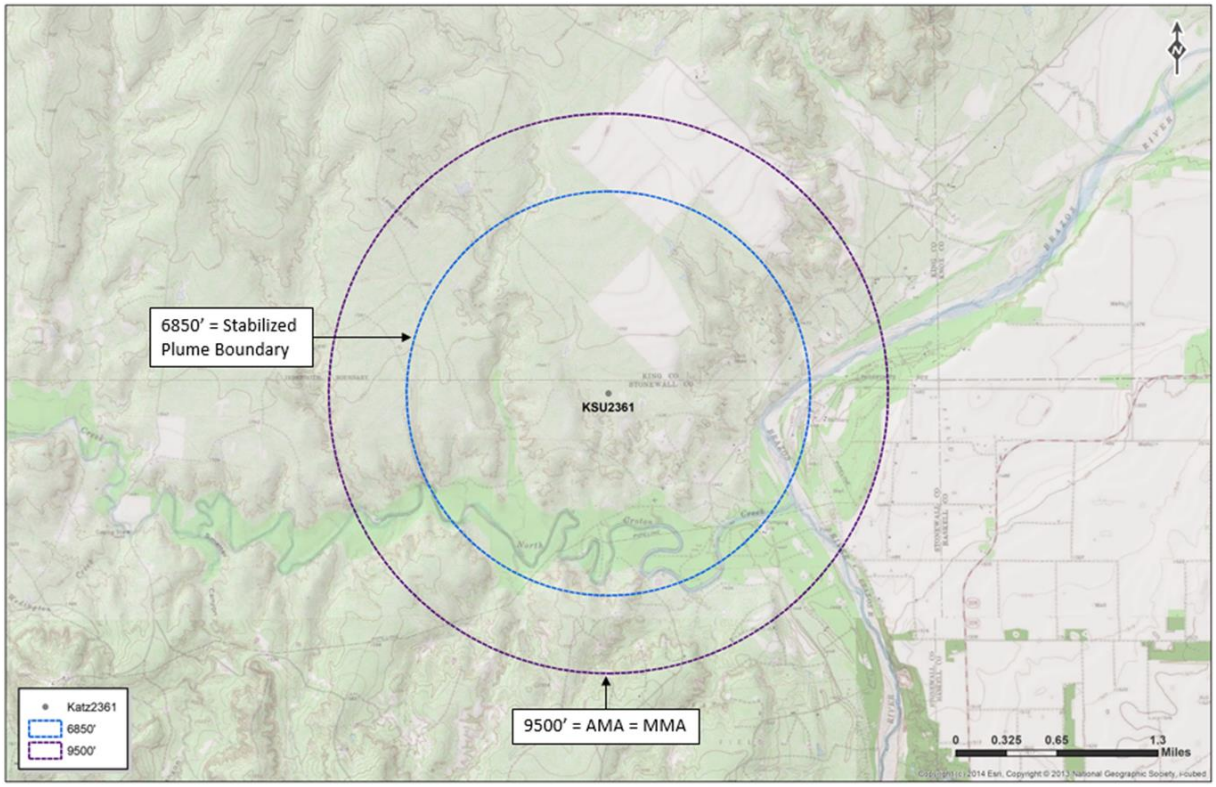


Figure 39 – Stabilized Plume Boundary, Active Monitoring Area and Maximum Monitoring Area

## 3.2 Active Monitoring Area

Per 40 CFR 98.449, the boundary of the AMA is established by superimposing two different boundary conditions. For the first condition, Kinder Morgan defines year t as occurring 30 years after the cessation of injection, when the modeled plume has stabilized with a maximum extent radius of 6,850'. The addition of a half-mile buffer results in a maximum extent of 9,500', satisfying the first condition. For the second condition, since Kinder Morgan defines year t as when the plume stabilizes, 30 years after the cessation of injection, the projected radius of the plume for t + 5 is also 6,850'. Superimposing the results of these two conditions results in Kinder Morgan defining the AMA with a radius of 9,500', or 3,384 acres, as shown in Figure 39.

# SECTION 4 – POTENTIAL PATHWAYS FOR LEAKAGE

This section identifies the potential pathways for $CO_2$ to leak to the surface within the MMA. Also included are the likelihood, magnitude, and timing of such leakage. The potential leakage pathways are:

- Leakage from surface equipment
- Leakage through existing wells within the MMA
- Leakage through faults and fractures
- Leakage through the confining layer
- Leakage from Natural or Induced Seismicity

## 4.1 Leakage from Surface Equipment

The surface facilities at the KSU 2361 well are designed for injecting acid gas primarily consisting of $CO_2$. One additional pipeline will be constructed to carry the acid gas from the custody transfer meter to the KSU 2361 wellhead, as shown in Figure 40. The wellbore of the KSU 2361 is designed for acid gas, as seen in the wellbore schematic in Figure 41. The facilities have been designed to minimize leakage and failure points. The design and construction of these facilities followed industry standards and best practices. $CO_2$ monitors are located around the facility and the well site. These gas monitor alarms will be triggered at levels set upon completion of a baseline study of the ambient air quality, followed by a gas dispersion model. An emergency shutdown valve (ESD) is located at the wellhead and is locally controlled by pressure, with a high-pressure and low-pressure shut-off.

The facilities have been designed and constructed with other safety systems to provide for safe operations. These systems include ESD valves to isolate portions of the pipeline, pressure relief valves along the pipeline to prevent over-pressurization, and venting to allow piping and equipment to be de-pressured under safe and controlled operating conditions in the event of a leak. More information on these systems and be found in Appendix C. Should Kinder Morgan construct additional $CO_2$ facilities other meters will be installed as needed to comply with the 40 CFR **§98.448(a)(5**) measurement. These meters will be near the existing facilities and utilize the existing monitoring programs discussed previously. Additionally, $CO_2$ monitors will be installed near the new meters and tied into the facility monitoring systems. No additional wells are included within this MRV facility.

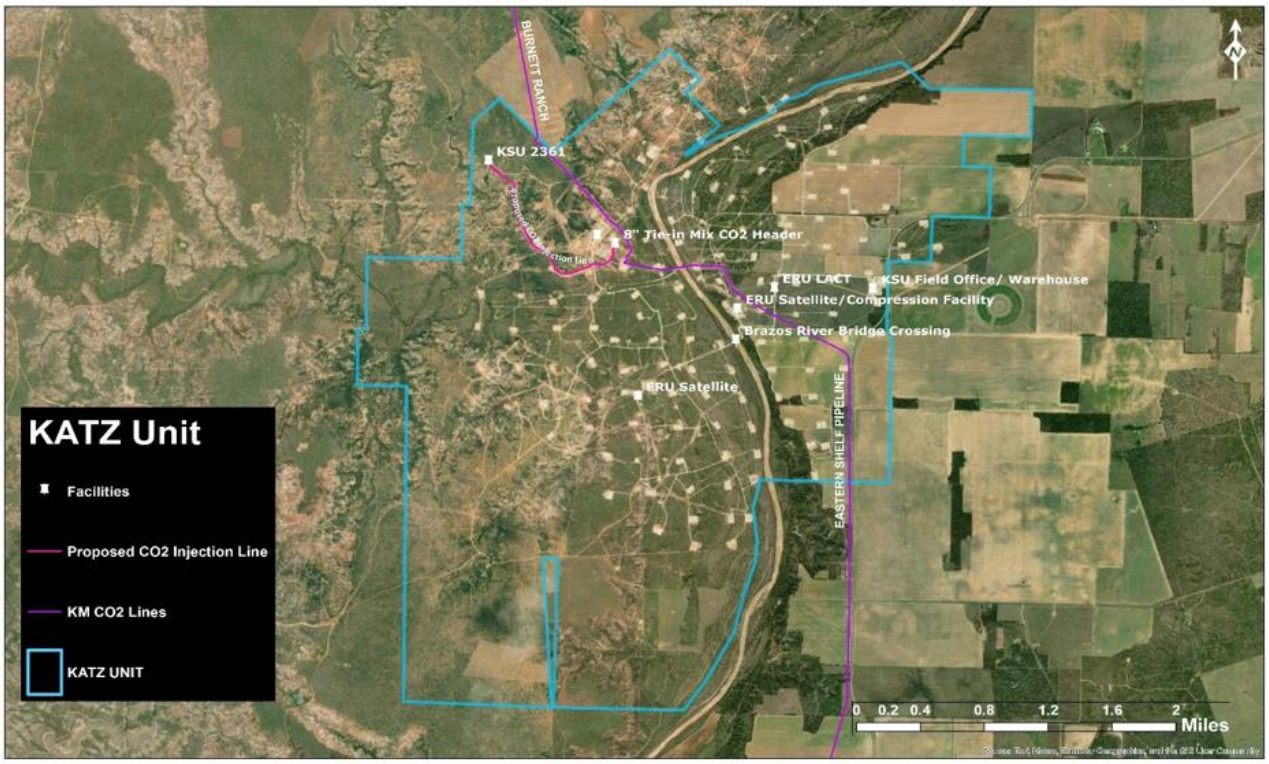


Figure 40 – Site Plan

With the level of monitoring implemented at the KSU 2361 well, a release of $CO_2$ would be quickly identified, and the safety systems would minimize the release volume. The $CO_2$ stream injected into KSU 2361 could include small amounts of methane and nitrogen, as seen in Appendix B. The CO2 injected into the Katz 2361 well is supplied by a number of different sources into the pipeline system and the composition is not expected to change over time. If any leakage were to be detected, the volume of $CO_2$ released will be quantified based on the operating conditions at the time of release, as stated in Section 7 in accordance with 40 CFR **§98.448(a)(5)**. Kinder Morgan concludes that leakage of $CO_2$ through the surface equipment as unlikely.

## 4.2 Leakage from Existing Wells within MMA

### 4.2.1 Oil and Gas Operations within Monitoring Area

A significant number of wells have historically been drilled within the area of the KSU 2361 well. However, production has primarily been from the shallower Strawn formation in the Katz Field. The Strawn is separated from the Ellenburger-Cambrian interval by 665' in this area. In addition to the primary Strawn production, a few wells have produced from the Mississippian. The mid-Mississippian is separated from the Ellenburger-Cambrian interval by 133'. KSU 2361 is the only well penetrating the injection interval within the projected plume area of the MMA for the KSU 2361. Therefore, it is the only well that will be monitored for surface leakage. This well is designed to handle and inject acid gas, which reduces the risk and likelihood of leakage through the existing well to near-zero.

The KSU 2361 well was designed to prevent migration from the injection interval to the surface through the casing and cement placed in the well, as depicted in the schematic denoted in Figure 41. Mechanical integrity tests (MIT), required under Statewide Rule (SWR) **§3.46** [40 CFR **§146.23 (b)(3)**], will take place every five years to verify that the well and wellhead can contain the appropriate operating pressures. If the MIT were to indicate a leak, the well would be isolated and the leak mitigated to prevent leakage of the injectate to the atmosphere.

A map of all oil and gas wells within the MMA is shown in Figure 42. The MMA review map and a summary of all the wells in the MMA are provided in Appendix D. Figure 43 highlights that no wells penetrate the MMA's gross injection zone.

KINDER MORGAN

**Schematic - Current**

**Well Name: KSU #2361**

| API/UWI | Surface Location | Field Name | State | Well Configuration Type | RRC/COGC... | Account Cat/Prop... |
|---|---|---|---|---|---|---|
| 42-433-33712 | SEC 2 LONG, CB | KATZ | Texas | Vertical | | 26039 |

| Estimated KB Elevation (ft) | KB-Tubing Head Distance (ft) | Original Well Spud Date | Rig Release Date | PBTD (All) (ftKB) | Total Depth All (TVD) (ftKB) |
|---|---|---|---|---|---|
| 1,531.00 | 13.00 | 8/23/2012 18:00 | 9/13/2012 06:00 | Original Hole - 6,431.0 | |

**Most Recent Job**

| Job Category | Primary Job Type | Secondary Job Type | Start Date | End Date |
|---|---|---|---|---|
| Non-Rig Activity | Coil Tubing | | 4/2/2019 | 4/4/2019 |

**TD: 6,625.0** Vertical, Original Hole, 2/21/2022 10:06:22 AM

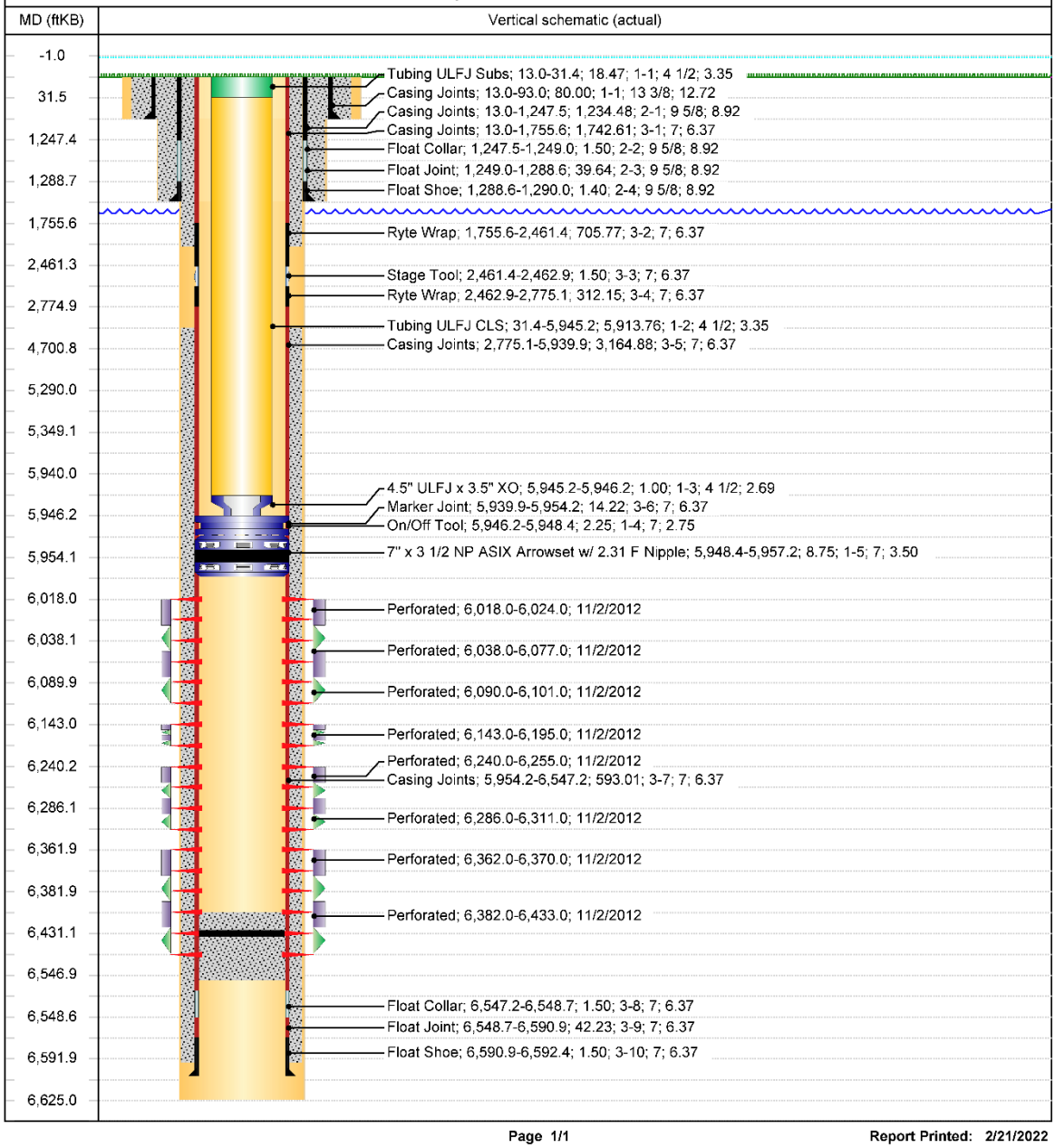


Page 1/1 Report Printed: 2/21/2022

Figure 41 – KSU 2361 Wellbore Schematic

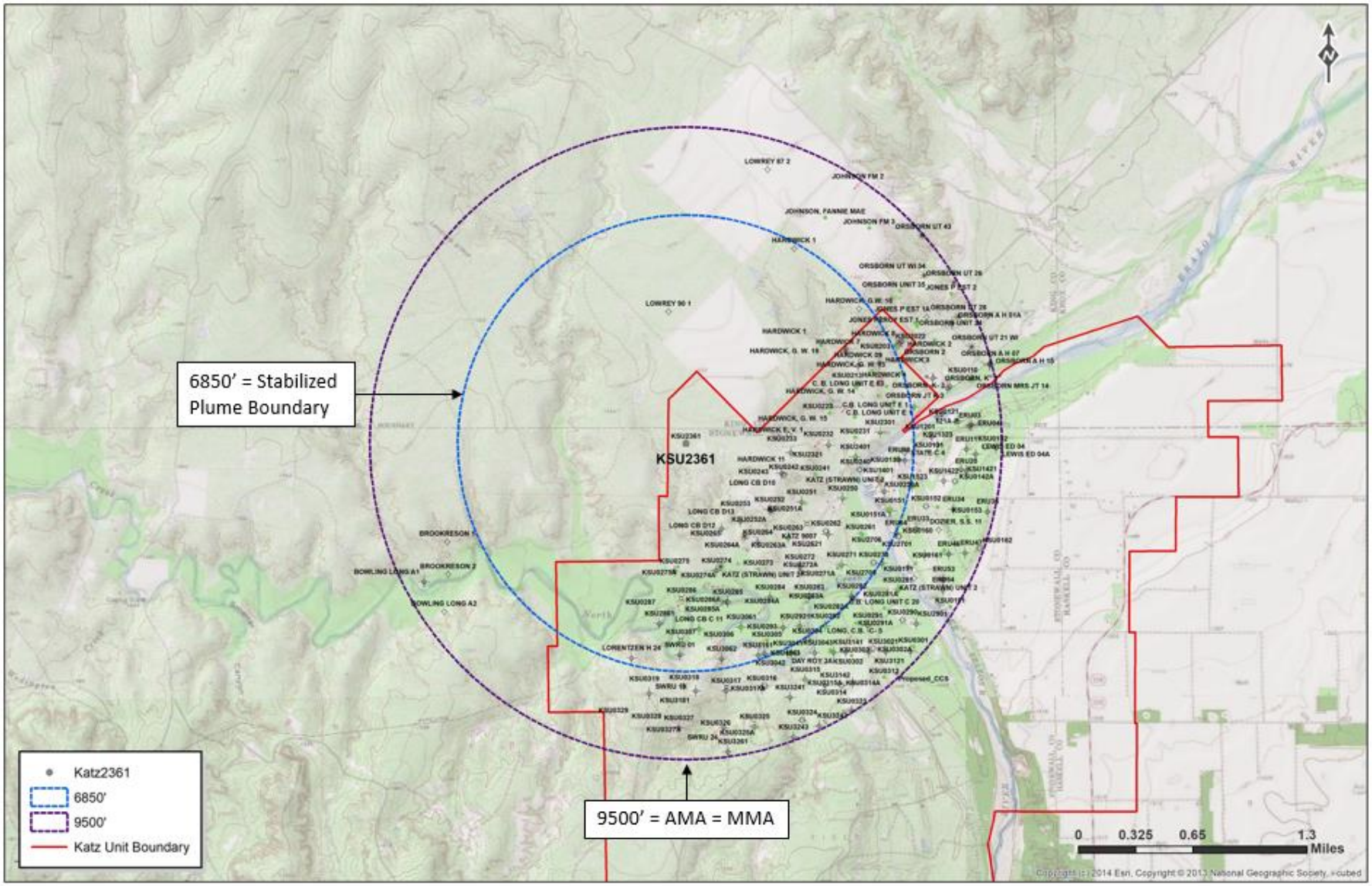


Figure 42 – All Oil and Gas Wells within the MMA

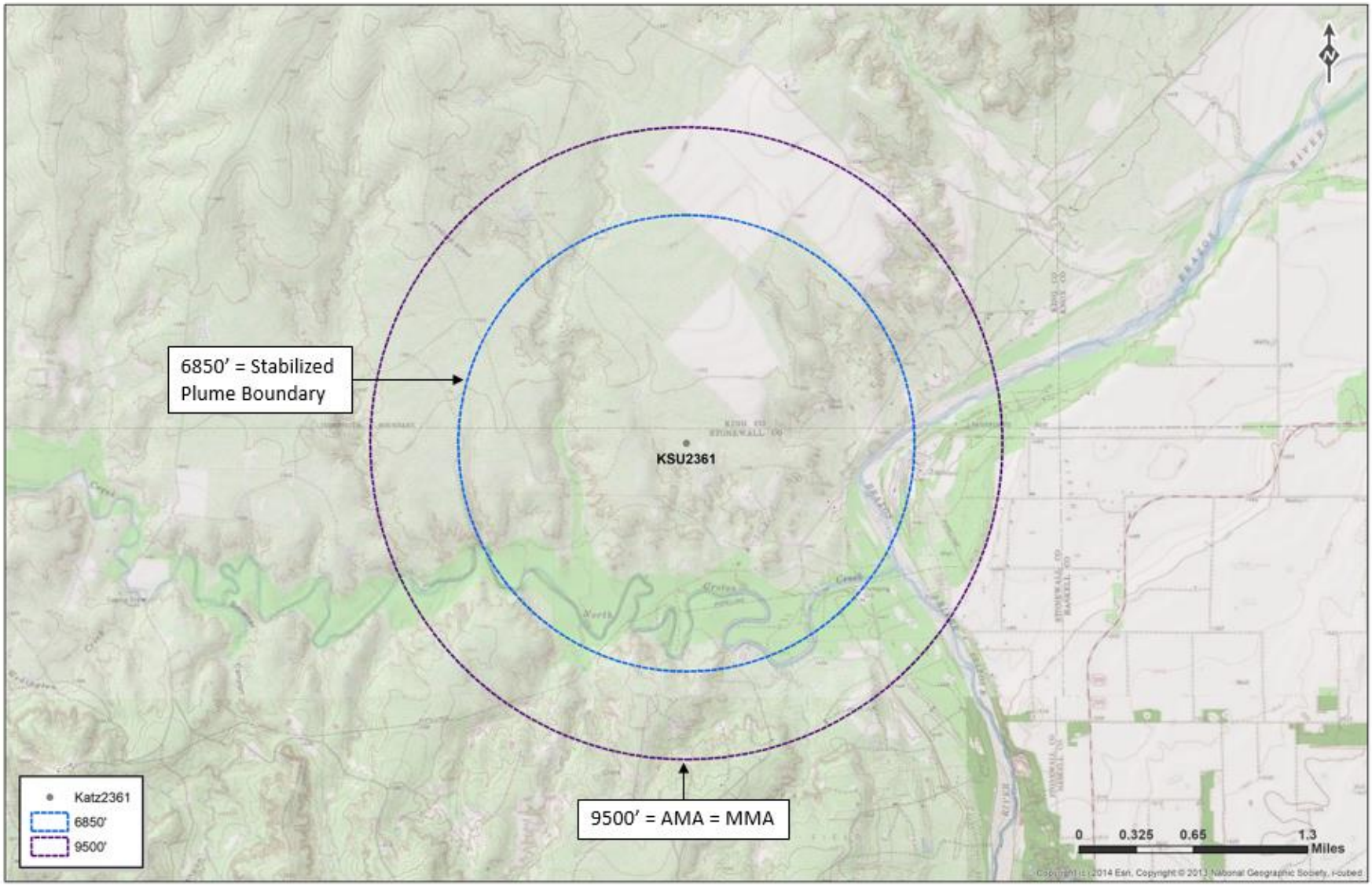


Figure 43 – Oil and Gas Wells Penetrating the Gross Injection Interval within the MMA

**Future Drilling**

Potential leak pathways caused by future drilling in the area are not expected to occur. The deeper formations, such as the Pre-Cambrian, have proven to date to be less productive or non-productive in this area, which is why the location was selected for injection. Furthermore, any drilling permits issued by the TRRC in the area of KSU 2361 include a list of formations for which oil and gas operators are required to comply with TRRC Rule 13 (entitled "Casing, Cementing, Drilling, Well Control, and Completion Requirements"), 16 TAC **§3.13**. By way of example, see the KSU 2361 well drilling permit provided in Appendix A. The Ellenburger and Cambrian Sands are among the formations listed for which operators in Stonewall County and district 7B (where the KSU 2361 is located) are required to comply with TRCC Rule 13. TRRC Rule 13 requires oil and gas operators to set steel casing and cement across and above all formations permitted for injection under TRRC Rule 9 or immediately above all formations permitted for injection under Rule 46 for any well proposed within a one-quarter mile radius of an injection well. In this instance, any new well permitted and drilled to the KSU 2361 well's injection zone, and located within a one-quarter-mile radius of the KSU 2361 well, will be required under TRRC Rule 13 to set steel casing and cement above the KSU 2361 well injection zone. Additionally, Rule 13 requires operators to case and cement across and above *all* potential flow zones and zones with corrosive formation fluids. The TRRC maintains a list of such known zones by TRRC district and county and provides that list with each drilling permit issued, which is also shown in the permit mentioned above in Appendix A.

### 4.2.2 Groundwater wells

A groundwater well search resulted in zero groundwater wells found within the MMA, as identified by the Texas Water Development Board.

The surface and intermediate casings of the KSU 2361 well, as shown in Figure 41, are designed to protect the shallow freshwater aquifers consistent with applicable TRRC regulations and the GAU letter issued for this location. See the GAU letter included in Appendix A. The wellbore casings and cements also prevent $CO_2$ leakage to the surface along the borehole. Kinder Morgan concludes that leakage of the sequestered $CO_2$ to the groundwater wells as unlikely.

## 4.3 Leakage Through Faults and Fractures

One fault was interpreted within the seismic coverage projecting 12,000' east of the KSU 2361 location. Initial plume models do not indicate an interaction between the injectate and the fault plane. Additionally, this fault dies within the Mississippian formation and does not penetrate the Lower Strawn Shale that acts as the upper confining unit. In the unlikely scenario in which the injection plume reaches the fault, and the fault acts as a transmissive pathway, the upper confining shale above the fault will act as an ideal sealant from injectate leaking outside of the permitted injection zone.

Should an unmapped fault exist within the plume boundary, the offset would be below 3D seismic resolution. The offset would be less than the thickness of the Lower Strawn Shale, juxtaposing it against itself, preventing vertical migration.

Fractures and subsequent subaerial exposure are responsible for porosity development within the injection intervals. Open hole logs show little to no porosity development indicating the Lower Strawn Shale or Mississippian Lime were not exposed at this location. Therefore, upward migration of injected gas through confining bed fractures is unlikely.

## 4.4 Leakage Through the Confining Layer

The Ellenburger and Cambrian injection zones have competent sealing rocks above and below the sand and carbonate formations. The properties of the overlying Lower Strawn Shale and its high composition of shale and mudstone make an excellent sealing rock to the underlying Ellenburger formation. Tight Mississippian Lime of roughly 266' lies between the Ellenburger and Lower Strawn Shale formations forming an impermeable upper buffer seal from the injection interval to the upper confining zone. Above this confining unit, shales found within the Homecreek Shale above the Desmoinesian formation will act as additional sealants between the injection interval and the USDW. The USDW lies above the sealing properties of the formations outlined above, making stratigraphic migration of fluids into the USDW highly unlikely. Precambrian basement rock's underlying low porosity and permeability minimizes the likelihood of downward migration of injected fluids. The relative buoyancy of injected gas to the in-situ reservoir fluid makes migration below the lower confining layer unlikely.

## 4.5 Leakage from Natural or Induced Seismicity

The location of KSU 2361 is in an area of the Midland Basin that is inactive from a seismicity perspective, whether induced or natural. A review of historical seismic events on the USGS's Advanced National Seismic System site (from 1971 to present) and the Bureau of Economic Geology's TexNet catalog (from 2017 to present), as shown in Figure 44, indicates the nearest seismic event (unspecified whether natural or induced) occurred more than 40 miles away.

There is no indication of seismic activity posing a risk for loss of $CO_2$ to the surface within the MMA. Therefore, Kinder Morgan concludes that leakage of the sequestered $CO_2$ through seismicity as unlikely.

Pressures will be kept significantly below the fracture gradient of the injection and confining intervals. Additionally, continuous well monitoring combined with seismic monitoring will identify any operational anomalies associated with a seismicity event.

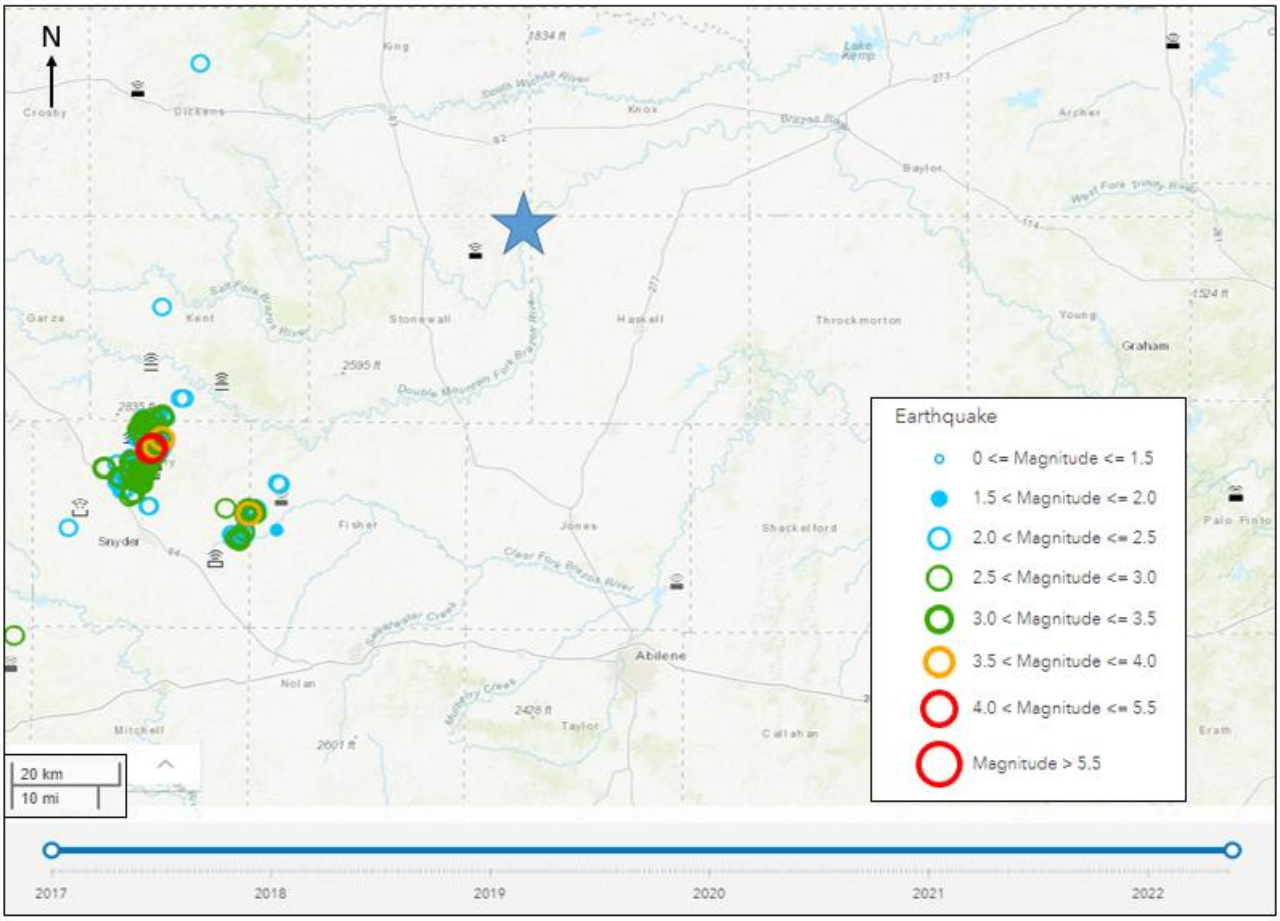


Figure 44 – Seismicity Review (TexNet – 06/01/2022)

# SECTION 5 – MONITORING FOR LEAKAGE

This section discusses the strategy that Kinder Morgan will employ for detecting and quantifying surface leakage of $CO_2$ through the pathways identified in Section 4 to meet the requirements of 40 CFR **§98.448(a)(3)**. Table 10 summarizes the monitoring of potential leakage pathways to the surface. Monitoring will occur during the planned 21-year injection period or cessation of injection operations, plus a proposed 5-year post-injection period.

- Leakage from surface equipment failure
- Leakage through existing and future wells within MMA
- Leakage through faults, fractures, or confining seals
- Leakage through natural or induced seismicity

Table 10 – Summary of Leakage Monitoring Methods

| Leakage Pathway | Monitoring Method |
|---|---|
| Leakage from surface equipment | Fixed $CO_2$ monitors throughout the AGI facility |
| | Daily visual inspections |
| | Supervisory Control and Data Acquisition (SCADA) |
| Leakage through existing wells | Fixed $CO_2$ monitor at the the AGI well |
| | SCADA continuous monitoring at the AGI Well |
| | Mechanical Integrity Tests (MIT) of the AGI Well every 5 years |
| | Visual inspections |
| | Quarterly atmospheric $CO_2$ measurements at well locations within the AMA |
| Leakage through groundwater wells | Annual groundwater samples from monitoring wells |
| Leakage from future wells | $CO_2$ monitoring during offset drilling operations |
| Leakage through faults and fractures | SCADA continuous monitoring at the AGI Well (volumes and pressures) |
| | In-field $CO_2$ monitors |
| Leakage through confining layer | SCADA continuous monitoring at the AGI Well (volumes and pressures) |
| | In-field $CO_2$ monitors |
| Leakage from natural or induced seismicity | Existing TexNet seismic monitoring station to be implemented |

## 5.1 Leakage from Surface Equipment

As the facility and the KSU 2361 well are designed to handle $CO_2$, leakage from surface equipment is unlikely to occur and would be quickly detected and addressed. The facility design minimizes leak points through the equipment used, and the connections are designed to minimize corrosion points. A baseline atmospheric $CO_2$ concentration will be established before injection operations begin. The facility and well site contain several $CO_2$ alarms with locations in close proximity.

The AGI complex is continuously monitored through automated systems. Details surrounding these systems can be found in Appendix C. In addition, field personnel conduct daily visual field inspections of gauges, monitors, and leak indicators such as vapor plumes. The effectiveness of the internal and external corrosion control program is monitored through the periodic inspection of the surface equipment associated with the sequestered CO2 and inspection of the cathodic protection system. These inspections and the automated systems allow Kinder Morgan to respond to any leakage situation quickly. The surface equipment will be monitored for the injection and post-injection period. Should leakage be detected during active injection operations, the volume of $CO_2$ released will be calculated based on operating conditions at the time of the event, per 40 CFR **§98.448(a)(5)**.

Pressures and flow rates through the surface equipment are continuously monitored during operations. If a release occurred from surface equipment, the amount of $CO_2$ released would be quantified based on the operating conditions, including pressure, flow rate, size of the leak point opening, and duration of the leak. In the unlikely event a leak occurs, Kinder Morgan will quantify the leak per the strategies discussed in Section 7, below.

## 5.2 Leakage From Existing and Future Wells within MMA

Kinder Morgan continuously monitors and collects injection volumes, pressures and temperatures through their SCADA systems, for the KSU 2361 well. This data is reviewed by qualified personnel and will follow response and reporting procedures when data exceeds acceptable performance limits. KSU 2361 has a pressure and temperature gauge placed in the injection stream at its wellhead and a pressure gauge on the casing annulus. A change of pressure on the annulus would indicate the presence of a possible leak. In addition, mechanical integrity tests (MIT) performed every 5 years, as expected by the TRRC and UIC, would also indicate the presence of a leak. Upon a negative MIT, the well would be isolated and the leak mitigated.

As discussed previously, Rule 13 would ensure that new wells in the field would be constructed to prevent migration from the injection interval.

In addition to the fixed monitors described previously, Kinder Morgan will also establish and operate an in-field monitoring program to detect $CO_2$ leakage within the MMA. The scope of work will include $CO_2$ monitoring at the AGI well site and, at minimum, quarterly atmospheric monitoring near any wells identified that penetrate the injection interval within the MMA. The collection of these measurements will be carried out by using a qualified third party. Upon approval of the MRV and through the post-injection monitoring period, Kinder Morgan will have these monitoring systems in

place. No wells have been identified within the MMA that penetrate the injection interval. Additional monitoring will be added as the MMA is updated over time. In the unlikely event a leak occurs, Kinder Morgan will quantify the leak per the strategies discussed in Section 7, below.

**Groundwater Quality Monitoring**

Kinder Morgan will monitor the groundwater quality in fluids above the confining interval by sampling from groundwater wells in the area of the facility and analyzing the sample with a third-party laboratory on an annual basis. In the case of KSU 2361, no existing groundwater wells have been identified within the MMA. At least two groundwater monitoring wells will be drilled within 1500' of KSU 2361 at a depth of approximately 100'. The final number, locations, and depths of the wells will be determined by a study completed by a certified 3rd party firm. The approximate location and depths of these wells are shown in Figure 45. A baseline sampling from these wells will occur before injection starts. The parameters to be measured will include pH, total dissolved solids, total inorganic and organic carbons, density, temperature, and other standard laboratory measurements. Any significant differences in these parameters from the baseline sample will be evaluated to determine if leakage of $CO_2$ to the USDW may have occurred.

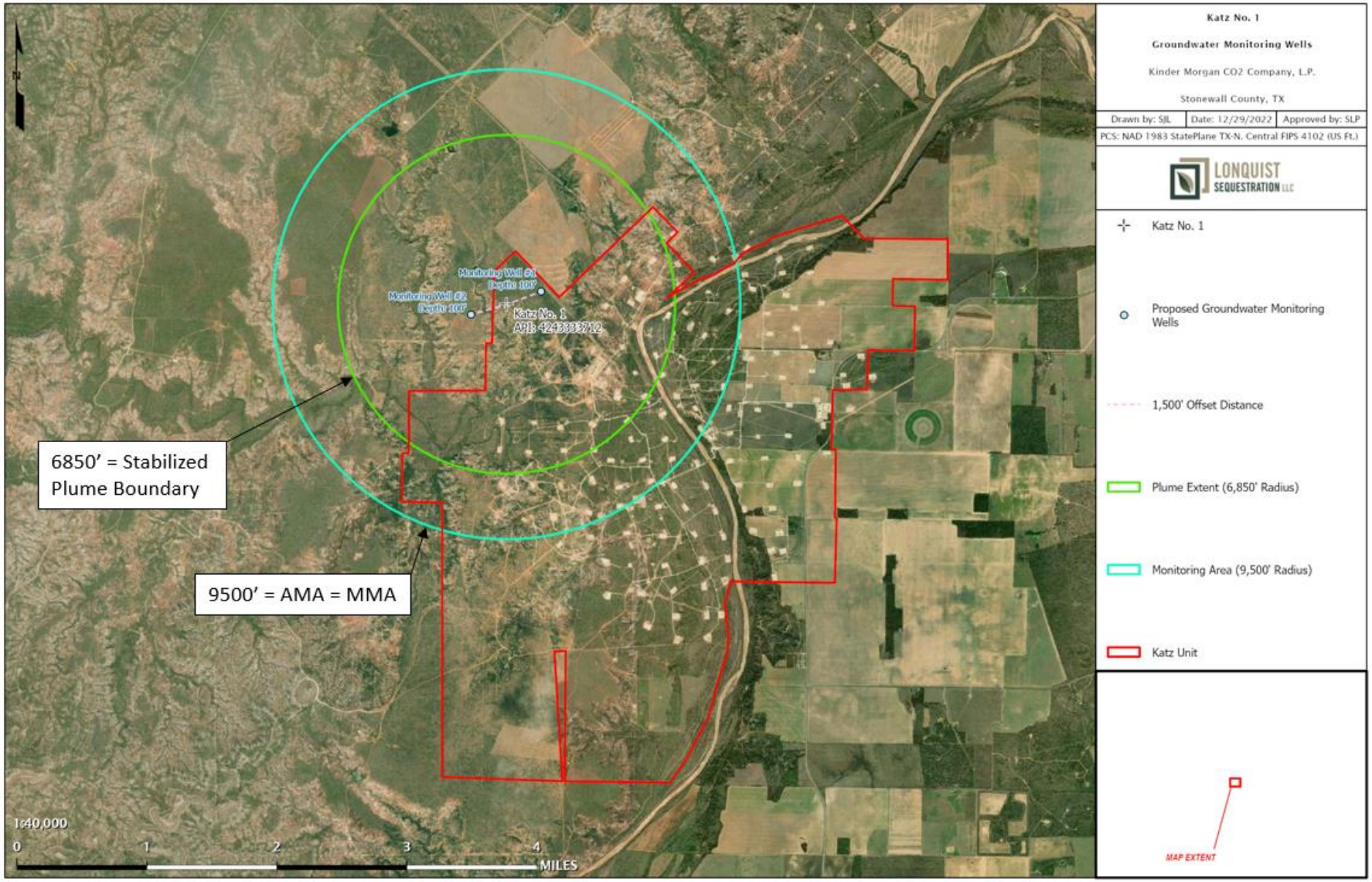


Figure 45 – Groundwater Monitoring Wells

## 5.3 Leakage through Faults, Fractures or Confining Seals

Kinder Morgan continuously monitors the operations of the KSU 2361 well through automated systems. Any deviation from normal operating conditions indicating movement into a potential pathway, such as a fault or breakthrough of the confining seal would trigger an alert. Any such alert would be reviewed by field personnel and action taken to shut in the well, if necessary. In addition, a field monitoring system is proposed to measure the shallow topsoil $CO_2$ concentrations across the MMA. These measurements will be taken quarterly by in-field gas sensors. The field $CO_2$ monitoring systems would alert field personnel for any release of $CO_2$ caused by such leakage. In the unlikely event a leak occurs, Kinder Morgan will quantify the leak per the strategies discussed in Section 7, below.

## 5.4 Leakage through Natural or Induced Seismicity

While the likelihood of a natural or induced seismicity event is extremely low, Kinder Morgan plans to use the nearest TexNet seismic monitoring station to monitor the area of the KSU 2361 well. This station is 7.29 miles southwest of the well location, as shown below in Figure 46. This is a sufficient distance to allow for accurate and detailed monitoring of the seismic activity surrounding the Katz Unit. Kinder Morgan will monitor this station for any seismic activity that occurs near the well. If a seismic event of 3.0 magnitude or greater is detected, Kinder Morgan will review the injection volumes and pressures at the KSU 2361 well to determine if any significant changes occur that would indicate potential leakage. In the unlikely event a leak occurs, Kinder Morgan will quantify the leak per the strategies discussed in Section 7, below.


Figure 46 – Nearest TexNet Seismic Station

# SECTION 6 – BASELINE DETERMINATIONS

This section identifies the strategies Kinder Morgan will undertake to establish the expected baselines for monitoring $CO_2$ surface leakage per 40 CFR **§98.448(a)(4).** Kinder Morgan will use the existing SCADA monitoring systems to identify changes from the expected performance that may indicate leakage of $CO_2$. Once the baseline concentrations are determined over a 12 month period prior to injection, the $CO_2$ monitors will be set to alarm at concentrations that are statistically significant deviation from baseline.

## 6.1 Visual Inspections

Daily inspections will be conducted by field personnel at the facility and the KSU 2361 well. These inspections will aid with identifying and addressing possible issues in order to minimize the possibility of leakage. If any issues are identified, such as vapor clouds or ice formations, corrective actions will be taken to address such issues.

## 6.2 $CO_2$ Detection

In addition to the well site fixed monitors described previously, Kinder Morgan will establish and operate an in-field monitoring program to detect any $CO_2$ leakage within the MMA. The scope of baseline determination will include atmospheric $CO_2$ measurements at the AGI well site and near identified penetrations within the MMA. Topsoil $CO_2$ concentrations will also be measured, at pre-determined locations within the MMA, as baseline values before injection activities begin.

## 6.3 Operational Data

Upon starting injection operations, baseline measurements of injection volumes and pressures will be taken. Any significant deviations over time will be analyzed for indication of leakage of $CO_2$.

## 6.4 Continuous Monitoring

The total mass of $CO_2$ emitted by surface leakage and equipment leaks will not be measured directly as the injection stream for this project are well beyond the OSHA PEL 8-hour TWA limit of 5,000 ppm. Direct leak surveys are dangerous and present a hazard to personnel. Continuous monitoring systems should trigger an alarm upon a release. The mass of the $CO_2$ released would be calculated for the operating conditions, including pressure, flow rate, size of the leak point opening, and duration of the leak. This method is consistent with 40 CFR **§98.448(a)(5)**, allowing the operator to calculate site-specific variables used in the mass balance equation.

In the case of a blowdown event, emissions will be sent to vent stacks and will be reported as required for the operation of the well.

## 6.5 Groundwater Monitoring

Initial samples will be taken from the groundwater monitoring wells drilled within 1,500 feet of the KSU 2361 well upon approval of Kinder Morgan's MRV and before commencing injection of $CO_2$. A third-party laboratory will analyze the samples to establish the baseline properties of the groundwater.

# SECTION 7 – SITE-SPECIFIC CONSIDERATIONS FOR MASS BALANCE EQUATION

This section identifies how Kinder Morgan will calculate the mass of $CO_2$ injected, emitted, and sequestered. This also includes site-specific variables for calculating the $CO_2$ emissions from equipment leaks and vented emissions of $CO_2$ between the injection flow meter and the injection well, per 40 CFR **§98.448(a)(5)**.

## 7.1 Mass of $CO_2$ Received

Per 40 CFR **§98.443**, the mass of $CO_2$ received must be calculated using the specified $CO_2$ received equations "unless you follow the procedures in 40 CFR **§98.444(a)(4**)." 40 CFR **§98.444(a)(4)** states that "if the $CO_2$ you receive is wholly injected and is not mixed with any other supply of $CO_2$, you may report the annual mass of $CO_2$ injected that you determined following the requirements under paragraph (b) of this section as the total annual mass of $CO_2$ received instead of using Equation RR-1 or RR-2 of this subpart to calculate $CO_2$ received." The $CO_2$ received for this injection well is wholly injected and not mixed with any other supply; the annual mass of $CO_2$ injected will equal the amount received. Any future streams would be metered separately before being combined into the calculated stream.

## 7.2 Mass of $CO_2$ Injected

Per 40 CFR **§98.444(b)**, since the flow rate of $CO_2$ injected will be measured with a volumetric flow meter, the total annual mass of $CO_2$, in metric tons, will be calculated by multiplying the mass flow by the $CO_2$ concentration in the flow according to Equation RR-5:

$$CO_{2,u} = \sum_{p=1}^{4} Q_{p,u} * D * C_{CO_{2,p,u}}$$

Where:

$CO_{2,u}$ = Annual $CO_2$ mass injected (metric tons) as measured by flow meter u

$Q_{p,u}$ = Quarterly volumetric flow rate measurement for flow meter u in quarter p (standard cubic meters per quarter)

D = Density of $CO_2$ at standard conditions (metric tons per standard cubic meter): 0.0018682

$C_{CO2,p,u}$ = Quarterly $CO_2$ concentration measurement in flow for flow meter u in quarter p (volume percent $CO_2$, expressed as a decimal fraction)

p = Quarter of the year

u = Flow meter

## 7.3 Mass of $CO_2$ Produced

The KSU 2361 well is not part of an enhanced oil recovery project; therefore, no $CO_2$ will be produced.

## 7.4 Mass of $CO_2$ Emitted by Surface Leakage

The mass of $CO_2$ emitted by surface leakage and equipment leaks will not be measured directly as the injection stream for this well contains concentrations well beyond the OSHA PEL 8-hour TWA limit of 5,000 ppm. Direct leak surveys are dangerous and present a hazard to personnel. Any leakage would be detected and managed as an upset event. An upset event is any unlikely event that results in the failure of any mass of $CO_2$ to remain permanently sequestered in the target reservoir. Continuous monitoring systems should trigger an alarm upon a release. The mass of the $CO_2$ released would be calculated for the operating conditions, including pressure, flow rate, size of the leak point opening, and duration of the leak. This method is consistent with 40 CFR **§98.448(a)(5)**, allowing the operator to calculate site-specific variables used in the mass balance equation.

In the unlikely event that $CO_2$ was released as a result of surface leakage, the mass emitted would be calculated for each surface pathway according to methods outlined in the plan and totaled using Equation RR-10 as follows:

$$CO_{2E} = \sum_{x=1}^{X} CO_{2,x}$$

Where:

$CO_2$ = Total annual $CO_2$ mass emitted by surface leakage (metric tons) in the reporting year

$CO_{2,x}$ = Annual $CO_2$ mass emitted (metric tons) at leakage pathway x in the reporting year

X = Leakage pathway

Calculation methods using equations from subpart W will be used to calculate $CO_2$ emissions due to any surface leakage between the flow meter used to measure injection quantity and the injection wellhead.

As discussed previously, the potential for pathways for all previously mentioned forms of leakage are unlikely. Given the possibility of uncertainty around the cause of a leakage pathway that is mentioned above, Kinder Morgan believes the most appropriate method to quantify the mass of $CO_2$ released will be determined on a case-by-case basis. Any mass of $CO_2$ detected leaking to the surface will be quantified by using industry proven engineering methods including, but not limited

to engineering analysis on surface and subsurface measurement data, dynamic reservoir modeling, history-matching of the sequestering reservoir performance, among others. In the unlikely event that a leak occurs, it will be addressed, quantified and documented within the appropriate timeline. Any records of leakage events will be kept and stored as stated in Section 10, below.

## 7.5 Mass of $CO_2$ Sequestered

The mass of $CO_2$ sequestered in subsurface geologic formations will be calculated based on Equation RR-12, assuming an expected injection start date of June 1, 2024, as this well will not actively produce oil or natural gas, or any other fluids, as follows:

$$CO_2 = CO_{2I} - CO_{2E} - CO_{2FI}$$

Where:

$CO_2$ = Total annual $CO_2$ mass sequestered in subsurface geologic formations (metric tons) at the facility in the reporting year

$CO_{2I}$ = Total annual $CO_2$ mass injected (metric tons) in the well or group of wells covered by this source category in the reporting year

$CO_{2E}$ = Total annual $CO_2$ mass emitted (metric tons) by surface leakage in the reporting year

$CO_{2FI}$ = Total annual $CO_2$ mass emitted (metric tons) from equipment leaks and vented emissions of $CO_2$ from equipment located on the surface between the flow meter used to measure injection quantity and the injection wellhead

$CO_{2FI}$ will be calculated in accordance with Subpart W reporting of GHGs. Because no venting is expected to occur, the calculations would be based on the unusual event that a blowdown is required and those emissions sent to flares and reported as part of the required GHG reporting for the gas plant.

- Calculation methods from subpart W will be used to calculate $CO_2$ emissions from equipment located on the surface between the flow meter used to measure injection quantity and the injection wellhead.

# SECTION 8 – IMPLEMENTATION SCHEDULE FOR MRV PLAN

The KSU 2361 well currently reports GHGs under Subpart UU, but Kinder Morgan has elected to submit an MRV plan under, and otherwise comply with, Subpart RR. The MRV plan will be implemented upon receiving EPA approval. The Annual Subpart RR Report will be filed by March 31st of the year following the reporting year.

# SECTION 9 – QUALITY ASSURANCE

This section identifies how Kinder Morgan plans to manage quality assurance and control to meet the requirements of 40 CFR **§98.444.**

## 9.1 Monitoring QA/QC

$CO_2$ *Injected*

- The flow rate of the $CO_2$ being injected will be measured with a volumetric flow meter, consistent with industry best practices. These flow rates will be compiled quarterly.
- The composition of the $CO_2$ stream will be measured upstream of the volumetric flow meter with a continuous gas composition analyzer or representative sampling consistent with industry best practices.
- The gas composition measurements of the injected stream will be averaged quarterly.
- The $CO_2$ measurement equipment will be calibrated per the requirements of 40 CFR 98.444(e) and 98.3(i) of the GHGRP.

$CO_2$ *Emissions from Leaks and Vented Emissions*

- Gas monitors will be operated continuously, except for maintenance and calibration.
- Gas monitors will be calibrated according to the requirements of 40 CFR 98.444(e) and 98.3(i) of the GHGRP.
- Calculation methods from subpart W will be used to calculate $CO_2$ emissions from equipment located on the surface between the flow meter used to measure injection quantity and the injection wellhead.

*Measurement Devices*

- Flow meters will be continuously operated except for maintenance and calibration.
- Flow meters will be calibrated according to 40 CFR §98.3(i) requirements**.**
- Flow meters will be operated per an appropriate standard method as published by a consensus-based standards organization.

All measured volumes of $CO_2$ will be converted to standard cubic meters at a temperature of 60 degrees Fahrenheit and an absolute pressure of 1 atmosphere.

## 9.2 Missing Data

In accordance with 40 CFR **§98.445**, Kinder Morgan will use the following procedures to estimate missing data if unable to collect the data needed for the mass balance calculations:

- If a quarterly quantity of $CO_2$ injected is missing, the amount will be estimated using a representative quantity of $CO_2$ injected from the nearest previous period at a similar injection pressure.
- Fugitive $CO_2$ emissions from equipment leaks from facility surface equipment will be estimated and reported per the procedures specified in subpart W of 40 CFR **§98.**

## 9.3 MRV Plan Revisions

If any changes outlined in 40 CFR **§98.448(d)** occur, Kinder Morgan will revise and submit an amended MRV plan within 180 days to the Administrator for approval.

# SECTION 10 – RECORDS RETENTION

Kinder Morgan will retain records as required by 40 CFR **§98.3(g)**. These records will be retained for at least three years and include the following:

- Quarterly records of the $CO_2$ injected
  - Volumetric flow at standard conditions
  - Volumetric flow at operating conditions
  - Operating temperature and pressure
  - Concentration of the $CO_2$ stream
- Annual records of the information used to calculate the $CO_2$ emitted by surface leakage from leakage pathways.
- Annual records of the information used to calculate $CO_2$ emitted from equipment leaks and vented emissions of $CO_2$ from equipment located on the surface between the flow meter used to measure injection quantity and the injection wellhead.

# SECTION 11 - REFERENCES

Adams, Donald & Keller, Randy. (1996). Precambrian Basement Geology of the Permian Basin Region of West Texas and Eastern New Mexico: A Geophysical Perspective. AAPG Bulletin. 80. 410-431. 10.1306/64ED87FA-1724-11D7-8645000102C1865D.

Broadhead, Ronald E., 2005. Regional Aspects of the Wristen petroleum system, southeastern New Mexico: New Mexico Bureau of Geology and Mineral Resources Open File Report, no. 485.

Comer, John B., 1991. Stratigraphic Analysis of the Upper Devonian Woodford Formation, Permian Basin, West Texas and Southeastern New Mexico: Bureau of Economic Geology Report of Investigations, no. 201.

Conselman, F. B. (1954). Preliminary Report on the Geology of the Cambrian Trend of West Central Texas. *Abilene Geologic Society*.

Ewing et al. (2004). Groundwater Availability Model for the Seymour Aquifer. *Texas Water Development Board.*

Galley, J. (1958). Oil and Geology in the Permian Basin of Texas and New Mexico. *Basin or Areal Analysis or Evaluation*.

George, Peter G., Mace, Robert E., and Petrossian, Rima, 2011. Aquifers of Texas: Texas Water Development Board Report, no 380.

Gunn, R. D. (1982). Desmoinesian Depositional Systems in the Knox Baylor Trough. *North Texas Geological Society*.

Harding, R.W. and Associates. (1978). THE SEYMOUR AQUIFER: Ground-Water Quality and Availability in Haskell and Knox Counties, Texas. *Texas Department of Water Resources.*

Hendricks, L. (1964). STRATIGRAPHIC SUMMARY OF THE ELLENBURGER GROUP OF NORTH TEXAS. *Tulsa Geological Society Digest, Volume 32*.

Hoak, T., Sundberg, K., and Ortoleva, P. Overview of the Structural Geology and Tectonics of the Central Basin Platform, Delaware Basin, and Midland Basin, West Texas and New Mexico: Department of Energy Open File Report.

Holtz, M.H., and Kerans, C. (1992). Characterization and categorization of West Texas Ellenburger reservoirs. *Permian Basin Section SEPM Publication No. 92-22, p. 31-44.*

Hornhach, M. J. (2016). Ellenburger wastewater injection and seismicity in North Texas. *Physics of the Earth and Planetary Interiors*.

Jesse G. White, P. P. (2014). Reconstruction of Paleoenvironments through Integrative Sedimentology and Ichnology of the Pennsylvanian Strawn Formation. *AAPG Southwest Section Annual Convention, Midland, Texas*.

Kane, S. C. (n.d.). THE MISSISSIPPIAN BARNETT FORMATION: A SOURCE-ROCK, SEAL, AND RESERVOIR PRODUCED BY EARLYCARBONIFEROUS FLOODING OF THE TEXAS CRATON. *BEG*.

Kerans, C. (1989). Karst-controlled reservoir heterogeneity and an example from the Ellenburger Group (Lower Ordovician) of West Texas. *Bureau of Economic Geology.*

Kerans, C. (1990). Depositional Systems and Karst Geology of the Ellenburger Group (Lower Ordovician), Subsurface West Texas. *Bureau of Economic Geology*.

Kupecz, J.A., and L.S. Land. (1991). Late-stage dolomitization of the Lower Ordovician Ellenburger Group, West Texas. *Journal of Sedimentary Petrology.*

Kyle, J.R. and E.F. McBride. (2014). Geology of the Voca Frac Sand District, western Llano Uplift, Texas. *Arizona Geological Survey Special Paper #9, Chapter 2, p. 1-13.*

Loucks, R. (2003). REVIEW OF THE LOWER ORDOVICIAN ELLENBURGER GROUP OF THE PERMIAN BASIN, WEST TEXAS. *Bureau of Economic Geology*.

Mason, C. C. (1961). GROUND-WATER GEOLOGY OF THE HICKORYSANDSTONE MEMBER OF THE RILEY FORMATION. McCULLOCH COUNTY. TEXAS. *TEXAS BOARD OF WATER ENGINEERS*.

Molina, Oscar, Vilarras, Victor, and Zeidouni, Mehdi, 2016. Geologic carbon storage for shale gas recovery: 13th International Conference on Greenhouse Gas Control Technologies, GHGT-13, 14-18.

Ruppel, Stephen C. and Holtz, Mark H., 1994. Depositional and Diagenetic Facies Patterns and Reservoir Development in Silurian and Devonian Rocks of the Permian Basin: Bureau of Economic Geology Report of Investigations, no. 216.

Snee, Jens-Erik Lund and Zoback, Mark D., 2016. State of stress in the Permian Basin, Texas and New Mexico: Implications for induced seismicity.

Teeple, Andrew P., Ging, Patricia B., Thomas, Jonathan V., Wallace, David S., and Payne, Jason D., 2021. Hydrogeologic Framework, Geochemistry, Groundwater-Flow System, and Aquifer Hydraulic Properties Used in the Development of a Conceptual Model of the Ogallala, Edwards-Trinity (High Plains), and Dockum Aquifers In and Near Gaines, Terry, and Yoakum Counties, Texas: USGS Scientific Investigations Report 2021-5009.

# SECTION 12 - APPENDICES